UNIVERSITAT POLITÈCNICA DE VALÈNCIA

Departamento de Comunicaciones

NOVEL 5G-MODULATION FORMATS AND THEIR APPLICATION IN OPTICAL WIRELESS COMMUNICATIONS

Ph. D. Thesis

by

Mohammed Bahaaelden

Supervisors: Prof. Beatriz Ortega Tamarit

Prof. Rafael Pérez Jiménez

Valencia, March 2024

Universitat Politècnica de València

Institute of Telecommunications and Multimedia Applications

Photonics Research Labs

8G Building

Cno. de Vera, s/n

46022, Valencia

Spain

Tel: +34 963879580

E-mail: MOBA2@DOCTOR.UPV.ES

In loving memory of my father,

for his pride that his son finishes a Ph. D.

To my loved ones,

for their support and encouragement

About the author

Mohammed Bahaaelden was born in Diyala, IRAQ, in 1984. He received the B.Sc. Degree in Electronic Engineering from Mosul University, Iraq (2008), and M.Sc. Degree in Electrical and Electronic Engineering from Near East University, North Cyprus (2015), where the presented his Final project on using the artificial neural network in power plant. Besides, he received his Master's Degree in Engineering Physics from Sofia university, Bulgaria (2017) with a Master Project based on experimental demonstration of using visible light communication to send data information by using Arduino.

From February 2010 to March 2012, he worked as an operator Engineering, in particular with operation turbine and monitoring, at MASS global company, Erbil, Iraq. From October 2014 to September 2015, he worked as Radio frequence Engineering to provide technical guidance to program stuff and junior engineers, at Newroz Telecom company, Erbil, Iraq.

In February 2019, he started his Ph. D. and joined the Instituto de Telecomunicaciones y Aplicaciones Multimedia, Universitat Politecnica de Valencia (UPV), Valencia (Spain). His Ph. D. has been focused on future optical wireless communications, advanced modulation formats and indoor communications, under the supervision of Prof. Beatriz Ortega Tamarit and Prof. Rafael Pérez Jiménez. During this period, he has collaborated in FOCAL and OPTIMISE national projects, and he has published several international journal and conferences papers.

His current research focuses on visible light communications, FBMC modulation, data transmission over hybrid indoor/outdoor transmission, Internet of Things and optical access networks.

He can be contacted at Moba2@doctor.upv.es and mohammedbahaaelden@yahoo.com

OrCID: 0000-0001-6232-5546

Valencia, Spain, March 2024

Contents

List of figures

List of tables

List of acronyms

QoS	Quality of service
RF	Radio frequency
VLC	Visible light communication
5G	Fifth generation
OWC	Optical wireless communication
6G	Sixth generation
LEDs	Light Emitting Diodes
WRC	World Radio Conference
mmWave	Millimeter wave
THz	Terahertz
VR	Virtual reality
Tbps	Terabit-per-second
KPIs	Key performance indicators
Li-Fi	Light fidelity
LANs	Local area networks
LDs	Laser diodes
OFDM	Orthogonal frequency division multiplexing
QAM	Quadrature amplitude modulation
IM/DD	Intensity modulation and direct detection
CP	Cyclic prefix
DCO-OFDM	Direct current biased optical OFDM
CFO	Channel frequency offset
STO	Symbol timing offset
OQAM	Offset-QAM
FBMC	Filter bank multicarrier
IAM	Interference approximation method
4G	Fourth generation
IAM-R/C	Special types of IAM sequence
D/A	Digital-to-analog
A/D	Analog-to-digital
PD	Photodetector
TIA	Trans-Impedance Amplifier
TOV	Turn-on voltage
PIN	Positive intrinsic negative
APD	Avalanche photodetector
OLED	Organic LED
BJT	Bipolar-junction transistor
LOS	Line of sight
B5G	Beyond 5G
OOK	On-OFF Keying
NRZ	Non-return to zero
PAM	Pulse amplitude modulation
BW	Bandwidth

CAP	Amplitude and phase modulation
PAPR	Peak-to-average power ratio
WDM	Wavelength-division-multiplexing
ACO	Asymmetric clipped optical OFDM
GPS	Global positioning system
NFV	Network function virtualization
FPGA	Field Programmable Gate Array
Li-Fi	Light fidelity
IPMS	Institute for Photonic Microsystems
MIMO	Multiple input multiple output
Mb/s	Megabits per second
COTS	Commercial off-the-shelf
Gbps	Gigabit-per-second
CMOS	Metal-Oxide Semiconductor
PAR	Project Authorization Request
CSD	Criteria for Standards Development
HCF	Hybrid coordination function
OBSS	Overlapping basic service set
GFDM	Generalized Frequency Division Multiplexing
UFMC	Universal Filtered Multicarrier
OOBE	Out-of-band emission
ICI	Inter Carrier Interference
IFFT	Inverse Fast Fourier Transform
ISI	Inter Symbol Interference
CMT	Cosine modulated multitone
SMT	staggered modulation multitone
FMT	Filtered multitone
PSD	Power Spectral Density
C2R	Complex-to-real
R2C	Real-to-Complex
SFB	Synthesis filter bank
AFB	Analysis filter banks
PR	Perfect reconstruction
PHYDYAS	PHYsical layer for DYnamic AccesS and cognitive radio
FT	Frequency-time
IR	Infrared
TMUX	Transmultiplexer
SIR	Signal-to-interference ratio
CE	Channel estimation
CAPI	Coded Auxiliary Pilot
IMI	Intrinsic imaginary interference
EGF	Extended Gaussian Function
Po-De	Polyphase decomposition
SER	Symbol error rate
PON	Passive optical network
ZF	Zero-forcing

MSLR	Main to side lobe ratio

Abstract

The sixth generation (6G) network is the potential solution to meet the exponentially increasing requirements of the emerging services and applications. The 6G platform expects to offer high data rates, ultra-high connectivity, and low latency based on the required key performance indicators (KPIs). The visible light communication (VLC) technology represents a key technology for 6G network but requires an efficient advanced modulation technique to support such requirements. In the last decades, optical signals based on Orthogonal Frequency Division Multiplexing (OFDM) scheme has attracted a lot of attention and become the most popular modulation among several multicarrier access schemes, thanks to its robustness and simplicity against multipath fading using the cyclic prefix (CP). However, besides the downsides of OFDM-rectangular prototype filter, high leakage powers and carrier frequency offset can significantly deteriorate the performance of OFDM signals since the extra CP and guard band samples leads to redundant data information that decreases its spectral efficiency.

One of the most candidate waveforms that is considered as the promising modulation technique for the next generation requirements and applications is Filter Bank MultiCarrier (FBMC) multiplexing. The major benefit of FBMC scheme is non-reliance on CP and high numbers of guard band samples, thereby, it employs several well time-frequency localized pulse functions with high side-lobe suppression ratio instead, which allows enhancing the spectral efficiency and system performance as key factors in next generation optical networks, and provides a good alternative to CP-OFDM technique.

This Thesis aims to make a step forward in proposing modulation formats to be used in VLC systems as enabling technology in 6G networks. Hence, Flip-FBMC system with a truncation algorithm is proposed to offer a high-speed transmission with low latency by tackling the doubled-overhead tails at the subframes of Flip-FBMC burst by the use of the isotropic orthogonal transformation algorithm (IOTA) and PHYsical layer for DYnamic AccesS and cognitive radio (PHYDYAS) filters. However, due to the intrinsic imaginary interference (IMI), the enhancement in recovered-optical FBMC signal over Flip-OFDM system is limited to the propagation over a link with low delays profile and/or low constellation mapping. Thereby, multitap equalization is proposed for the sake of mitigating the IMI over a channel with high delays profile.

Moreover, for indoor VLC system, the possibility to enhance the error performance of non-coherent FBMC signals is delivered by analysing the property of time-frequency localization with Extended Gaussian Function (EGF), where the spreading factor plays a crucial role in determining the trade-off between the spectral features and optimal reconstruction of signal quality. In such scenario, due to the limited dynamic range of light emitting diode (LED), improving in the accuracy of estimation depends on the power-levels of pseudo pilots with the use of Interference Approximation Method (IAM) architecture. Thereby, the analysis reveals that IAM sequence is not suitable for a real transmission scenario due to high power of IAM over the payload data which conflicts with VLC purposes of illumination and communication simultaneously. Additionally, the Thesis provides the first theoretical analysis reporting the degradation of estimation accuracy for several clipping ratios based on the impact of imaginary interference level outside the first order neighbourhood zone that cannot be estimated by IAM preamble. However, the value of Flip-FBMC/IAM technique in providing the unipolar model must be emphasized compared to the use of Direct Current biased Optical FBMC (DCO-FBMC) format that suffers from a reduction in estimating accuracy. Thereby, the downfall performance with DCO-FBMC system has been reported because of the induced IMI that spreads out

the first neighbourhood symbols, which is more evident when low levels of the added DC-bias are required.

From such perspective, the frame repetition technique with Flip-FBMC signals has been demonstrated as a major solution for minimizing the induced interference. Therefore, in this Thesis, Flip-FBMC/frame repetition with PHYDYAS profile is proposed as a viable candidate to cope with the restricted dynamic range of the LED, compared to the performance for each Flip-CP-OFDM and Flip-FBMC/IAM system in future 6G networks based on VLC access.

Resumen

La red de sexta generación (6G) es la solución potencial para satisfacer los requisitos exponencialmente crecientes de los servicios y aplicaciones emergentes. La plataforma 6G espera ofrecer altas velocidades de datos, conectividad ultra alta y baja latencia en función de los indicadores clave de rendimiento (KPI) requeridos. La tecnología de comunicación por luz visible (VLC) representa una tecnología clave para la red 6G, pero requiere una técnica de modulación avanzada eficiente para cumplir con dichos requisitos. En las últimas décadas, las señales ópticas basadas en el esquema de multiplexación por división de frecuencia ortogonal (OFDM) han atraído mucha atención y se han convertido en la modulación más popular entre varios esquemas de acceso multiportadora, gracias a su robustez y simplicidad frente a la cancelación por trayectos múltiples utilizando el prefijo cíclico (CP). Sin embargo, además de las desventajas del prototipo de filtro rectangular OFDM, la pérdida de potencia y el desplazamiento de la frecuencia pueden deteriorar significativamente el rendimiento de las señales OFDM, ya que las muestras adicionales de CP y banda de guarda implican información de datos redundante que disminuye su eficiencia espectral.

Una de las formas de onda más prometedoras para redes de próxima generación es la técnica de modulación Filter Bank MultiCarrier (FBMC). El principal beneficio del esquema FBMC es que no depende de CP y de un gran número de muestras de banda de guarda, por lo tanto, emplea varias funciones de pulso localizadas en el tiempo con una alta relación de supresión de lóbulos laterales, lo que permite mejorar la eficiencia espectral y el rendimiento del sistema como factores clave en las redes ópticas de próxima generación, y proporciona una buena alternativa a la técnica CP-OFDM.

Esta Tesis pretende dar un paso adelante en la propuesta de formatos de modulación para ser utilizados en sistemas VLC como tecnología habilitadora en redes 6G. Por lo tanto, se propone el sistema Flip-FBMC con un algoritmo de truncamiento para ofrecer una transmisión de alta velocidad con baja latencia Flip-FBMC mediante el uso del algoritmo de transformación ortogonal isotrópica (IOTA) y la capa PHYsical para DYnamic AccesS y filtros de radio cognitiva (PHYDYAS). Sin embargo, debido a la interferencia imaginaria intrínseca (IMI), la mejora de la calidad de la señal FBMC óptica recuperada a través del sistema Flip-OFDM se limita a la propagación a través de un enlace con un perfil de retardos cortos y/o constelaciones de orden bajo. De este modo, se propone la ecualización multitap con el fin de mitigar el IMI en un canal con perfiles de retardos elevado.

Además, para los sistemas VLC en interiores, la posibilidad de mejorar el rendimiento de error de las señales FBMC no coherentes se ofrece mediante el análisis de la propiedad de la localización de tiempo-frecuencia con la función gaussiana extendida (EGF), donde el factor de dispersión desempeña un papel crucial en la determinación del equilibrio entre las características espectrales y la reconstrucción óptima de la calidad de la señal. En tal escenario, debido al rango dinámico limitado del diodo emisor de luz (LED), la mejora de la precisión de la estimación depende de los niveles de potencia de los pseudopilotos con el uso de la arquitectura del Método de Aproximación de Interferencia (IAM). Por lo tanto, el análisis revela que la secuencia IAM no es adecuada para un escenario de transmisión real debido a la alta potencia de IAM sobre los datos de la carga útil, lo que entra en conflicto con la condición simultánea de iluminación y comunicación en los sistemas VLC. Además, la Tesis proporciona el primer análisis teórico que informa de la degradación en la estimación para varios factores de *clipping* basada en el impacto del nivel de interferencia imaginario fuera de la zona de primer orden que no puede ser estimada mediante el preámbulo de IAM. Sin

embargo, se debe enfatizar en el valor de la técnica Flip-FBMC/IAM para proporcionar el modelo unipolar en comparación con el uso del formato FBMC óptico polarizado con corriente continua (DCO-FBMC) que sufre una reducción en la estimación de la precisión.

Por lo tanto, se ha demostrado el descenso del rendimiento con el sistema DCO-FBMC debido al IMI inducido fuera de los símbolos de orden cero, y que es más evidente cuando se requieren niveles bajos de corriente DC. Desde esta perspectiva, la técnica de repetición de tramas con señales Flip-FBMC ha demostrado ser una solución importante para minimizar la interferencia inducida. Por lo tanto, en esta Tesis, la modulación Flip-FBMC con repetición de tramas y perfil de filtro PHYDYAS se propone como un candidato viable para hacer frente al rango dinámico restringido del LED, en comparación con el rendimiento de los sistemas Flip-CP-OFDM y Flip-FBMC/IAM en futuras redes 6G basadas en acceso VLC.

Resum

La xarxa de sexta generació (6G) és la solució potencial per a satisfer els requisits exponencialment creixents dels servicis i aplicacions emergents. La plataforma 6G espera oferir altes velocitats de dades, connectivitat ultra alta i baixa latència en funció dels indicadors clau de rendiment (KPI) requerits. La tecnologia de comunicació per llum visible (VLC) representa una tecnologia clau per a la xarxa 6G, però requerix una tècnica de modulació avançada eficient per a complir amb estos requisits. En les últimes dècades, els senyals òptics basats en l'esquema de multiplexació per divisió de freqüència ortogonal (OFDM) han atret molta atenció i s'han convertit en la modulació més popular entre diversos esquemes d'accés multiportadora, gràcies a la seua robustesa i simplicitat enfront de la cancel·lació per trajectes múltiples utilitzant el prefix cíclic (CP). No obstant això, a més dels desavantatges del prototip de filtre rectangular OFDM, la pèrdua de potència i el desplaçament de la freqüència poden deteriorar significativament el rendiment dels senyals OFDM, ja que les mostres addicionals de CP i banda de guarda impliquen informació de dades redundant que disminuïx la seua eficiència espectral.

Una de les formes d'ona més prometedores per a xarxes de pròxima generació és la tècnica de modulació Filter Bank MultiCarrier (FBMC). El principal benefici de l'esquema FBMC és que no depén de CP i d'un gran nombre de mostres de banda de guarda, per tant, empra diverses funcions de pols localitzades en el temps amb una alta relació de supressió de lòbuls laterals, la qual cosa permet millorar l'eficiència espectral i el rendiment del sistema com a factors clau en les xarxes òptiques de pròxima generació, i proporciona una bona alternativa a la tècnica CP-OFDM.

Esta Tesi pretén fer un pas avant en la proposta de formats de modulació per a ser utilitzats en sistemes VLC com a tecnologia habilitadora en xarxes 6G. Per tant, es proposa el sistema Flip-FBMC amb un algoritme de truncament per a oferir una transmissió d'alta velocitat amb baixa latència Flip-FBMC mitjançant l'ús de l'algoritme de transformació ortogonal isotròpica (IOTA) i la capa PHYsical per a DYnamic AccesS i filtres de ràdio cognitiva (PHYDYAS). No obstant això, a causa de la interferència imaginària intrínseca (IMI), la millora de la qualitat del senyal FBMC òptica recuperada a través del sistema Flip-OFDM es limita a la propagació a través d'un enllaç amb un perfil de retards curts i/o constel·lacions d'orde baix. D'esta manera, es proposa l'equalització multitap amb la finalitat de mitigar el IMI en un canal amb perfils de retards elevat.

A més, per als sistemes VLC en interiors, la possibilitat de millorar el rendiment d'error dels senyals FBMC no coherents s'oferix mitjançant l'anàlisi de la propietat de la localització de temps-freqüència amb la funció gaussiana estesa (EGF), on el factor de dispersió exercix un paper crucial en la determinació de l'equilibri entre les característiques espectrals i la reconstrucció òptima de la qualitat del senyal. En tal escenari, a causa del rang dinàmic limitat del díode emissor de llum (LED), la millora de la precisió de l'estimació depén dels nivells de potència dels pseudopilots amb l'ús de l'arquitectura del Mètode d'Aproximació d'Interferència (IAM). Per tant, l'anàlisi revela que la seqüència IAM no és adequada per a un escenari de transmissió real a causa de l'alta potència de IAM sobre les dades de la càrrega útil, la qual cosa entra en conflicte amb la condició simultània d'il·luminació i comunicació en els sistemes VLC. A més, la Tesi proporciona la primera anàlisi teòrica que informa de la degradació en l'estimació per a diversos factors de clipping basada en l'impacte del nivell d'interferència imaginari fora de la zona de primer orde que no pot ser estimada mitjançant el preàmbul de IAM. No obstant això, s'ha d'emfatitzar en el valor de la tècnica Flip-FBMC/IAM per a proporcionar el model unipolar en comparació amb l'ús del format FBMC òptic polaritzat amb corrent continu (DCO-FBMC) que patix una reducció en l'estimació de la precisió.

Per tant, s'ha demostrat el descens del rendiment amb el sistema DCO-FBMC a causa del IMI induït fora dels símbols d'orde zero, i que és més evident quan es requerixen nivells baixos de corrent DC. Des d'esta perspectiva, la tècnica de repetició de trames amb senyals Flip-FBMC ha demostrat ser una solució important per a minimitzar la interferència induïda. Per tant, en esta Tesi, la modulació Flip-FBMC amb repetició de trames i perfil de filtre PHYDYAS es proposa com un candidat viable per a fer front al rang dinàmic restringit del LED, en comparació amb el rendiment dels sistemes Flip-CP-OFDM i Flip-FBMC/IAM en futures xarxes 6G basades en accés VLC.

Chapter 1. Introduction

"*The best scientists are open to the possibility that they may be wrong, and they are willing to change their minds in the face of new evidence*".

– Richard Feynman

The goal of this Chapter is to provide the motivation, concept, requirements, and objectives of this Thesis. A brief survey of the evolution of the various generations of optical wireless communication networks is exhibited to address the main limitations and motivations in this work. Based on the sixth-generation challenges arising from the new emerging services and increasing demands, the objectives of this dissertation are identified. Finally, this Chapter also describes the structure of this Thesis, summarizing the contents of each section.

1.1. An overview of visible light communications

The concept of communicating through light is not new. Optical wireless communications (OWC) has actually existed for over three centuries. Ship flags, semaphore, and fire beacons are examples of early OW techniques. Another early form of optical communication is the reflection of sunlight via mirrors. The heliograph depicted in Figure 1.1 is an excellent illustration of such a system, where mirror movement generates light flashes that can be utilized to transmit Morse code [1]. This technique was a very useful tool for optical communication over 50 miles or more in the 19th century. This gadget was mostly used by the military, for protection of forests and surveys that was in operation until 1935 [1].

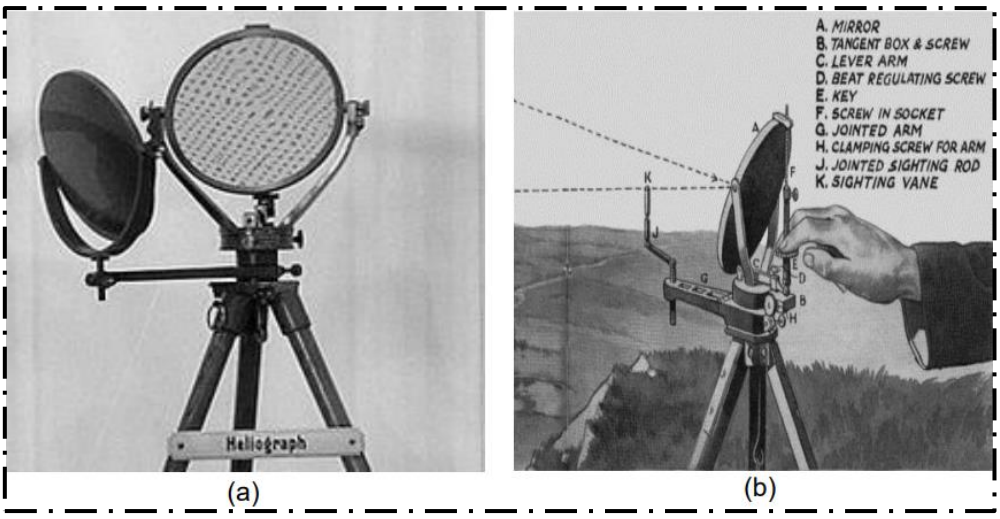

Figure 1.1. The heliograph, (a) the British army model, and schematic structure and assembly for (b) [1].

As a free-space communication device based on light, the photophone was created in 1880 by Alexander Graham Bell and Sumner Trainer. The apparatus was utilized to convey sounds onto a laser beam. As observed in Figure 1.2, the detection system of the device relies on a selenium crystal within the receiver that converts the optical signal into a flowing current of electrons. Bell's photophone relied on the electrical conductivity of selenium crystals, whose conductivity is influenced by the amount of light they are exposed to [2]. It is acknowledged that the photophone served as the forerunner of contemporary fiber optics, which carry more than 80% of global telecommunications traffic. In comparison to earlier techniques, optical communication systems nowadays demonstrate significantly higher data rates and improved quality of service (QoS).

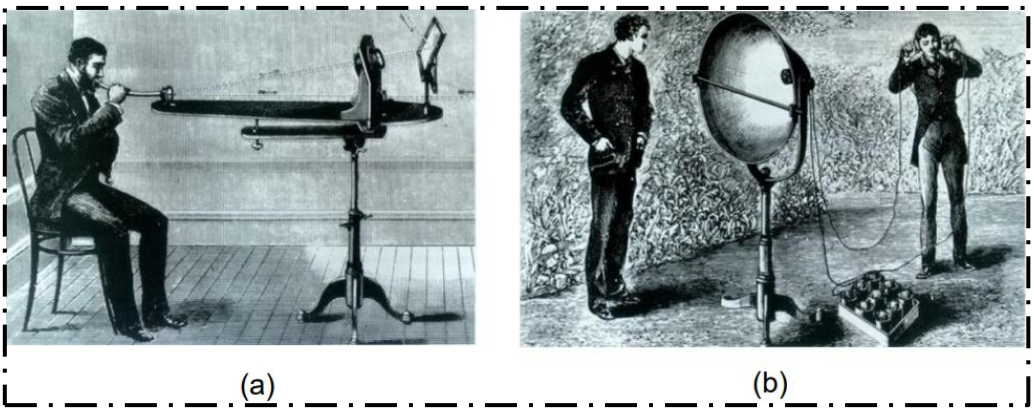

Figure 1.2. The transmitter with Bell's photophone for (a), and the receiver for (b) [2].

However, the demand for an alternative technology is being driven by a number of issues, such as the radio frequency (RF) spectrum congestion. A promising technique to overcome the limitations in the radio spectrum for wireless communication systems is the visible light communication (VLC) technology, thereby, VLC technique emerges as a promising solution to RF signals. By varying the intensity of an optical source operating in the visible area of the electromagnetic spectrum at a rate faster than the human eye's response time, information can be sent in VLC and is effectively perceived as a constant glow.

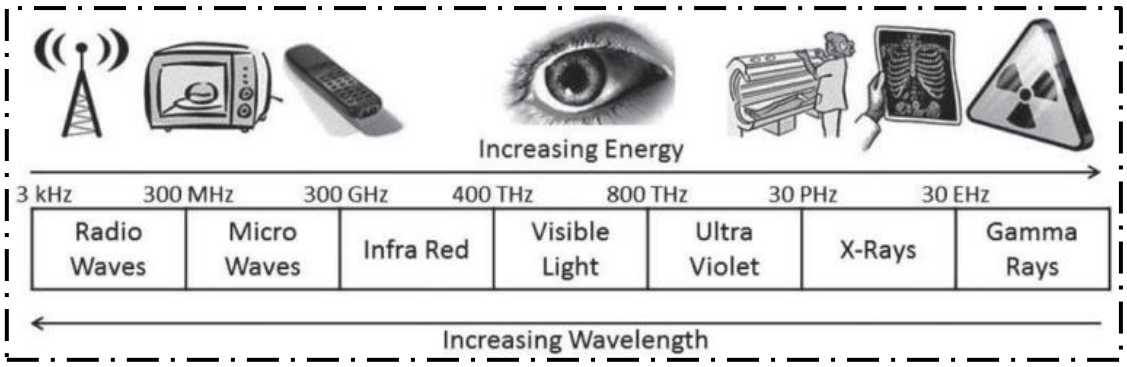

Figure 1.3. Electromagnetic spectrum [3].

As observed in Figure 1.3, utilizing an unlicensed segment of the electromagnetic spectrum, such as the optical band (430-790THz), presents itself as a feasible avenue for enhancing the capacity of wireless communication in the spectrum that transcends the boundaries of five generation (5G) and ventures into the territory of 6G. OWC is the name of this new technology, which has the important benefit of making extensive use of uncontrolled, unrestricted optical spectrum. As shown in Figure 1.4, OWC is often divided into several groups according to the transceiver technology and application scenarios, where satellite, vehicle-to-vehicle (V2V), underwater, free space optics between buildings or indoor VLC systems for high speed-transmission rate appear as potential applications in 6G-platform.

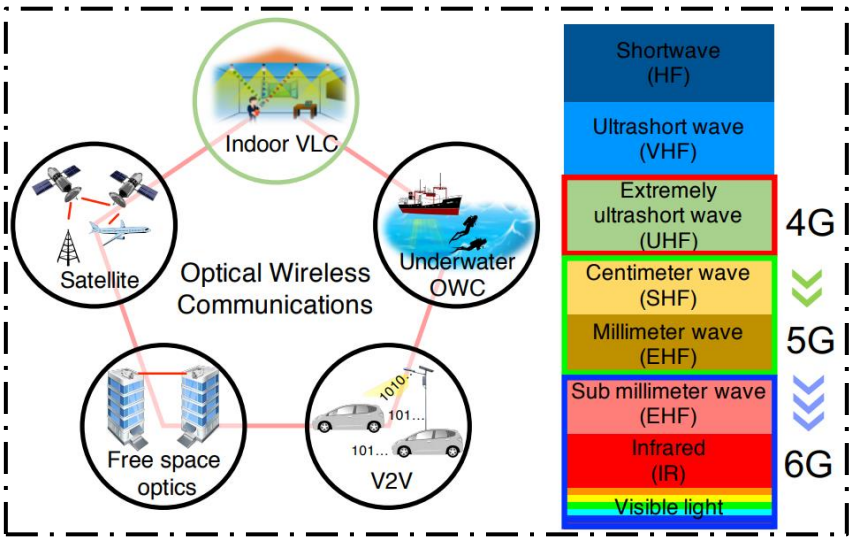

Figure 1.4. The potential applications for optical communication over various parts of spectrum resource [4].

Over the past 20 years, VLC has drawn a lot of attention from researchers among the several types of OWC. Light Emitting Diodes (LEDs) are used by VLC for data transmission as well as indoor lighting. The quick switch to LEDs for indoor illumination from traditional incandescent and fluorescent lightbulbs served as the impetus for VLC. LEDs are perfect for high-speed wireless transmission because of their direct modulation capability at very high frequencies in addition to their energy efficiency. The VLC transmission data rate has skyrocketed from Mbps to Gbps, positioning it as a formidable rival for future wireless networks, thanks to crucial technological advancements.

Although the World Radio Conference in 2019 (WRC-19) suggested that high-speed applications and ultra-low latency can be satisfied using the contiguous spectrum of millimeter wave

(mmWave), the assigned spectral resource for International Mobile Telecommunications 2020 services is still very limited to meet the 6G requirements. As a future vision for 6G networks, to verify such demands, the solution is to employ the large-scale abundant spectrum of terahertz (THz) and visible light communication bands, which are paving the way for 6G networks.

Moreover, such bands play a crucial rule to support i.e., the ultimate virtual reality (VR) services of high throughput rate of 2-Tbit-per-second (Tbps) that cannot be achieved by mmWave frequency band. Besides, the narrow pencil beamforming of THz wave compared to that with mmWave, contributes to minimize the interference with VR users in that example, although such narrow beamforming needs to redirected according to user moves, which leads the users to be out of VR services. Moreover, the positioning services of centimetres accuracy is obtained using 3-LEDs with VLC system, although the user mobility with dynamic selection of LEDs is not investigated in such works [5]-[6]. Therefore, the hybrid VLC/THz communication link is employed to enhance the VR services (to locate the VR-users accurately and sending high quality VR-images) [7]. Furthermore, the other main features of spectrum communication for mmWave of 5G and 6G including THz and VLC technologies are summarized in Table 1.1.

Table 1.1. Comparison of 5G based on mmWave and 6G of VLC and THz [8]-[9].

	5G-mmWave	**6G-VLC**	**6G-THz**
Technology used	mmWave	VLC	Sub mmWave (THz)
Peck data rate	Gb/s	In Tb/s range	Gb/s-Tb/s range
Operating frequency range	3 GHz -300 GHz	430 THz-790 THz	100 GHz-10 THz
Spectrum	Licensed	Unlicensed	Licensed
Transmitted power	High	Low	High
Underwater communication	No	YES	No
Electromagnetic interference	Yes	No	Yes
Usage environment	Indoor/outdoor	Mostly indoor	Indoor/outdoor
Challenges	Circuit design challenges and high propagation loss	Require RF at uplink transmission, low coverage, suffers from shot noise caused by another light source and prone to blockage	High penetration loss, higher propagation loss compared to mmWave, circuit design challenges and molecular absorption

From Table 1.1, the VLC band, as the highest frequency, can achieve higher speed-rate with compared to THz wave, thereby, the VLC data capacity can be in the order of Tbps as it operates on an unrestricted terahertz band of the electromagnetic spectrum. Nevertheless, the utilization of VLC band is limited by the speed of the state-of-the-art technologies, and yet there is no cost-effective equipment for commercial usages. Apart from the materials and devices, the currently available modulation techniques are also inadequate to support VLC spectrum, while the development of advanced modulation is still challenging.

Consequently, since the 6G network is expected to offer high data rates, ultra-high connectivity, and low latency based on the characteristics of key performance indicators (KPIs); we assume a platform based on mmWave band or a VLC system with the use of modulation waveforms that insufficient to meet the KPIs demands as a 5G network, the VLC system represents as a key

technology for 6G network that required an efficient modulation technique to support such requirements.

1.2. Motivation of this thesis

The high transmission rate and unlicensed spectrum band obtained by using VLC/Light fidelity (Li-Fi) systems aim to replace classical wireless local area networks (LANs) for indoor OWCs. Moreover, Li-Fi system is preferable over other wireless technologies, i.e. infrared communication, owing to the low cost and, ability to support high-speed transmission under safety criteria for human eyes with the use of LEDs. Although a transmission with laser diodes (LDs) can achieve higher throughput rate with long coverage distance, the transmitter/receiver precise alignment is considered as the main impairment, compared with wider divergence transmission in LEDs.

Apart from the development materials and devices, such as micro-LED and pre-equalization circuits that can be devoted to extending the system modulation bandwidth, the current LED bandwidth limitation is the major drawback in next generation high-speed Li-Fi systems. Therefore, a spectrally efficient modulation scheme, i.e. orthogonal frequency division multiplexing (OFDM) and/or Carrier-less Amplitude and Phase Modulation, is crucial for enhancing system transmission rate by enhancing bandwidth efficiency. Besides, such multidimensional technique of multilevel modulation, i.e. OFDM of 16/64 quadrature amplitude modulation (QAM) constitutes a suitable alternative for increasing the reduced spectral efficiency in single dimensional modulation schemes, i.e. typical on/off keying. From this perspective, OFDM format has become a predominant technique in indoor VLC context to deliver high throughput rates, since OFDM scheme can utilize the channel characteristics more effectively by using high modulation orders to fit the channel, making carrier-less amplitude and phase modulation technique less flexible than OFDM format [10]-[11].

To cope with intensity modulation and direct detection (IM/DD) channels, various techniques based on OFDM mechanism have been proposed and examined quite intensively in recent years due to the low implementation complexity, and ability to overcome the impact of inter-carrier interference and inter symbol interference, respectively, by using the overhead samples of cyclic prefix (CP), i.e. Flip-OFDM [12], and direct current-biased (DC bias) optical OFDM (DCO-OFDM) [13]. However, the redundant samples of CP, that are uploaded with useless information, drives to drop the system spectral efficiency. Besides, a significant spectral leakage is resulted according to the rectangular profile of fast Fourier transform filters [14]-[15], and as a consequence, extra guard bands at the edges of the spectrum are required to avoid the high out-of-band emission. Moreover, in real transmission, the impact of imperfect synchronization based on OFDM signalling, drives the system to be more sensitive to channel frequency offset (CFO) and symbol timing offset (STO) [16]-[17].

According to such restrictions, among several candidate waveforms that are considered as the promising modulation technique for the next generation requirements and applications, offset-QAM with filter bank multicarrier (FBMC-OQAM) modulation has recently achieved a lot of attention as an alternative to optical CP-OFDM technique [18]-[21]. The main characteristic of using FBMC modulation is the employment of the well time-frequency localized prototype pulse with high side-lobe suppression ratio instead of overhead CPs. Besides, according to [21], no guard bands are required at the edge of optical FBMC spectrum, thereby, the spectral efficiency can be furtherly enhanced. The spectral property of a minimum leakage can also be obtained by using FBMC technique with compared to other multicarrier modulation schemes. Additionally, asynchronous transmission from multiple users is simply separated in the frequency domain, hence, high flexibility for spectrum allocation can be supported [22]. Furthermore, compared to

CP-OFDM system, FBMC signalling shows more robustness against the residual impact of STO and CFO [23]. However, despite these crucial advantages, high hardware complexity, and the impact of imaginary interference that inherits into received FBMC signals, are currently the major drawbacks in FBMC systems [24].

Nevertheless, in RF domain, the impact of residual interference can be mitigated with the use of FBMC-frame duplication technique based on different prototype filters [25]-[26], although RF-OFDM system still offers better performance than the FBMC-frame duplication technique, and even at the low QAM order, i.e. 4-QAM where the imaginary interference is not significant. However, such influence could be differed due to the combinational nature of optical signal (real positive format), the retrieved optical FBMC signal that is obtained after transmission over a real optical channel has a different level of imaginary interference than that with RF signals.

The significant difference between the FBMC-frame duplication and classical FBMC-OQAM technique, is that the latter needs special reference symbols, i.e. Interference approximation method (IAM) of high power over the payload data, to mitigate the imaginary interference from estimated signals. However, maximizing the IAM power over payload data can drive the optical FBMC transmission burst to falls out the restricted dynamic range of LED (nonlinearity impact), which is considered as one of the major drawbacks for indoor-VLC system-based LED in a realistic transmission scenario [27]-[28].

Moreover, another drawback arises at the expense of using FBMC system, where the pulse shaping filter requires to be more spread out in time domain in order to obtain higher spectral selectivity, so higher latency can be induced in such scenario. For this perspective, tail truncation and pre-loading techniques have been proposed to mitigate such impact [29]-[30]. However, in such techniques, the out of band emission level has a significant impact to evaluate the truncation performance. Consequently, since the leakage power has less influence on the optical signal, the expected tail-shortening mechanism should impose different criteria in evaluating the system performance.

1.3. Objectives

The scope of this Thesis is to model, characterize and investigate the major limiting factors in indoor VLC systems and to propose efficient modulation formats based on FBMC for the sake of providing high throughput rate and minimum latency according to 6G requirements. More specifically, the fundamental objectives can be summarized below:

- To investigate the proposal of a Flip-FBMC system as a good alternative to optical CP-OFDM system, also considering different prototype filters and lengths to deliver the optimum spectral efficiency with minimum latency.
- To investigate the imaginary interference impact over different propagation links and constellation mapping.
- To propose multitap equalization for the sake of mitigating the residual interference over high delays profile links.
- To evaluate the property of time-frequency localization with extended Gaussian function in non-coherent FBMC signals and analyse the role of the spreading factor in determining the trade-off between the spectral features and optimal reconstruction of signal quality.
- To investigate the influence of IAM-C/IAM-R preambles on the amplitude of Flip-FBMC data packet and illumination conditions when a commercial LED is employed.
- To analyse the role of using Flip-FBMC in avoiding the interference outside the first order zone, compared to the addition of different DC bias levels with DCO-FBMC scheme.

- To propose a theoretical analysis of a novel Flip-FBMC based on frame repetition model and its performance over a realistic transmission scenario.
- To analyse the influence of impulse/frequency response of different filter profiles and their roles to avoid the clipping distortion, compared to other optical multicarrier schemes.

1.4. Thesis structure

The structure of this manuscript is based on six chapters as follows.

Chapter 2 is dedicated to the description of general components in VLC systems. We review the main drawbacks of 4G-5G modulation formats that are commonly employed in indoor VLC systems. Besides, the limited modulation bandwidth and the non-linear characteristics of LED are also addressed. The future challenges and limitations for indoor OWC systems are introduced in this chapter. The potential use and vision of VLC for a 6G technological platform is also described together with the main market players with VLC products.

Chapter 3 exhibits the enabling architectures and technologies for future modulation waveforms, i.e. FBMC-OQAM scheme-based transmultiplexer model, compared to other waveform candidates, and as a potential-alternative technique to OFDM format that drains its spectral efficiency by using extra CP and guard band samples. This chapter also includes a brief introduction of the properties of most well-localized filters, also analyses the impact of residual interference in FBMC signals, and the role of deterministic preamble sequence in minimizing such effects.

Chapter 4 presents a novel Flip-FBMC scheme based on a biorthogonal format for an indoor VLC system. Besides, a tail-shortening algorithm is proposed to reduce the system penalty in throughput rate and system latency, while such algorithm is investigated over several prototype filters of different lengths. Moreover, his chapter presents the role of using Flip-FBMC system to avoid the induced interference outside the first tap zone, compared with DCO-FBMC signals. This chapter includes the evaluation of multitap equalization to mitigate the impact of intrinsic interference over a multipath link with high delays profile.

Chapter 5 describes the impact of confining high power at the first order zone on the noise floor level, the time-frequency localization property, and amplitudes of pseudo pilots with IAM preamble that are controlled by tuning spreading factor in extended gaussian function. Moreover, it includes the main downsides of employing the deterministic preamble sequence over a restricted operation range of LED and dimming control issue and the first theoretical analysis of the impact of the clipping ratios on the imaginary interference outside the 1-tap neighbourhood blocks is also presented. Furthermore, we analyse the role of the prototype filter profile based on Flip-FBMC/frame repletion model in minimizing the clipping distortion and enhancing the dimming challenge, compared to Flip-FBMC system with IAM sequence. Also, this chapter includes the simulation results of throughput rate, hardware complexity and the comparison performance between the proposed system, Flip-FBMC/IAM and Flip-CP-OFDM schemes over different types of propagation indoor links and constellation orders.

Finally, chapter 6 summarizes the major contributions of thesis and some possible steps for future research.

Chapter 2. Fundamentals of indoor optical wireless communication systems

"No amount of experimentation can ever prove me right; a single experiment can prove me wrong."

– Albert Einstein

This chapter provides a general overview of the concept of indoor visible light communication systems. Comparison between optical wireless and RF systems is highlighted to confirm the value of VLC in next generation applications. It also shows the main structure of visible light communication systems structure, including transmitter/receiver components and optical wireless link configurations. Moreover, this chapter outlines the design challenges of indoor optical wireless communication and the most common signal modulation techniques based on OFDM modulation. Furthermore, the importance value of visible light communication in next generation network is highlighted and the possibility to provide a short connectivity reaching the Tbps range by 2027. This chapter also includes the potential use and vision of VLC for a 6G platform, and the main market players with VLC products.

2.1. Evolution of visible Light communication systems

The motivation behind visible light communication systems raised from the fast replacement of classical lights, i.e. fluorescent and incandescent bulbs, by the energy efficiency of LEDs, which can be directly modulated at a rate much faster than the response time of the human eye. The VLC technology exploits optical wireless communications to transmit high data rate over unlicensed electromagnetic spectrum with 375 nm to 780 nm wavelength. Such technology has

emerged to cope with the RF-spectrum crunch up to 300 GHz since VLC spectrum bandwidth is larger than RF spectrum by more than 1000 times, and serves as an alternative technique for communication and illumination requirements and applications.

Compared to RF principle, the VLC-key idea is simple since the input data modulates the intensity of the LED. A photosensitive element at the receiver side extracts the information from the fluctuation of light intensity for the sake of satisfying the fundamental objectives of illumination and communication simultaneously for various VLC applications. From such perspective, the implementation cost of the transmission link is notably minimized. Additionally, compared with the considerable crosstalk interference of RF signals, the propagation of visible light is not interfered by electromagnetic waves. Thereby, VLC delivers unique advantages over scenarios that are sensitive to electromagnetic interference, i.e. airports, underground mines hospitals and nuclear power plants.

Over the past decades, according to the framework of cities and industries communication, the information rate using VLC technique has risen from a few Mbps to several tens of Gbps, by using multicarrier modulation techniques providing high data rates, and making it as a promising candidate for future applications based optical wireless communication, i.e. Internet of things services, underwater communication, indoor localization, vehicle to traffic light/vehicle communication and optical camera communication [31]-[32].

2.2. Architecture of visible light communication systems

In order to transmit the input message, LEDs are employed to modulate the light intensity, while the corresponding photodetectors PDs, at the receiver node, are in charge of direct detection and converting the detected light back into the information stream.

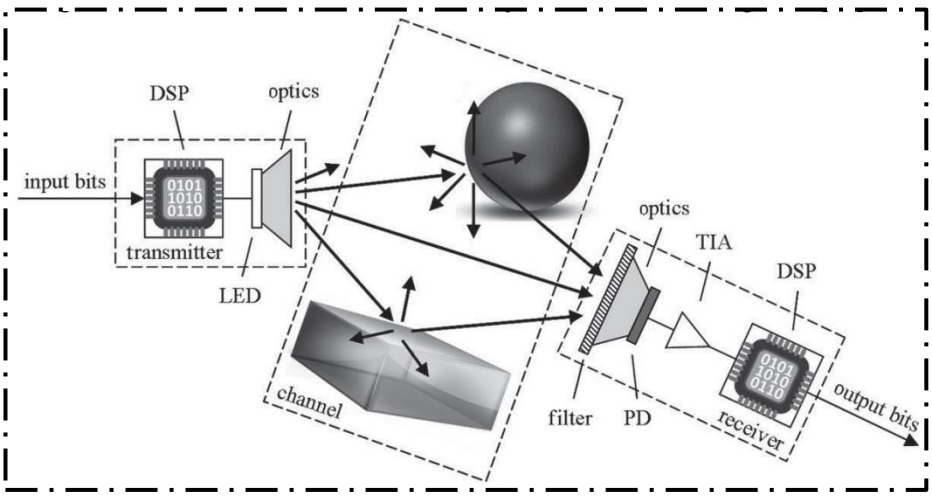

Figure 2.1. VLC architecture [33].

A filter at the inception of photosensor can be utilized to minimize the interference as a result of ambient light. Moreover, a front-end amplifier is required to minimize the noise and interference from the detected signal, as shown in Figure 2.1. Consequently, for practical VLC transmitter, by using digital-to-analog (D/A) convertor, the data-bits are modulated and converted to an electrical signal, which is uploaded to LED to modulate the light intensity.

Since LED is classified as a non-coherent source and to ensure the modulating signal in positive signal form, a direct current is usually added. At the receiver, the resulted photo-current form is generated by the means of Photodetector (PD), followed by pre-amplification stage with a Trans-Impedance Amplifier (TIA) circuit, and sampled by A/D convertor.

2.3. LED-based transmitters in VLC systems

An LED is a semiconductor PN junction (Consists of N-type and P-type materials) that releases energy in the shape of photons when fed with an electrical current. LEDs have tremendous advantages over other artificial lighting sources (fluorescent lamps and incandescent bulbs), i.e. lifetime, energy efficiency and compact size. Due to its fast response, LEDs can be employed for illuminating and communicating purposes simultaneously. For general illumination, white light is considered one of the most desirable colors among several produced colors by LED in the visible region.

An LED emits the white light as a result of the combination of phosphors with blue/UV LED emission or by mixture different colors of that LED. There are several sorts of white LEDs, but the significant ones are: Phosphor Converted LEDs (pc-LEDs), red-green-Blue (RGB) LEDs (multi-chip LEDs), micro-LEDs and Organic LEDs (OLEDs). However, the latter is still inefficient in terms of durability and frequency compared to other LED types [34]. Although, the high-speed transmission demand of 6G network is mainly restricted with the nonlinearity and bandwidth emitter source, research groups have focused on proposing novel wide-bandwidth light sources, such as OLEDs and micro-LEDs, to be served in next generation OWC platform [35]-[36].

Due to the limited modulation bandwidth of several MHz in typical white LEDs, the modulation characteristics of LED are required to be investigated before application in real time transmission. Hence, the LED frequency response is calculated according to its parasitic capacitance and carrier lifetime. Moreover, the nonlinear characteristic of LEDs is considered as the most important factor that should be taken into account in practical scenarios to avoid the degradation in signal quality. Moreover, as presented in Figure 2.2, the turn-on voltage (TOV) as the lower limit, and cut-off region (upper limit) of restricted dynamic range of LED represents a crucial aspect in determining the clipped signal outside the operation range of used LED. To avoid the overheating issue, the upper limit of saturation voltage is determined by the manufacturer. The TOV refers to the minimum driving voltage, where the LED status is cut-off below this point (a saturation region where LED is not conducting current) [34] and [36]. Notably, for the sake of evaluating the clipping distortion as a result of avoiding the nonlinearity impact, the permissible difference between the maximum/minimum voltage of a commercially available LED in [27] is considered in section 5.4.

Since only unipolar real signal can be employed in VLC system, the intensity modulation and direct detection (IM/DD) should be provided, since the phase/frequency of conveyed signal cannot be acknowledged as the non-coherent nature of used photoreactor. Hence, the instantaneous electrical current provided by the photodetector, i.e. the baseband-received signal, is denoted by $r(t)$ and can be expressed as:

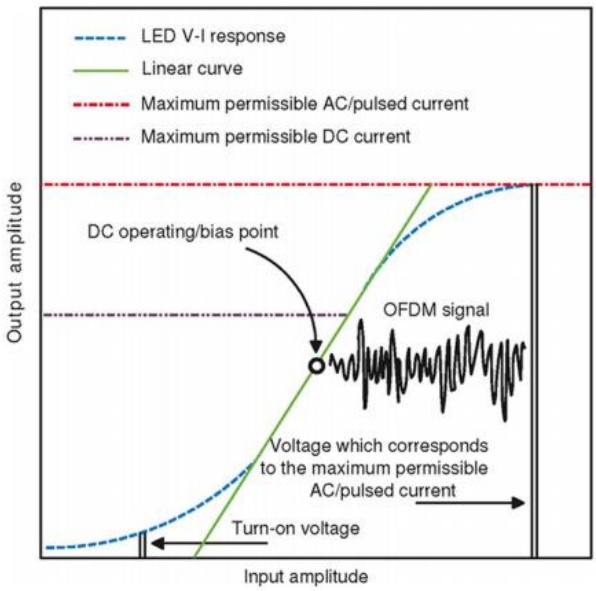

Figure 2.2. Nonlinear and linearized LED transfer characteristic [36].

$$r(t) = G \times RS \times X(t) \otimes h(t) + z(t) \tag{2.1}$$

where *z(t)* term is an Additive white Gaussian noise (AWGN) with variance of σ_n^2, the term RS refers to the responsivity of used photodetector and $X(t)$ is referred as the instantaneous optical power of LED.

From this perspective, a summary of several VLC-high throughput rate systems can be observed in Table 2.1, where in such investigation the high transmission rate is achieved based on OFDM technique. It is noteworthy mentioning that the characteristics of maximum bandwidth for white LED (CRE EXML2) in [21] is adopted for the sake of calculating the maximum throughput rate in section 4.8 of this Thesis. Besides, a positive intrinsic negative (PIN) diode or avalanche photodetector (APD) is considered as the mainstream optical receiver source, where a higher gain is reported with APDs. Although, the typical excessive noise in APDs can be overcome by biasing the APD above its breakdown voltage. While a low cost and the ideal response when a PD is flooded with high intensity light are the main features of PIN PD.

The use of Micro and organic LEDs is seen to support the Gbps throughput rate in next optical generation requirements. Micro-LEDs are considered the ideal light sources for various applications of high-speed VLC, due to the low self-heating and capacitance. Besides, the resulted optimum current dispersion, higher modulation bandwidths and shorter carrier lifetimes. On the other hand, the organic LED has gained a lot of attention due to the low cost and flexible manufactured structure. Besides, although such emitter is characterized with high-speed transmission of Gbps rate, the high capacitance is considered as the main downside in such LED [34]. Moreover, recently in [37], Micro-LEDs have emerged as next generation display technology because of their superior ability to withstand moisture and provide ultrahigh luminance, and long lifespan compared to OLED displays and liquid crystal displays, thereby, Micro-LED can be considered as a suitable emitter source for the 6G requirements.

From such perspective, Table 2.1 summarizes the maximum throughput rate by using different high-speed micro-LED in recent VLC studies.

Table 2.1. Research progress summary of employing Micro-LEDs with OFDM modulation format for VLC systems.

YEAR	Light source	Throughput Rate
2024 [38]	60 Micrometer-Blue Micro-LED	8.649 Gbps
2023 [39]	Semipolar blue/green Micro-LED	3.495/3.483 Gbps
2022 [40]	Ultravioleta Micro-LED	6.94 Gbps
2021 [41]	Semipolar green Micro-LED	4.343 Gbps
2017 [42]	violate Micro-LED	7.91 Gbps
2016 [43]	Blue Micro-LED	5.0 Gbps
2014 [44]	blue Micro-LED	1.68 Gbps

As presented in the academic research list, the different throughput rates rely on the applied distance, number of LEDs, pre- and/or post-equalization technique, multiplexing and type of receiver.

2.4. Optical receivers in VLC systems

In the VLC system, the primary noises associated with photodetector are the thermal noise (Johnson noise) and the quantum noise current (shot noise) induced by the arbitrary fluctuation of photons. Such haphazardness can be processed as a Poisson model, while the Gaussian distribution is resulted at the high number of photons in the induced photocurrent. In such scenario, a negligible impact of primary photons is resulted, thereby, the shot noise degree is small and cannot recognized from Gaussian distribution. Hence, the low impact of shot noise can modeled as AWGN with a variance of [45]:

$$\sigma_{\text{shot}}^2 = 2I_{\text{bg}}\ q_e\ I_2\ \text{BW} \tag{2.2}$$

The I_{bg} term denotes the background current as a result of the ambient light, where the noise bandwidth (BW) term is 0.562 $\left(I_2 = 0.562\right)$, and q_e term is the charge of electron.

The noise-tolerant in the received signal can be captured by choosing the TIA with high ability of noise rejection. Since the thermal noise is generated because of the random motion of electrons with load resistance in the TIA circuit, a model of field-effect transistor (FET) based TIA is assumed according to the low noise compared to the TIA based on a bipolar-junction transistor (BJT) type. The variance of thermal noise, which can be modeled as AWGN, is determined as [45]-[46]:

$$\sigma_{\text{Thermal}}^2 = \frac{8\pi K_{\text{B}} T_{\text{K}}}{G_{\text{TIA}}}\ Ca_{\text{PD}}\ A_{\text{PD}} I_2\ BW^2 + \frac{16\pi^2 K_{\text{B}} T_{\text{K}}}{g_{\text{FET}}}\ Ca^2{}_{\text{PD}}\ A^2{}_{\text{PD}}\ I_3 BW^3 \tag{2.3}$$

and the total variance noise can be represented as:

$$\sigma_n^2 = \sigma_{\text{Thermal}}^2 + \sigma_{\text{Shot}}^2 \tag{2.4}$$

where K_{B} term is referred to the Boltzmann constant, the PD-detection area is represented by A_{PD} term, the Ca_{PD} represents the PD-capacitance, where the absolute temperature is

represented by T_{K} term, and $I_3 = 0.0868$, while the transconductance of the FET is symbolized by g_{FET} and G_{TIA} refers to the open loop voltage gain.

According to [47], in the presence of optical background noise that generated with AC driven LED or fluorescent light, the impact of shot and thermal noises can be neglected in bit-error-rate (BER) calculation.

2.5. Types of propagation links

As shown in Figure 2.3, each propagation of Line of sight (LOS) and non-LOS determines whether the transmitter and receiver have an unobstructed vision to each other, which can be classified into three scenarios: directed, non-directed and Hybrid propagation scenarios, which is expressed according to the degree of directionality and barriers between the sender and receiver.

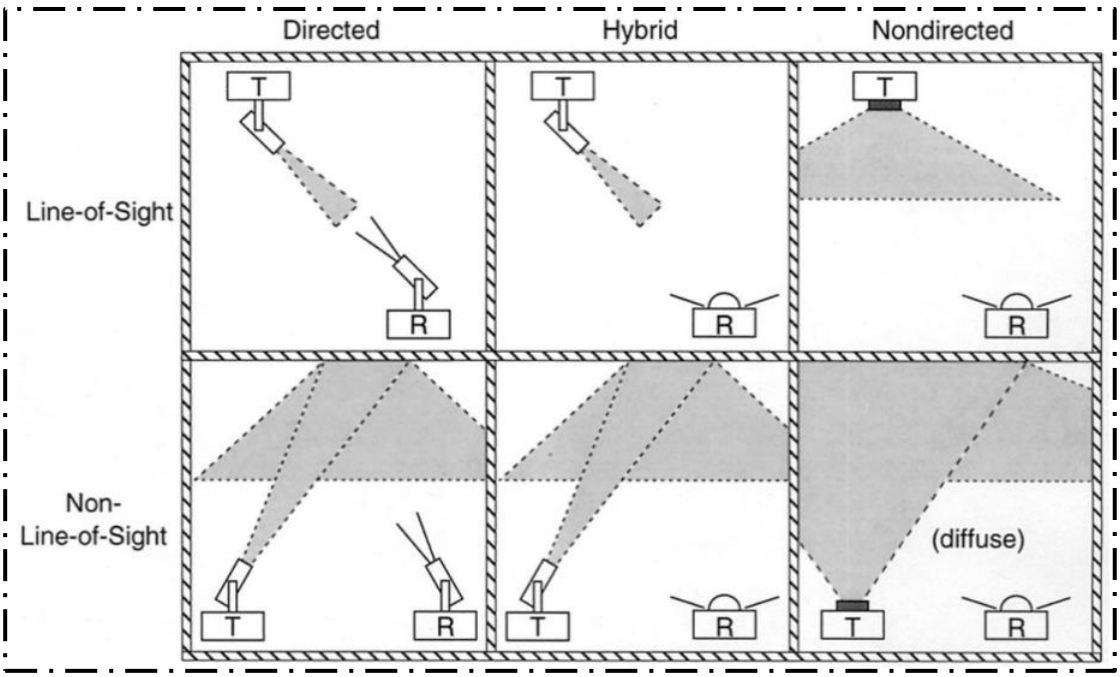

Figure 2.3. Configuration types of VLC-links [48].

According to the LOS link, the PD-received optical power can be calculated as:

$$p_r = h_{\mathrm{LOS}} \underbrace{\lim_{T\to\infty} \frac{1}{2T} \int_{-T}^{T} X(t)\, dt}_{p_t} \tag{2.5}$$

where the p_t term is referred to the LED transmitter power, and the channel DC gain h_{LOS} can be given as:

$$h_{Los} = \begin{cases} \dfrac{(Q+1)A_{\mathrm{PD}}}{2\pi d^2} \cos^Q(\theta) T_S(\Psi) g(\Psi) \cos(\Psi) & 0 \le \Psi \le \Psi_C \\ 0, & \text{elsewhere} \end{cases} \tag{2.6}$$

where Ψ is the incident angle, θ is the irradiance angle and Ψ_C is the receiver field of view (FOV). The $T_S(\Psi)$ term is the gain of the optical filter, and *d* represents the distance between LED and PD. The Q parameter describes the order of Lambertian emission with a semi-angle at half power $\phi_{1/2}$ that can be computed according to [48]-[50]:

$$Q = -\frac{\ln(2)}{\ln\left(\cos\phi_{1/2}\right)} \tag{2.7}$$

and *g(Ψ)* is the gain for the optical concentrator of the PD that can be given as:

$$g(\Psi) = \begin{cases} \dfrac{n_r}{\sin^2 \Psi_C} & 0 \le \Psi \le \Psi_C \\ 0, & \text{elsewhere} \end{cases} \tag{2.8}$$

where n_r is the refractive index. For the non-LOS scenario, the DC channel gain is computed by:

$$h_{\text{Non\_LOS}} = \begin{cases} \dfrac{(Q+1)A_{\text{PD}}}{2\pi D_1 D_2} \cos(\varnothing)\ \cos(\hat{\lambda})\ dA_{wall}\ \cos^Q(\theta)\ T_S(\Psi)\ g(\Psi)\ \cos(\Psi) & 0 \le \Psi \le \Psi_C \\ 0, & \text{elsewhere} \end{cases} \tag{2.9}$$

And the total received power can be given as:

$$p_r = p_t\ H_{\text{LOS}} + \int_{\text{wall}} p_t H_{\text{Non\_LOS}} \tag{2.10}$$

where $\hat{\lambda}$ is the angle of irradiance to the wall, and the angle of irradiance from the reflective area of the wall is denoted by $\varnothing$. The term D_1 represents the distance between the transmitter and the wall, while D_2 is the distance between the wall and PD surface.

The propagation links of multipath scenario take place due to reflections off surrounding environments. The received data-information consists of weighted and delayed copies of the conveyed message since the original signal is propagated over several links of different lengths. Thereby, the received optical signal is stretched in time yielding in the so-called temporal dispersion. According to its channel impulse response, the mean excess delay μ_τ can be computed as [52]- [53]:

$$\mu_\tau = \frac{\sum_i t_i\ h^2{}_i(t)}{\sum_i h^2{}_i(t)} \tag{2.11}$$

where *t* is the propagation time, then the RMS delay spread D_{RMS} can be expressed according to [52]-[53]:

$$D_{\text{RMS}} = \sqrt{\frac{\sum_i \left(t-\mu_\tau\right)^2 t_i\ h^2{}_i(t)dt}{\sum_i h^2{}_i(t)dt}} \tag{2.12}$$

2.6. Modulation schemes for VLC signals

Apart from optimizing LEDs with novel structures and mechanisms, the fundamental downside of the limited linear operation range of commercially available LED can impede the research avenue toward B5G and 6G transmission rate requirement. Nevertheless, high-speed VLC systems can be supported by using advanced modulation techniques [54] so the most widespread modulation schemes are revised in this section.

The earliest modulation scheme in a communication system is referred to On-OFF Keying (OOK) technique, which transmits bit 1 and bit 0 by tuning the LED on and off, respectively, to modulate the input data. Fujimoto *et al.* exploited a single blue LED to achieve 662 Mbps with the use of OOK with non-return to zero (NRZ) modulation [55]. Another low cost 1-dimentional multilevel modulation is PAM technique, where the input message is modulated according to the signal amplitude, which has an efficient bandwidth usage compared with OOK. Over a free space transmission link of 0.6 m, 2 Gbps is obtained based on 4-PAM modulation [56]. Although the in-phase and quadrature channels cannot be fully exploited in one-dimension techniques, an amplitude and phase modulation (CAP) modulation scheme can overcome such impairment. CAP technique consists of two orthogonal finite impulse response (FIR) digital filters to separate the data streams, followed by adding a DC bias value to provide the unipolar signalling, thereby, a simple implementation is obtained without the necessity to inverse FFT (IFFT)/FFT processing blocks.

The major aspect with the use of CAP modulation is the low peak-to-average power ratio (PAPR) with respect to optical OFDM scheme [57]. Thus, the conveyed signals based on CAP modulation is less susceptible to nonlinear impairments induced by modulating the LED with signals of high amplitudes. Consequently, CAP modulation scheme has been attracted much of attention in VLC systems, i.e. the aggregate data rates of 1.32 Gbps is enhanced to 3.22 Gbps by the aid of the wavelength-division-multiplexing (WDM) [58]. Nevertheless, the main downside of CAP modulation format is the sensitivity to non-ideal spectral channels, which leads to a severe degradation in system performance, and it is susceptible to timing jitter. Thereby, complex equalizers are required to minimize the induced cross-channel interference and ISI influence [59].

Alternatively, OFDM is an attractive multiple subcarrier modulation format that has extensively been used in optical wireless and RF systems. The concept idea of OFDM is that one single high data-rate stream is divided into several streams of lower data-rate, which are transmitted in parallel on different sub-carriers. Thereby, the period of each sub-carrier is higher than that of the equivalent single-carrier system. Besides, guard-interval of CPs is inserted to supress the ICI effect while a simple channel equalization is employed at the receiver.

Due to the above features and to overcome the LED-limited modulation bandwidth, OFDM modulation scheme have widely been employed in indoor optical signals. Before the intensity modulation of the LED, the data signal must be positive and real format. Therefore, several optical techniques have been proposed to guarantee the OFDM signal in real and unipolar format such as: DC-offset OFDM (DCO-OFDM), asymmetric clipped optical OFDM (ACO-OFDM) and Flip-OFDM [60].

2.6.1. DCO-OFDM system

The DCO-OFDM processing blocks are presented in Figure 2.4, the input data message is mapped onto a complex value by employing M-ary QAM modulation. Then, the input-complex mapped onto a vector of *X*, which is imposed to have a condition of Hermitian symmetry, can be expressed as below:

$$X = [X(0) \underbrace{X(1)...X\left(M/2-1\right)}_{\text{Original Values}} X\left(M/2\right) \underbrace{X^*\left(M/2-1\right)...X^*(1)\ X^*(0)}_{\text{Hermitian Symmetry}}] \tag{2.13}$$

where

$$X_0 = X_{M/2} = 0 \tag{2.14}$$

The * term represents the complex conjugate. The first (DC) and M/2 subcarriers are set to zero in order to achieve a real bipolar signal. Due to the Hermitian condition, the 50% of spectral efficiency is lost as only (M/2-1) is modulated, and the resulting signal is fed to M-points IFFT to produce the bipolar-real time signal. The OFDM signal at k^{th} time instant at the output of IFFT processing block can be written as [60]-[61]:

$$x_k = \frac{1}{M}\sum_{m=0}^{M-1} X_m \exp\left(\frac{j2\pi mk}{M}\right) \tag{2.15}$$

As a results of the central limit theorem, the non-distorted signal x_k follows a Gaussian distribution of zero mean and a variance σ^2 [61]:

$$p_x(x) = \left(x;0,\sigma^2\right) = \frac{1}{\sqrt{2\pi}\ \sigma}\ \exp\left\{-\frac{x^2}{2\sigma^2}\right\} \tag{2.16}$$

Then, a guard band of CPs is added to the beginning of each transmitted OFDM-block. Following by D/A processing block, which is converted to an electrical current signal. To achieve a non-negative signal form (unipolar format), a suitable addition of DC bias β_{DC} value is required, which is set to the relative the standard deviation of $x(t)$ [60]:

$$\beta_{DC} = \varepsilon\sqrt{E\left\{x^2(t)\right\}} \tag{2.17}$$

where ε term refers to the proportionality constant, and the level of β_{DC} is defined as a bias of $10\log_{10}\left(\varepsilon^2+1\right)$ dB.

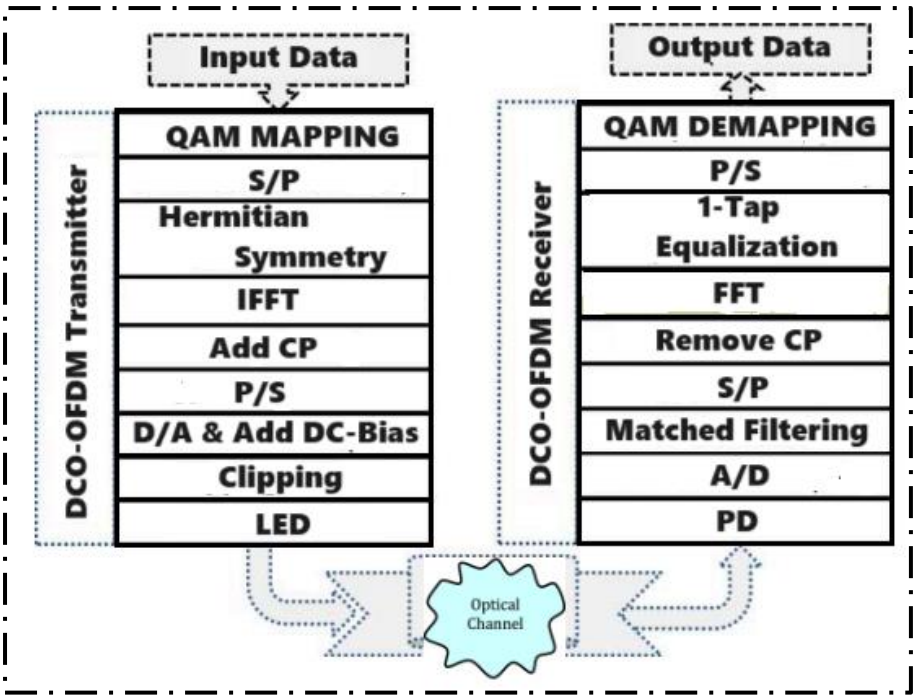

Figure 2.4. Implementation blocks of DCO-OFDM system

Afterwards, to generate an optical signal that is employed to drive the LED, the required clipping of signal amplitude, which goes beyond the linear restricted dynamic range of LED (upper and lower limits), is performed as [60]-[62]:

$$x_{Clip} = \begin{cases} \kappa\sqrt{E\left\{x^2(t)\right\}}, & x(t) > \kappa\sqrt{E\left\{x^2(t)\right\}} \\ x(t), & -\kappa\sqrt{E\left\{x^2(t)\right\}} \le x(t) \le \kappa\sqrt{E\left\{x^2(t)\right\}} \\ -\kappa\sqrt{E\left\{x^2(t)\right\}}, & x(t) > \kappa\sqrt{E\left\{x^2(t)\right\}} \end{cases} \tag{2.18}$$

Moreover, the spectral efficiency of DCO-OFDM for M $\text{IFFT}_{\text{size}}$ can be expressed as:

$$\eta_{\text{DCO-OFDM}} = \frac{\log_2(M)\left(\text{IFFT}_{\text{size}} - 2\right)}{2\left(M + M_{\text{CP}}\right)} \text{ bits/s/Hz} \tag{2.19}$$

Where M_{CP} refers to the sample size of cyclic prefix. Although such system is easy to implement, the main drawback of DCO-OFDM modulation technique is a waste of optical power, since extra DC bias is used to obtain the unipolar form. Besides, a significant clipping noise is resulted when a low β_{DC} level is employed [62].

2.6.2. ACO-OFDM signals

To avoid the penalty of insufficient power for DCO-OFDM signals, ACO-OFDM system is considered as shown in Figure 2.5. In ACO-OFDM, DC bias is not required to obtain the unipolar format since an anti-symmetric property of time-domain symbols is resulting at the output of IFFT block, where the only odd subcarriers are modulated. The input information to the IFFT processing block is given as [63]:

$$X = [0, X(0),\ 0, X(1) \ldots X\left(M/2-1\right),\ 0,\ X^{*}\left(M/2-1\right),\ 0, \ldots X^{*}(0)] \tag{2.20}$$

From equation (2.20), the even frequency subcarriers are clipped to zero, where a free-information lost is reported, to achieve the positive unipolar signal, as shown below [62]:

$$x_{ACO-OFDM} = \begin{cases} x(k), & x(k) > 0 \\ 0, & x(k) \le 0 \end{cases} \tag{2.21}$$

Although ACO-OFDM modulation format offers high optical power efficiency compared to DCO-OFDM system, only M/4 subcarriers are used to carry a useful information. Consequently, ACO-OFDM is spectrally less efficient than DCO-OFDM by 50%, as expressed below [64]-[66]:

$$\eta_{\text{ACO-OFDM}} = \frac{\log_2(M)\left(\text{IFFT}_{\text{size}}\right)}{4\left(M + M_{CP}\right)} \quad \text{bits/s/Hz} \tag{2.22}$$

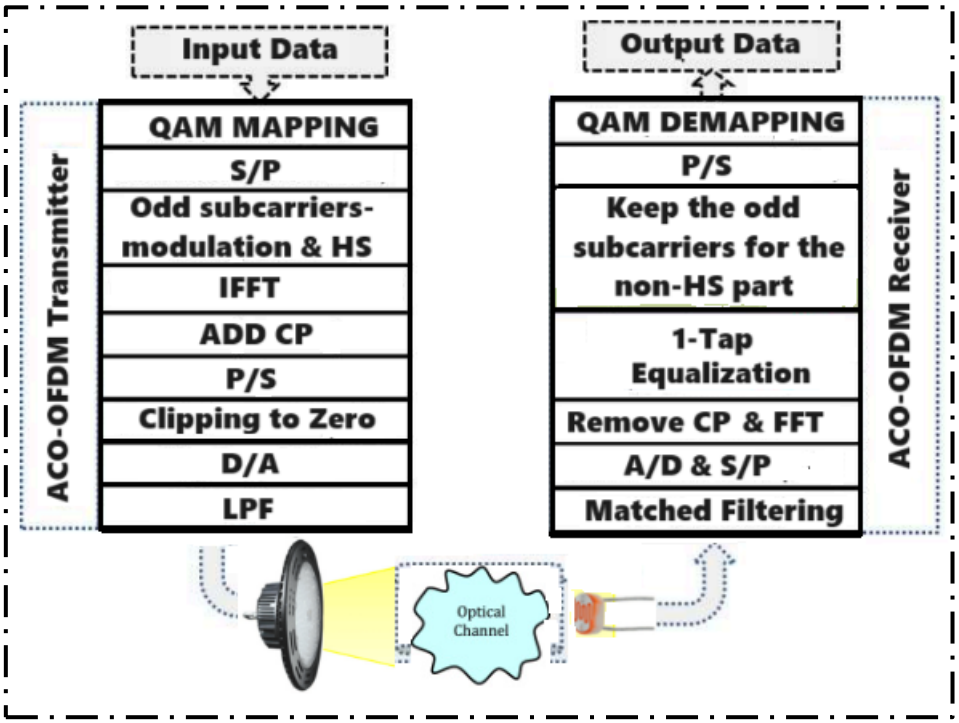

Figure 2.5. Implementation blocks of ACO-OFDM system

2.6.3. Unipolar Flip-OFDM scheme

The block diagram of Flip-OFDM system is exhibited in Figure 2.6. Let X_n term be the conveyed QAM message, where the OFDM signal at k^{th} time instant at the output of IFFT processing block is given by [67]

$$x_k = \frac{1}{N}\sum_{n=0}^{N-1} X_n \exp\left(\frac{j2\pi nk}{N}\right) \tag{2.23}$$

Like DCO-OFDM, the condition of Hermitian symmetry is imposed of the input-complex QAM ($X_0 = X_{N/2} = 0$), and ($X_n = X^{*}_{N-n}$) where n = 0, 1, …, N/2-1. Thereby, the bipolar real time-domain signal at the IFFT-output can be rewritten as [68]:

$$x_k = X_0 + \sum_{n=1}^{N/2-1} X_n \exp\left(\frac{j2\pi nk}{N}\right) + X_{N/2}\exp\left(j\pi k\right) + \sum_{n=N/2+1}^{N-1} X^*_{N-n} \exp\left(\frac{j2\pi nk}{N}\right) \tag{2.24}$$

Afterwards, the unipolar data-information is achieved by splitting the original bipolar signal into positive and negative successive subframes using the flipping technique, as expressed in the equation below:

$$x(k) = x^+(k) + x^-(k) \tag{2.25}$$

where

$$x^+(k) = \begin{cases} x(k), & x(k) \geq 0 \\ 0, & \text{otherwise} \end{cases}$$

$$x^-(k) = \begin{cases} x(k), & x(k) < 0 \\ 0, & \text{otherwise} \end{cases} \tag{2.26}$$

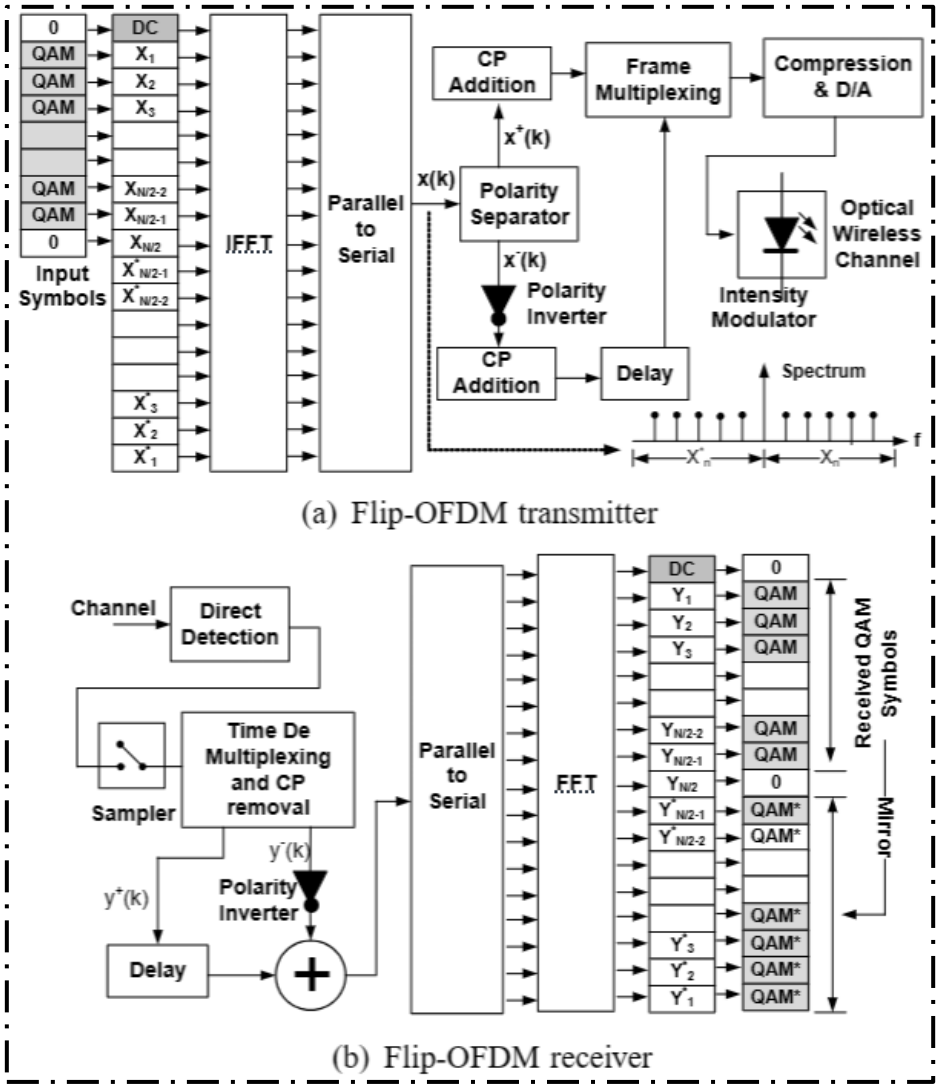

Figure 2.6. Implementation blocks of transmitter and receiver Flip-OFDM system [69]

As presented in Figure 2.6, the cyclic prefix samples are added to each OFDM subframe, which are removed at the reconstruction and detection process of bipolar subframes:

$$y(k) = \underbrace{y_1(k)}_{\text{received positive subframe}} - \underbrace{y_2(k)}_{\text{received negative subframe}} \tag{2.27}$$

The equivalent signal to noise ratio SNR can be expressed according to [69]:

$$SNR = \frac{E[x_t^2(k)]}{2\sigma_n^2} \tag{2.28}$$

where the $E[x_t^2(k)]$ term denotes the total transmitted Flip-OFDM energy. Flip-OFDM signal has identical error performance, and 50% less of the computational complexity, compared to ACO-OFDM system, as expressed below:

Table 2.2. Complexity comparison between ACO-OFDM and Flip-OFDM systems

	ACO-OFDM	**Flip-OFDM**
Transmitter	$2\left(\frac{IFFT_{size}}{2}\right)log\left(\frac{IFFT_{size}}{2}\right)$	$IFFT_{size}\ log(IFFT_{size})$
Receiver	$2IFFT_{size}\ log\left(IFFT_{size}\right)$	$IFFT_{size}\ log(IFFT_{size})$

Although Flip-OFDM and ACO-OFDM schemes show 50% of bandwidth penalty compared to DCO-OFDM system, the loss in their spectral efficiency can be avoided using multilayers (depth-streams) technique (layered ACO-OFDM [70 and Layered Flip-OFDM [71]).

The η of layered Flip-OFDM is the sum of spectral efficiencies of the data-information at the chosen modulation depth:

$$\eta_{\text{layered Flip-OFDM}} = \eta_{\text{Flip-OFDM}} \sum_{d=1}^{\text{Dep}} \frac{1}{2^d - 1} \tag{2.29}$$

where the Dep term represents maximum modulation depth. The η of layered Flip-OFDM can achieve 98.6% of the DCO-OFDM spectral efficiency by using a maximum modulation depth of 5.

However, the main implication of transmitting multiple layers for optical bursts simultaneously is that requires iterative decoding and high computational loads [72].

2.7. VLC vision in next generation optical wireless communications

Classical RF solutions cannot satisfy the traffic capacity growing requirements. Hence, as a consequence of the scarcity of frequencies, the new technologies required to developed for the sake of supporting the next generation of wireless communications demands.

One strategy to maintain high service quality is 5G technology. A broad bandwidth, or a frequency range spanning the low band (less than 1 GHz), the medium band (1-6 GHz), and the high or mmWave band (above 6 GHz), is needed for 5G to enable downlink data speeds of up to 1 Gbps. However, the weakness of this technology is the high cost of infrastructure

development. The backhaul and licensing processes for 5G small-cell technology, for instance, are very expensive. Furthermore, 5G technology is not likely to be able to handle the growing volume of traffic and applications that demand extremely high data rates.

It is anticipated that 6G will appear in 2025 if mobile wireless technology keeps developing in this manner. The purpose of the new technology is to address 5G's technological shortcomings. More than 5G, 6G is anticipated to be able to guarantee flawless use, especially when handling rapid increases in traffic and the effectiveness of indoor network performance. Meanwhile, researchers have started looking at the possible use of radio communications over the Terahertz spectrum, with VLC being the main technology utilized on it, in an attempt to build a new technological platform for 6G.

The VLC system is one of the more promising technologies to meet the demands of 6G. In particular, VLC's unique operating characteristics, such as its capacity to support Tbps order data rates (because large amounts of unregulated spectrum are available), inherent security, high positioning accuracy, and support for environmentally friendly and sustainable communication, can play a pivotal role in enabling 6G [35]. Moreover, from such perspective, VLC system can be considered as a complementary potential technology to be employed in certain applications of 6G platform, where the THz and mmWave cannot be supported or may be inefficient. Moreover, as an example, in eHealth applications, unwanted electromagnetic interference can be induced with THz wave, and the connection continuity is not guaranteed with mmWave.

According to KPI Research, the 6G system combines 5G and satellite networks, utilizing satellite telecommunication for data, internet, audio, video, earth imaging, navigation, and global positioning system (GPS). Research indicates that the core architecture of 6G facilitates advanced access-backhaul integration, disaggregation, a 3D network architecture, a smooth handover and multiple-frequency integration, and energy savings. It also virtualizes networking equipment from the physical layer to the network function virtualization (NFV).

Table 2.3 provides a comparison of 5G and 6G technology along with key performance indicators for 6G. Variations in data rate with respect to operational frequency are among the technical parameters. It is evident that downlink data rates should exceed 1 Tbps. Less than 0.1 milliseconds of latency make it appropriate for any crucial application, including vehicle-to-vehicle services, and the autonomous systems such as robotics that need for higher reliability [73]-[76].

Table 2.3. A comparison of 5G and 6G KPIs

KPI-Technical parametrs	5G	6G
Technology used	VLC or RF	Hybrid RF/VLC
Peck data rate	20 Gb/s	> Tb/s
Latency	Low	Ultra low
Operating frequency range	Up to 300 GHz	THz range
Jitter	NS	NS
Modulation waveform	OFDM/CAP	FBMC
Leakage energy	High	Low
Reliability	99.9%	>99.999%
Satellite integration	No	Yes

Numerous academics have identified FBMC waveform as a possible 6G modulation since the OFDM system's mechanism has the ability to violate some of the aforementioned KPIs [76]-[77]. Some features that suggest that VLC could be used as a basis for 6G technology are as follows:

- Similar to the 5G platform, 6G is expected to include diverse networks, such as macrocells, metro cells, micro-cells, picocells, and femtocells for indoor spaces. In these situations, VLC can be used to support high-capacity data platforms in an indoor space. One example of merging pre-existing infrastructure networks is hybrid wireless fidelity (WiFi)-VLC. High capacity and high-quality physical experience will be obtained by WiFi-VLC in accordance with 6G use scenarios.
- The unlicensed VLC spectrum band, which creates a bandwidth range of roughly 360 THz, is depicted in Table 1.1 as an option for larger data rates. Ultimately, this large bandwidth will result in a high data rate, which is anticipated to be over 1 Tbps as given in Table 2.3. Furthermore, in terms of security, the physical layer of 6G technology security depends on offering a layer of protection. It is claimed that VLC offers greater security than alternative wireless protocols. The gadget that is exposed to light is the only area that VLC can cover. As a result, compared to RF technology, there is less chance of security flaws. Therefore, some examples of service applications suitable for VLC include intelligent transport system to minimize accidents, telemedicine applications, smart homes/cities and 6G indoor flying network [73] and [78], amongst others.

2.7.1. VLC market status

Based on the review made in [79]-[80], a comparison of VLC main market actors is summarized below.

Products related to VLC and light fidelity (Li-Fi) are already available, mainly in the Business-to-Business market but also with an increasing presence in the Business to Consumer market. Even though Li-Fi products are available to consumers, they are typically more expensive than RF alternatives. This section delves into a thorough examination of the products on the market, illuminating the possibilities of VLC technology, especially in smart cities and industrial settings.

Li-Fi product specialist pureLiFi is a prominent participant in the industry. Li-Fi devices with an infrared uplink channel and a visible-light downlink channel are part of their product line. After developing products that worked with cellphones and laptops, pureLiFi branched out at 2019's Mobile World Congress with the introduction of the Gigabit Li-Fi. Recently, in April 2021, the company launched Kitefin, a product designed to facilitate the large-scale deployment of Li-Fi.

Pioneering Li-Fi solutions have found early adopters in office spaces, homes, and educational institutions as a promising alternative to Wi-Fi. In 2016, Oledcomm made waves with its debut Li-Fi products, including a desk lamp that transmits broadband internet through visible light. Since then, their offerings have expanded, and they now champion "High-speed Internet through invisible light" as their tagline. Notably, their current Li-Fi products, marketed under the same name, utilize infrared for both data transmission and reception.

While an outdoor version of their newest product, LiFiMax equipment, is not yet available, indoor speeds of up to 100 Mbit/s are achievable. In May 2016, Philips Lighting NV adopted "Signify." Under the "Trulifi" brand, signify sells a variety of smart lights with sensors and controllable features, in addition to Li-Fi equipment, though this is not their only focus. White light panels with Li-Fi were their original offering, but now they're focusing on two-way infrared communication. Signify boasts an impressive net data rate of around 845 Mbit/s on their website,

although they did not provide specific details about the main areas of application for their projects.

Since 2007, the German research institute known as Fraunhofer IPMS (Institute for Photonic Microsystems) has focused on developing electronic and photonic microsystems. These systems have a wide range of potential applications, including in the health and industrial sectors.

In 2018, a notable addition to the Li-Fi catalogue was the "Li-Fi HotSpot Evaluation Kit," boasting the capacity to transmit bidirectionally at speeds up to 100 Mbit/s using infrared technology. Comprising two infrared emitter/receiver units facilitating communication in both directions, the kit features a master and a slave for effective point-to-multipoint communication. These devices maintain optimal performance within an indoor range spanning from 0.5 m to a maximum of 5 m. Remarkably, the current iteration of the product, available on their website, is upgraded to transmit at an impressive speed of 1 Gbit/s.

Another pioneer in the industry, Velmenni, began with visible-light solutions before moving on to ultra-fast infrared products. At this time, the business is offering specialized indoor connectivity devices, such as a Wi-Fi dongle and an access point. More than that, they've unveiled an outdoor solution they call "LC," though they haven't said whether it uses lasers or LEDs. The majority of VLC devices on the market today are designed for high-data-rate applications and primarily target Li-Fi with visible or infrared light.

There are now a plethora of companies offering these cutting-edge products all over the world. According to market research, there is a growing customer base for indoor Li-Fi products. Private companies and schools are particularly interested in these products. Figure 2.7 summarizes the performance of different brands in the field by providing an aesthetically appealing representation of the distance and throughput they offer. The recommended distances for VLC products usually fall between 3.5 and 5 meters.

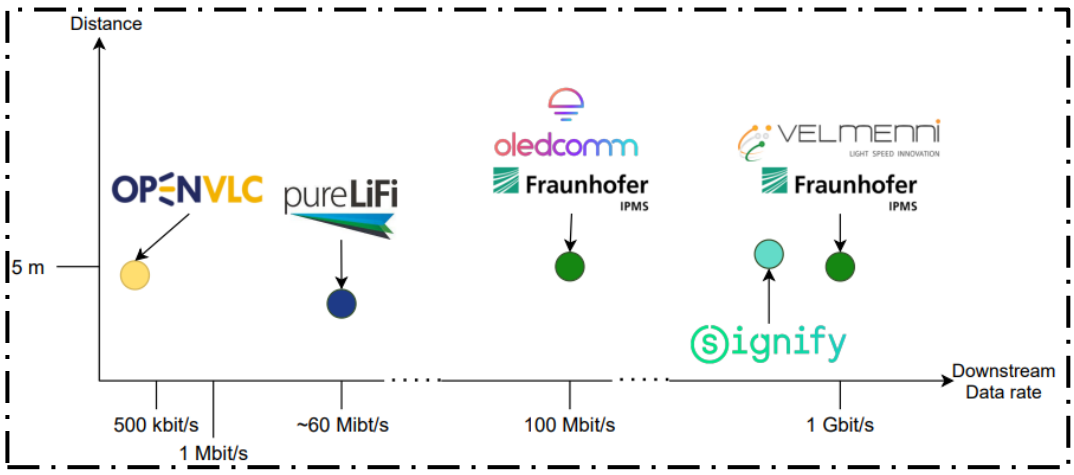

Figure 2.7. Comparison of the performance promised by several VLC/Li-Fi market players [79]

In recent years, significant experimental progress has been made by researchers from universities and private organizations worldwide, yielding practical laboratory findings. Here are some of the most important investigations:

Researchers at the University of Oxford achieved a transmission speed of 224 Gbps using a prototype of bidirectional Li-Fi. The Li-Fi covered a field of view of 60° and was divided into 6 aggregated links of 37.4 Gbps, with a range of about 3 meters. They achieved 112 Gbps using 3

links at 37.4 Gbps and covered a 36° field of view. This configuration is the first example of a wireless connection that can cover a room with a speed greater than 100Gbps and has routes for these networks. A group of German researchers conducted Li-Fi tests at Motol University Hospital in Prague, Czech Republic. The tests aimed to showcase the potential of Li-Fi in areas where Wi-Fi is not possible. The goal was to create a "smart hospital" by combining individual channels into a multi-user virtual multiple input multiple output (MIMO) link.

LVX System is a Florida-based company providing Li-Fi products and services in the US. This company collaborates with the US government through an agreement with NASA, developing applications for visible light communication. These advances may be used in future missions to Mars and also have the potential to improve the lives of Americans. Hyperion Technologies is a Turkish company specializing in optical wireless communication for next-generation wireless networks. The company played a significant role in the 802.15.7rl regulatory project and still provides assistance to the 802.11 regulatory group for light communication and the 802.15.13 for optical wireless communication [81].

2.7.2. Roadmap of VLC systems for 6G services

To attain optical-fiber equivalent capabilities, a potential complementary approach for the evolution of 6G networks involves harnessing the visible spectrum through VLC techniques, particularly for short-range links spanning the range of just a couple of meters. In contrast to conventionally utilized RF bands, VLC system presents unprecedented advantages, including ultra-high bandwidth in the THz range, absence of electromagnetic interference, access to free, unlicensed spectrum, and exceptional frequency reuse opportunities.

Presently, indoor VLC technology is constrained to a throughput ranging from several tens of Megabits per second (Mb/s) to one hundred (Mb/s) within a spectrum of approximately five meters. The lack of beamforming and the usage of commercial off-the-shelf (COTS) light fixtures cause this restriction. However, this constraint is anticipated to be overcome through the introduction of cutting-edge light sources utilizing microLED technology. These innovative components are poised to offer bandwidths exceeding 1 GHz, with laboratory achievements already reaching nearly 10 Gb/s on a single diode LED. From our perspective, VLC holds immense potential for enhancement over the next decade, bridging the existing performance gap between VLC and 5G technologies, which have already demonstrated Gigabit-per-second (Gbps) capabilities [82].

As we envision it, VLC technology is set to achieve Tbps performance when 6G services are introduced. We anticipate VLC providing short-range indoor connectivity at Tbps levels, with fully operational demonstrators achieving maturity by 2027. The inaugural milestone, set for 2019, concurrent with the introduction of 5G services, aims to showcase a robust short-range capability of 1 Gbps indoors.

This demonstration involves the deployment of thousands of LED active sources catering to both illumination and communication functions. However, a near-term challenge arises in efficiently managing these extensive matrices while preserving the high bandwidth. Addressing this challenge necessitates the integration of microLED matrices and Complementary Metal-Oxide Semiconductor (CMOS) driver arrays into a unified chip. Looking ahead to 2024, the aspiration is to achieve the proclaimed highest 5G link capacity of 20 Gbps. This entails the development of a more intricate device involving the parallelization of multiple chips mentioned above and the incorporation of a specialized imaging optical system.

This optical beamforming approach spatially separates users, significantly augmenting cellular throughput. As technology progresses towards 2026, with both microLED advancements and

spatial multiplexing techniques attaining maturity and cost-effectiveness, the utilization of white light based on diverse wavelengths becomes pivotal. WDM comes into play, unlocking the potential for ultra-high data rate VLC access points, with throughput potentially exceeding 100 Gb/s. By 2027, further advancements emerge with the massive parallelization of microLED arrays. This milestone positions the aggregated throughput target at Tbps, marking a culmination of technological progress in VLC, microLED, and spatial multiplexing [82].

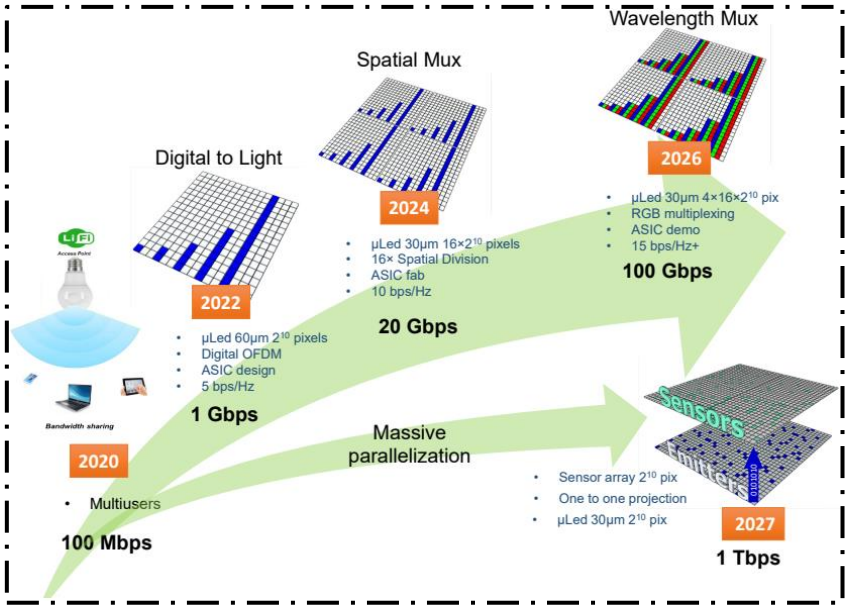

Figure 2.8. Roadmap for VLC systems from Mbps to Tbps [82]

2.7.3. VLC future challenges

Based on the review of VLC literature, we outline the key challenges that need to be addressed to enhance system performance. The required high speed transmission rate for next generation optical wireless networks can be restricted by the field of view (FOV) alignment and shadowing scenarios. In VLC-based indoor access network, the level of received optical power by a light sensor, that equipped with the receiver portable devices, is affected by the user motion, thereby, the resulted FOV misalignment between transmitter and receiver leads to a drop in received optical power. Regarding to the limited performance in shadowing scenario, a severe degradation in system performance is captured when the propagation link has been clogged by a potential obstacle, i.e. human passing by. Hence, for shadowing and FOV misalignment scenarios, it is imperative to invent a technique that can immediately react to the potential interruptions and changes in level of received optical power.

Furthermore, the limitation of non-linearity and signal clipping is extremely challenging for indoor VLC future research. Mitigating LED nonlinearity is crucial for efficient optical wireless communication systems to avoid high clipping distortion outside the restricted TOV, and saturation point of LED-dynamic range that can be identified according to the I-V characteristics. Although several techniques, i.e. pre-distortion/post-distortion, are submitted to tackle the nonlinearity effect [83] and [84], providing a LED with large operational range is a crucial key for supporting the next generation high speed requirements.

Signal clipping/attenuation is the simplest technique that has been proposed to avoid the impact of LED-nonlinearity, although such technique poses to degrade the transmitted signal power and violating the condition of VLC-dimming compatibility. Nevertheless, an optimum clipping threshold with acceptable error performance has been delivered by [85]. On the other hand, the signal power is directly related to the required illumination level, thereby, the chosen modulation format must support different levels of light intensity (very low/high of dimming levels). IEEE 802.15.7 standard defines sets of mechanisms to enable brightness control in the suggested modulation, also various formats have been introduced to be compatible with dimming control in optical OFDM signals [86]-[87]. Nevertheless, such scenario violates the light-off mode specifically at indoor VLC applications. Since the future VLC system exploits to offer simultaneous high-speed data transmission and illumination, several Mbps can only be achieved under a low brightness level, thereby, a hybrid VLC with RF and/or IR technologies has been suggested [88], i.e. integration optical wireless communication system with another communication standard has been demonstrated to has a cost efficiency of 47% and minimizing the power consumption by 49% compared to LED source [89]-[90]. However, the concurrent transmission, cost and complexity of such promising design still be a challenge.

The challenge of using VLC signals for uplink transmission has been gathered more attention in previous years. Besides, the eye safety problem at high-speed VLC requirement, light communication using LED with uplink transmission can interfere with downlink VLC path, and degrading the VLC system performance. Such implication drove researchers to exploits RF or ultraviolet wave for uplink transmission, although such technologies required high hardware complexity [91]-[92]. The promising IR wavelength is exploited to offload uplink traffic with mitigating the ISI of reflected signals and inter-user-interference from neighbour users by using angle diversity technology [93], where such technique is introduced to support the multi-users uplink mode with compared to several techniques that supporting a single user uplink transmission [94]-[96], but even so, further research is required to minimize the induced interference.

Moreover, employing a broad beam of light to overcome the high-cost beam-steering techniques, has a downside of power reduction with increase the coverage distance, due to the magnitude of the retrieved electrical signal is inversely proportional to square of the coverage distance [97].

The LED-modulation bandwidth keeps relatively restricted, although the rapid development in its manufactured structure to meet the high-speed 6G demands. Such requirements have been demonstrated only in a laboratory environment, where a highly cost optics are used. Therefore, to deliver the high-speed transmission of Terabit per second range, the VLC research community is currently investigating Li-Fi 2.0 with the use of the eye-safe laser of high modulation bandwidth [98]. Moreover, recent research has ensured eye-safe demands over high throughput rate of Gbps range by using vertical-cavity surface-emitting lasers [99].

A future trend of using a novel vertical handover for the heterogeneous network based on hybrid VLC (to satisfy high throughput rate) and RF (to overcome the interrupted connection with VLC propagation link), is proposed to ensure a continuous transmission with a low handover failure probability, where the handover times is further minimized [100]-[101], However, enhancing the quality of experience still challenging task in future indoor optical wireless networks.

The IEEE issued 802.11bb, a new standard that made Li-Fi technology widely available and compatible with WiFi. The standard outlines the system designs and physical layer requirements for light-wave-based wireless communication. The IEEE 802.11bb Task Group is working on modifying the IEEE 802.11 Stds for light communications - access to the Project Authorization

Request (PAR) and the (CSD) Criteria for Standards Development. The general scope of the Task Group is restricted to a specified area.

Uplink and downlink in 800 nm to 1,000 nm band achieve 10 Mb/s throughput at the MAC data service access point (SAP). Interoperability among solid state light sources with different modulation bandwidths. This amendment outlines alterations to the IEEE 802.11 MAC which are constrained to the subsequent:

The (HCF) Hybrid coordination function channel access, the overlapping basic service set (OBSS) detection, and power management modes. Analogous to the RF system's antenna chain, Light Antenna ONE allows for 802.11bb compliance. Li-Fi can be combined with WiFi chipsets already in use. Li-Fi is recognized by the system as a WiFi band [102]-[103].

2.8. Conclusions

In this chapter, the basic concepts of visible light communications have been reviewed, also considering the LEDs at the transmitterand the photodetector at the receiver. Besides, the characteristics of indoor optical wireless communication for various propagation models are given to analysis the impact of such parameter links and channel delay over system performance. The significant value of VLC technique has been provided to overcome some limited applications of RF systems. Afterwards, we first reviewed the fundamental principles of optical OFDM signaling, and the most common modulation technologies basic OFDM technique such as: DCO-OFDM, ACO-OFDM, Flip-OFDM and layered OFDM schemes have been systematically analyzed to identify the transmission performance as will be compared to advanced modulation techniques in the next chapters. The main implications for IM/DD communication technique are mainly based on the restricted dynamic range of LED, that is investigated over different optical OFDM format. Furthermore, the role of Micro-LED to overcome the limited modulation bandwidth is also presented. Furthermore, the importance of visible light communication is highlighted for future applications and services of 6G era (Mbps-Tbps roadmap). The current limitations, requirements, challenges, and the vision with applications of 6G network has been introduced based on the progress to date in VLC system.

Chapter 3. Fundamentals of FBMC-OQAM modulation systems

" When one door closes, another opens; but we often look so long and so regretfully upon the closed door that we do not see the one which has opened for us".

– Alexander Graham Bell

This chapter presents a solid framework for FBMC-OQAM system, also known as Staggered Multitone (SMT) method, as a promising modulation scheme for future optical wireless communication systems, compared to other waveform candidates. A comprehensive introduction of the fundamental theory for FBMC format based on transmultiplexing model and polyphase representations is provided as a potential-alternative technique to OFDM architecture that uses extra CP and guard band to obtain robustness against the inter symbol interference in different propagation scenarios. For such reason, the well-known prototype filters for FBMC-OQAM burst are considered to achieve an optimum spectral confinement. In such sense, the major benefit of FBMC with OQAM scheme is the requirement of well time-frequency localized pulse function with high side-lobe suppression ratio instead of guard band and CP samples, which enhances the spectral efficiency and system performance to be a key factor in next generation optical networks. In this chapter, we also analyse the intrinsic interference in FBMC signals, where a special preamble of IAM sequence is required for the channel estimation to minimize an intrinsic imaginary interference, which is classified as the main drawback in FBMC signals transmission.

3.1. Future candidate modulation-waveforms

The candidate waveforms that are considered as the promising modulation technique for the next generation requirements and applications are: Generalized Frequency Division Multiplexing (GFDM), Universal Filtered Multicarrier (UFMC) and Filter Bank Multicarrier (FBMC) schemes [77].

GFDM refers to the modulation format providing bandwidth that can be divided into either a minimum number of subchannels with wider bandwidth or a few numbers of narrowband subchannels. Such a non-orthogonal technique processes each subchannel by deploying a circular filtering to overcome the overhead tails at both sides of the transmitted burst. Moreover, employing the circular filtering rather than a linear convolution, with a chosen prototype filter leads to a signal of low latency. The spectral efficiency of GFDM signal is further enhanced compared to one in OFDM, due to the use of a single cyclic prefix for one block. Besides, GFDM offers an enhanced out-of-band emission (OOBE) compared to OFDM OOBE. However, since the GFDM system is based on a nonorthogonal transmission format, the induced Inter Carrier Interference (ICI) cannot be fully avoided.

Another candidate technique for supporting B5G/6G applications is UFMC, that is classified as an improved waveform with respect to CP-OFDM system. The essential blocks of UFMC technique are QAM modulation, serial-to-parallel conversion, the Inverse Fast Fourier Transform (IFFT) per group and group-wise filtering. In such system, the subchannel-wise filtering is performed to optimize OOBE impact, where such filter lengths are shorter than required in FBMC system. Moreover, since UFMC format does not require CP, the impact of Inter Symbol Interference (ISI) dominates over the performance of multipath fading channel. However, to enhance the system performance, optional blocks can be added, such as zero overhead-tail, discrete Fourier transform pre-coding and a sub-block of CP. Furthermore, it avoids extra processing blocks, i.e., OQAM block, as the orthogonality is achieved between sub-bands.

Filter Bank Multi-Carrier modulation based on transmitting real data-information as a result of splitting the input-QAM symbol into real and imaginary parts of a T/2 delay offset (OQAM instead of QAM modulation), where the orthogonality over adjacent subcarriers in verified by deploying OQAM modulation (the FBMC- orthogonality is only satisfied in a real domain). Besides, the cyclic prefix and guard band samples are not needed in FBMC mechanism if a well time-frequency localized prototype filter is applied. There are several ways to carry out the mechanism of FBMC, such as cosine modulated multitone (CMT), staggered modulation multitone (SMT) and filtered multitone (FMT). SMT or FBMC-OQAM modulation technique is classified as the major promising waveform for next-generation requirements because of its ability to combat the FBMC-intrinsic interference that results from OQAM signalling. Although such system offers an optimum spectral efficiency (no CPs/guard band employed), a training block and the integration of multiple-input multiple-output technique is not straight forward as occurs in 4G systems, i.e., OFDM scheme [104]-[108].

Several investigations have been performed in order to choose the optimum future candidate waveform with compared to OFDM format. In [109], a comparison study confirmed that FBMC and GFDM systems present equivalent and enhanced performance with respect to other waveforms, respectively, while in [110] the best error performance was obtained by using FBMC system. Besides, FBMC modulation shows optimum Power Spectral Density (PSD) [105]-[106]. Regarding to computational complexity [105], although FBMC has been presented as a high complexity technique compared to OFDM and UFMC modulation formats, it has presented a smaller number of real multiplication than GFDM format.

Consequently, FBMC has acquired a substantial attention from a large number of authors, i.e. [104] and [77], and the intensive worldwide research activities led to consider FBMC-OQAM system as a viable modulation technique for future requirements and applications. Moreover, compared to 4G modulation format, i.e. OFDM signals, higher spectral efficiency is obtained in FBMC. Besides, a few numbers of subcarriers as guard bands, is sufficient to verify the frequency emission masks and FBMC offers the lowest out-of-band emission. Hence, FBMC modulation format is considered throughout the rest of this thesis.

3.2. FBMC based transmultiplexer architecture.

In FBMC modulation, the core of the FBMC system with transmultiplexer (TMUX) configuration is the fundamental processing blocks of OQAM pre-processing and a synthesis filter bank that combines sub-band signals into one filtered signal. At a receiver side, the analysis filter bank includes matching receiver filters, and OQAM post-processing allows the retrieval of the complex input signal. OQAM lattice is used instead of a classical QAM, where each pair of staggered symbols in time at each subcarrier are presented as real and imaginary parts of one complex valued QAM symbol $C_{m,n}$. Thus, symbol density is identical for both FBMC and OFDM system models, as exhibited in forming a chequerboard lattice of Figure 3.1.

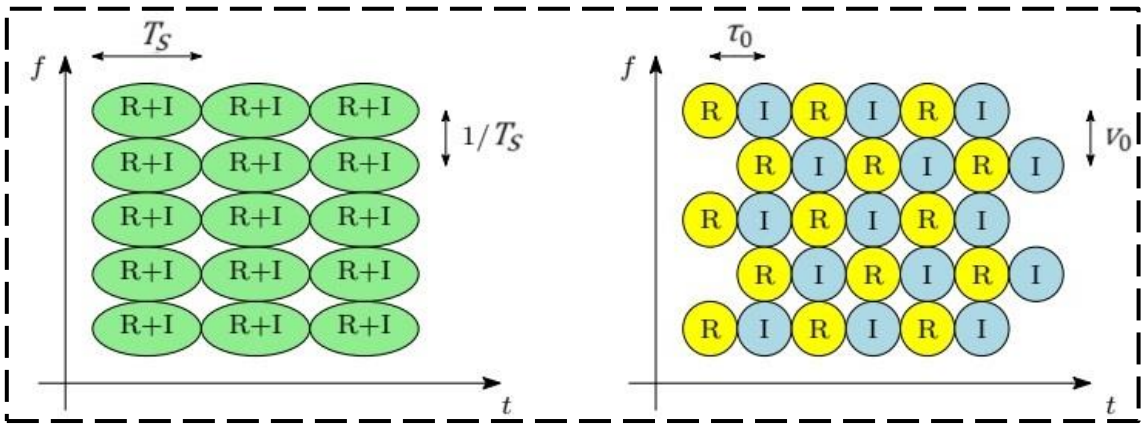

Figure 3.1. Time-frequency lattice for OFDM and OFDM-OQAM modulation.

The parameter T_S refers to the period of multicarrier symbol. The time and subcarriers spacing between two adjacent symbols is $\tau_0 = T_S / 2$ and $v_0 = 1/T_S$, respectively. For such scenario, in an FBMC-OQAM system, due to the complex-to-real (C2R$_{m,n}$) conversion process (staggering), we transmit two real pulse amplitude modulation (PAM) symbols $A_{m,n}$ at the m^{th} sub-carrier and n^{th} symbol. Notice that such conversion increases the sample rate by a factor of 2 (operate at twice rate of QAM blocks). The next step in staggering process is the multiplication of a phase-shift sequence $\varphi_{m,n}$ to enable the data reconstruction and enhance the orthogonality between the successive symbols [111]-[112].

$$A_{m,2n} = \begin{cases} \mathrm{Re}\left[C_{m,n}\right] & m \text{ even} \\ \mathrm{Im}\left[C_{m,n}\right], & m \text{ odd,} \end{cases} \tag{3.1}$$

and

$$A_{m,2n+1} = \begin{cases} \mathrm{Im}\left[C_{m,n}\right] & m \text{ even} \\ \mathrm{Re}\left[C_{m,n}\right], & m \text{ odd,} \end{cases} \tag{3.2}$$

Thus, the most standard option for phase-shift that will be adopted throughout the rest of this thesis is [111]-[113]:

$$\varphi_{m,n} = e^{j\frac{\pi}{2}(m+n)} = j^{(m+n)} \tag{3.3}$$

where

$$\varphi_{m,n} = \begin{cases} (-1)(-1)^{\lfloor m/2 \rfloor + \lfloor n/2 \rfloor} & m \text{ odd and } n \text{ odd} \\ -1^{(m+n)/2} & m \text{ even and } n \text{ even} \\ (-1)^{m/2+\lfloor n/2 \rfloor} i & m \text{ even and } n \text{ odd} \\ (-1)^{\lfloor m/2 \rfloor + n/2} i & m \text{ odd and } n \text{ even} \end{cases} \tag{3.4}$$

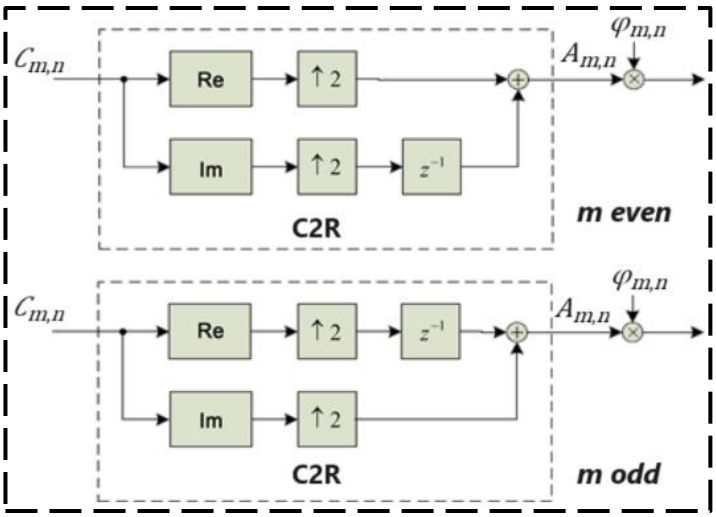

Figure 3.2. OQAM pre-processing (staggering).

Hence, it can be noticed that PAM symbols ($A_{m,2n}$ and $A_{m,2n+1}$ (in-phase and quadrature information)) of adjacent position are phase-shifted by a factor of π/2 radians, which is fed into synthesis filter bank (SFB).

3.3. Synthesis and analysis filter banks

According to equation (3.8), in communication based on FBMC modulation, the filter banks are deployed in the TMUX configuration with SFB and analysis filter banks (AFB) in the transmitter and receiver, respectively. The input signal ($A_{m,n}$ $\varphi_{m,n}$), at the inception of the SFB architecture, is processed convolutionally by a bank of *M* uniform-shifted replicas of a single linear-phase lowpass prototype filter *P[k]* with a symmetrical real-valued function [114]-[117]. Thus, the synthesis filters $g_m(k)$ represent the m^{th} shifted version of *P[k]* of L_p length at the transmitter side, and can be given as follows [113]:

$$g_m(k) = P[k]e^{j2\pi\frac{mk}{M} - j2\pi\frac{mDe}{M}} \tag{3.5}$$

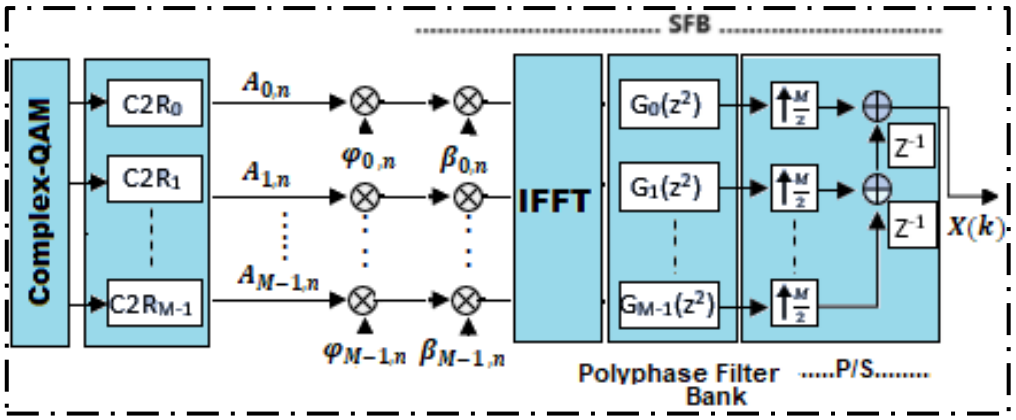

Figure 3.3. Efficient implementation for modulated the FBMC-OQAM signals.

The finite impulse response of *P[k]* function is a unit-energy of order $L_p - 1$, such as $\sum_{k=0}^{L_p-1} \left| p_{m,n}[k] \right|^2 = 1$. The delay term (*De*) of $\frac{L_p-1}{2}$ samples in equation (3.5) is proposed to impose the causality for the chosen prototype filter. It is noteworthy mentioning that the most popular values of filter length L_p are, $K \times M$, $K \times M + 1$ and $K \times M - 1$, where K is the overlapping factor and M refers to total number of used subcarriers. Shorter than $K \times M - 1$ prototype filter-length drives to degradation in system performance, whereas an extra latency is reported for higher than $K \times M + 1$ length option [118].

To obtain a very high stopband attenuation, a high value of overlapping factor should be considered in designing the prototype filter, thereby the overlapping factor controls the number of symbol-blocks that overlap in time domain. Without loss the generality the FBMC modulated burst can be written as [111]-[113]:

$$X(k) = \sum_{n=0}^{N-1} \sum_{m=0}^{M-1} A_{m,n} P_{m,n}[k]$$

$$X(k) = \sum_{n=0}^{N-1} \sum_{m=0}^{M-1} A_{m,n}\ \varphi_{m,n}\ \underbrace{e^{-j\frac{2\pi}{M} m \cdot De}}_{\beta_m}\ P\left[k - n\frac{M}{2}\right] e^{j2\pi \frac{mk}{M}} \tag{3.6}$$

The received data-information is fed to the AFB, where it down sampled by a factor of M/2 to be processed by a bank of complex-conjugated and time-reversed model of synthesis filters as:

$$f_m(k) = g^*\left[L_p - 1 - m\right] \tag{3.7}$$

where $f_m(k)$ term is the m^{th} analysis filter at the receiver. In ideal transmission scenario (free-distortion channel), the possibility to introduce the prototype filter with perfect reconstruction (PR), i.e., the received-estimated data sequence $A^{estimated}_{m_0,n_0} = A_{m,n}$ if the delay of the banks is ignored, is not valid in a real time transmission scenario due to channel impact. On the other hand, nearly PR (NPR) of designing the pulse-shaping filter should be considered instead. Such design suffers a marginal amount of interference even at a free-distortion channel.

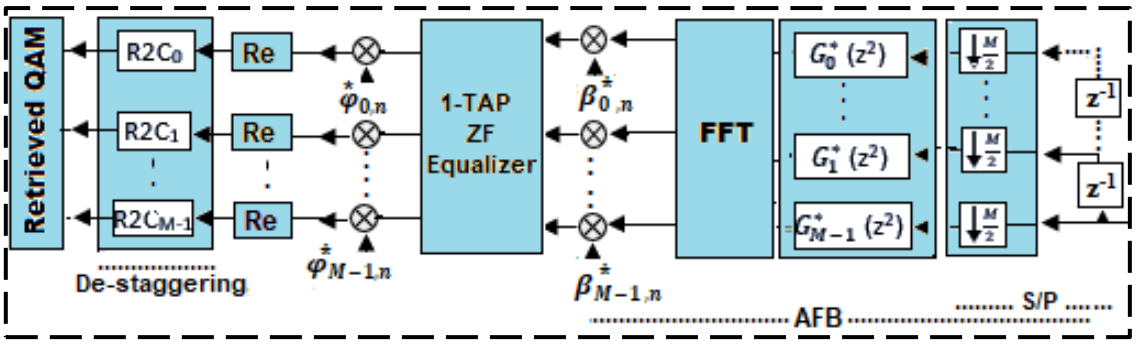

Figure 3.4. Efficient implementation for demodulated the FBMC-OQAM signals.

Therefore, a balance between the quality of reconstructed information and spectrum features needs to be pursued in the course of *P*[*k*] design. Since the FBMC-OQAM mechanism transmit a real PAM constellation, the estimated symbol $A^{estimated}{}_{m_0,n_0}$ can be reconstructed by taking the real part of the projection between the pulse function P_{m_0,n_0} and multiplexed signal *X*[*k*] as:

$$A^{estimated}{}_{m_0,n_0} = \mathrm{Re}\left\{\left\langle Y_{m,n}[k] \middle| P^{*}{}_{m_0,n_0}[k] \right\rangle\right\} \tag{3.8}$$

where $Y_{m,n}[k]$ term refers to the received data-information at the inception of AFB and, $\mathrm{Re}\{.\}$ is the real part operator. Over a channel of free-noise distortion (channel response equals to 1), the interference is a purely imaginary intrinsic interference as detailed in Tables 3.1 and 3.2, respectively, where the imaginary intrinsic interference $\zeta^{m,n}_{m_0,n_0}$ can be given as [26] and [119]-[121]:

$$\zeta^{m,n}_{m_0,n_0} = \left\langle P_{m,n}[k],\ P^{*}{}_{m_0,n_0}[k] \right\rangle \tag{3.9}$$

The intrinsic imaginary interference that is associated with received symbols is obtained by the use of PHYsical layer for DYnamic AccesS and cognitive radio abbreviated as (PHYDYAS) prototype filter, and which is a special case of Mirabbasi-Martin function (Mirabbasi-Martin function with overlapping factor (*K*) of 4) in [122].

Table 3.1. Imaginary interference $\zeta_{m_0,n_0}^{m,n}$ for transmitting $A_{m_0,n_0}=1$, based on PHYDYAS prototype filter with odd time index n_0

	n_0-2	n_0-1	n_0	n_0+1	n_0+2
m_0-1	$0.125j$	$0.205j$	$0.239j$	$0.205j$	$0.125j$
m_0	0	$0.564j$	1	$-0.564j$	0
m_0+1	$-0.125j$	$0.205j$	$-0.239j$	$0.205j$	$-0.125j$

Table 3.2. Imaginary interference $\zeta_{m_0,n_0}^{m,n}$ for transmitting $A_{m_0,n_0}=1$, based on PHYDYAS prototype filter with even time index n_0

	n_0-2	n_0-1	n_0	n_0+1	n_0+2
m_0-1	$-0.125j$	$-0.205j$	$-0.239j$	$-0.205j$	$-0.125j$
m_0	0	$0.564j$	1	$-0.564j$	0
m_0+1	$0.125j$	$-0.205j$	$0.239j$	$-0.205j$	$0.125j$

As detailed in Tables 3.1 and 3.2, the information-data signal has a purely imaginary intrinsic interference from the surrounding data (positioned on the imaginary part of the subchannel signal) even at ideal channel. Thereby, taking the real part leads to reconstruct the conveyed symbol $\mathrm{Re}\left\{\left\langle Y_{m,n}[k]\middle|P^{*}_{m_0,n_0}[k]\right\rangle\right\}$ = 1, and to validate the interference suppression ($\zeta_{m_0,n_0}^{m,n}$ shaded values that surrounding the transmitted data of 1). However, such intrinsic interference is not fixed at a receiver, because it is directly related to the employed prototype filter and its neighbouring subchannels (adjacent symbols). consequently, transmitting a known information at a known position is inadequate, since at the receiver, the intrinsic interference part depends on the neighbouring symbols [123].

According to Tables 3.1 and 3.2, for the first order neighborhood zone ((m_0, n_0) ∈ $\Omega_{(1,1)}$)) where Ω indicates the set points in the frequency-time (FT) grid, the following amplitude symmetry of $\zeta_{m_0,n_0}^{m,n}$ can be noted as [26] and [124]:

$$\zeta_{m_0,n_0}^{m_0+1,n_0+1}=-\zeta_{m_0,n_0}^{m_0-1,n_0+1}=\zeta_{m_0,n_0}^{m_0+1,n_0-1}=\zeta_{m_0,n_0}^{m_0-1,n_0-1} \tag{3.10}$$

$$\zeta_{m_0,n_0}^{m_0,n_0+1}=-\zeta_{m_0,n_0}^{m_0,n_0-1} \tag{3.11}$$

$$\zeta_{m_0,n_0}^{m_0+1,n_0}=-\zeta_{m_0,n_0}^{m_0-1,n_0} \tag{3.12}$$

The following properties contribute to identify the interference power on a certain subchannel in the FT grid, which can in turn, promote schemes for the deterministic preamble sequence of IAM method and interference cancellation to enhance the estimation accuracy [123].

According to equation (3.8), It is also noteworthy mentioning that the symbol estimation depends on the selection of employed prototype filter, where the estimation quality experiences a self-interference at the receiver (noise floor). Therefore, a signal-to-interference ratio (SIR) at ideal channel can be given as [124]:

$$\mathrm{SIR} = \frac{1}{\sum_{m=0}^{M-1}\sum_{n=0}^{\infty}\left(\mathrm{Re}\left\{\left\langle P_{m,n}[k]\middle|P^{*}_{m_0,n_0}[k]\right\rangle\right\}\right)^2} \tag{3.13}$$

However, FBMC burst based on a prototype filter with high SIR levels leads to overcome the impact of self-interference.

Extra attention is required at the TMUX-receiver side, the non-negative integers of the delay parameter $\Delta\delta$ arises to ensure causality at the inception of AFB, and the reconstructed delay (TMUX-latency) $\Delta\Upsilon$ is introduced at the evaluation of transmitted symbols, which can be written as [125]:

$$\Delta\Upsilon = \frac{2}{M}\left(L_p - 1 + \Delta\delta\right) \tag{3.14}$$

These parameters depend on the filter length used, where a longer prototype drives to higher latency at the TMUX output.

Regarding to the OQAM post-processing (de-staggering) which is the last stage to obtain the input complex QAM, as shown in Figure 3.5. The de-staggering processing blocks are summarized below, where the first processing step is the multiplication by a sequence of $\varphi_{m,n}$ conjugate $\left(\varphi^{*}_{m,n}\right)$, which is followed by taking the real part of demodulated received signal. Afterwards, the next processing block is real to complex ($R2C_{m,n}$) conversion that performs the inverse $C2R_{m,n}$ operation to recover back the complex data.

$$C^{\text{Reconstructed}}_{m,n} = \begin{cases} A^{\text{Estimated}}_{m,2n} + jA^{\text{Estimated}}_{m,2n+1} & m \text{ even} \\ A^{\text{Estimated}}_{m,2n+1} + A^{\text{Estimated}}_{m,2n} & m \text{ odd,} \end{cases} \tag{3.15}$$

In such scenario, due to the de-staggering processing blocks, the sampling rate is decreased by a factor of 2.

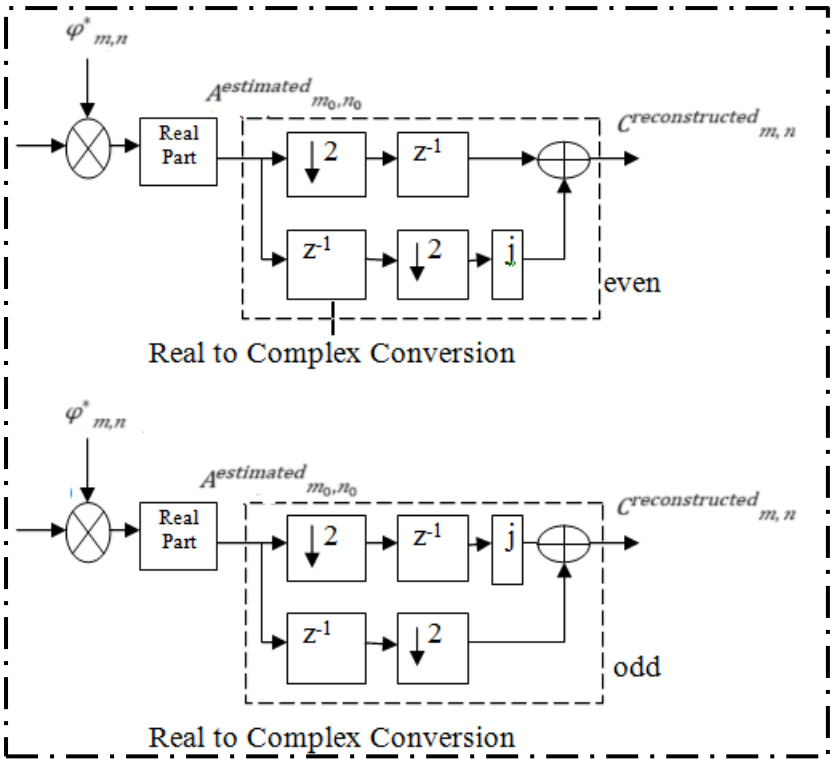

Figure 3.5. OQAM post-processing (de-staggering).

3.4. Channel Estimation in FBMC-OQAM

Channel estimation (CE) performs an essential aspect for reconstructing data-information through a propagating channel. However, in the presence of fading, CE provides the required knowledge about distortion by channel frequency response for the conveyed message, in order to design a suitable equalizer so that the fading impact can be compensated, and the transmitted signal can be correctly retrieved.

The required CE for OFDM system is a straightforward task due to the mechanism of OFDM modulation is based on an orthogonal frequency plan. Therefore, the received pilot burst is divided by its respective training symbols, which are previously known at the receiver, to estimate the channel response. However, the orthogonality in FBMC signal is satisfied only in the real field so that a special channel estimation technique is required to minimize the impact of intrinsic imaginary interference, which is classified as a major drawback in FBMC-OQAM system.

As the estimation strategy with OFDM system is not applicable for FBMC signals, several CE techniques are proposed in the literature to limit the intrinsic interference and to enhance the quality of estimation, such as coded Auxiliary Pilot (FBMC-CAPI) (scattered-pilot) [126] and the intrinsic imaginary interference (IMI) sequence (preamble-pilot). To satisfy the imaginary interference cancelation, FBMC-CAPI method deployed several auxiliary/coded training symbols to supress the imaginary interference on each scattered pilot. It is worth noting that the suggested method based on sending pilots that are surrounded by dummy symbol (auxiliary pilots), with the coding mechanism. Although such technique (FBMC-CAP) promotes the transmission performance, a high computational complexity is dominated is such transmission, due to the required surrounded pilots by high number of coded data to eliminate the imaginary interference.

Consequently, the most widely CE based on preamble-pilot in FBMC system is IAM sequence. A deterministic preamble sequence is a group of known training pilots with a duration of 1.5 complex symbols (3 columns pilots) at the inception of FBMC burst, which is deployed to enhance the estimation accuracy by minimizing the impact of intrinsic interference. Besides, preamble blocks can also be employed for synchronization purposes.

3.5. Imaginary interference with IAM sequence

In order to transmit the sequence of preamble-pilot, based on the TMUX-FBMC signal that is given by equation (3.6), the transmitter signal based on reference symbols can be expressed as below:

$$X(k) = \sum_{n=0}^{N-1} \sum_{m=0}^{M-1} T_{m,n} P_{m,n}[k] \tag{3.16}$$

where $T_{m,n}$ is the training symbols (pilots) for the m^{th} and n^{th} subchannel and timeslot, respectively. Whereas the received reference symbols at the output of AFB blocks can be formulated as:

$$\text{Received\_signal}_{\text{IAM}} = \left\{ \left\langle Y_{m,n}[k] \middle| P^{*}_{m_0,n_0}[k] \right\rangle \right\}$$

$$= H_{m_0,n_0} T_{m_0,n_0} + \underbrace{j \sum_{(m,n)\neq(m_0,n_0)} H_{m_0,n_0} T_{m,n} \zeta^{\text{m,n}}_{m_0,n_0}}_{I_{m_0,n_0}} + \underbrace{\sum_{k=-\infty}^{\infty} Z[k] P^{*}_{m_0,n_0}[k]}_{Z_{m_0,n_0}} \tag{3.17}$$

where Z_{m_0,n_0} and I_{m_0,n_0} terms are the gaussian noise and the associated intrinsic interference, respectively. The term H_{m_0,n_0} is the m^{th} channel frequency response at the frequency-time point (m_0, n_0).

As presented in Figure 3.6, for FBMC signal based on well time-frequency localization filter, the impact of I_{m_0,n_0} comes from the ≈98% immediate neighbours (1st order neighbourhood $\Omega_{(1,1)-(0,0)}$) of (m_0, n_0), which refers to following zone [127]:

$$\Omega_{(1,1)-(0,0)} = \left\{ (m_0 \pm 1, n_0),\ (m_0 \pm 1, n_0 \pm 1),\ (m_0, n_0 \pm 1) \right\} \tag{3.18}$$

Whereas the ≈2% of interference corresponding to outside of first order neighbourhood zone $(m_0, n_0) \notin \Omega_{(1,1)-(0,0)}$ is normally neglected.

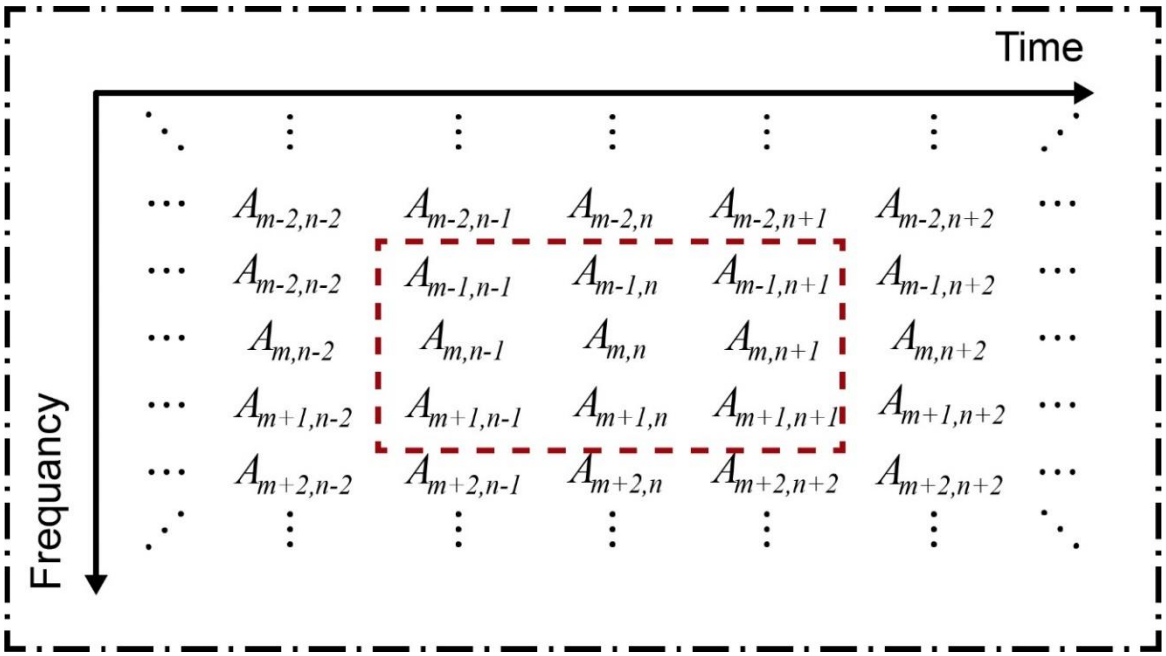

Figure 3.6. Inherent imaginary interference in received FBMC blocks

Furthermore, if such zone experiences a flat channel frequency response impact, then the quantity of equation (3.17) can be formulated as complex pseudo-pilots PLT_{m_0,n_0} :

$$PLT_{m_0,n_0} = T_{m_0,n_0} + j \underbrace{\sum_{(m,n)\in(m_0,n_0)} T_{m,n}\zeta_{m_0,n_0}^{m,n}}_{T_{m_0,n_0}^{Pilot\ imaginary\ interference}}$$

$$= T_{m_0,n_0} + jT_{m_0,n_0}^{Pilot\ imaginary\ interference} \tag{3.19}$$

where $T_{m_0,n_0}^{Imaginary\ interference}$ term refers to imaginary part of intrinsic interference, while the real part of interference can be overcome by deploying a prototype pulse with high level of SIR value. To this end, if known training symbols with the immediate neighbours of (m_0,n_0) are conveyed in FBMC system, then the approximation of the interference can be determined to estimate the channel frequency response (CFR) as:

$$H_{m,n}^{\wedge} = \frac{\overbrace{PLT_{m_0,n_0}}^{\text{Received pseudo-pilots}}}{T_{m_0,n_0} + \underbrace{jT_{m_0,n_0}^{Pilot\ imaginary\ interference}}_{\text{interference weights}}} \tag{3.20}$$

Thus, the objective of IAM technique is to evaluate the intrinsic interference from surrounding pilot-blocks (interference weights), where the previously computed weights, which depend on the pulse function, are stored in the receiver side for the channel estimation process. Note that higher value of $T_{m_0,n_0}^{Pilot\ imaginary\ interference}$ drives to enhance the estimation accuracy since it is inversely proportional to the noise in equation (3.20). Furthermore, if a well localized filter is employed, then 1.5 blocks is needed for training, while more blocks are required for less well time-localized filters. The characteristics of intrinsic imaginary interferences that generated by T_{m_0,n_0} symbol with the associated surrounding blocks are summarized in equations (3.10) - (3.12):

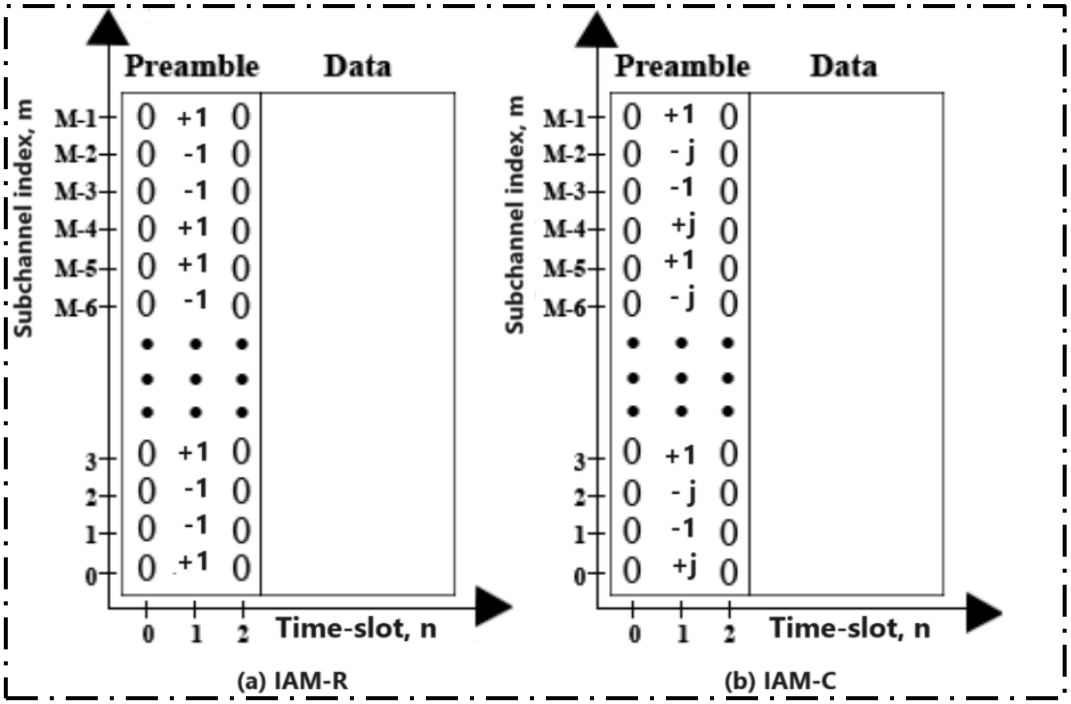

Figure 3.7. Preamble arrangements for the (a) IAM-R and (b) IAM-C techniques.

$$T_{m_0\pm1,n_0\pm1}^{Pilot\ imaginary\ interference} = -T_{m_0,n_0}(-1)^{m_0} e^{-j\frac{2\pi}{M}De} \sum_{k=M/2}^{L_p-1} P[k]\, P[k-\frac{M}{2}]\, e^{j\frac{2\pi k}{M}} \tag{3.21}$$

$$T_{m_0\pm1,n_0}^{Pilot\ imaginary\ interference} = \pm j\left(T_{m_0,n_0}\right) e^{-j\frac{2\pi}{M}De} \sum_{k=M/2}^{L_p-1} P^2[k]\, e^{j\frac{2\pi k}{M}} \tag{3.22}$$

$$T_{m_0,n_0\pm1}^{Pilot\ imaginary\ interference} = \mp j\left(T_{m_0,n_0}\right)(-1)^{m_0} \sum_{k=M/2}^{L_p-1} P[k]\, P[k-\frac{M}{2}]\, e^{j\frac{2\pi k}{M}} \tag{3.23}$$

Consecutively, in order to minimize the intrinsic imaginary interference, pseudo pilots are required as a preamble, which consists of three consecutive blocks ($T_{m,n-1}$, $T_{m,n}$, $T_{m,n+1}$) (1.5 complex QAM-blocks). The simplest way to cancel the interference in FBMC-OQAM system is to set a block of null values at the 1st and 3rd preamble structure. In the middle block $T_{m,n}$ (second timeslot), the level of training symbol is set to the maximum value allowed by the FBMC system, such as the intrinsic imaginary interference (IAM) of type R and type C as shown in Figure 3.7.

3.6. Prototype filter design

The PHYDYAS pulse function is classified as one of the widespread filters that was employed as the fundamental prototype filter in the European project with FBMC system, because of the fast spectrum decay and high quality for signal reconstruction. The PHYDYAS function is composed of 2×(*K*-0.5) taps, where PHYDYAS continuous frequency response can be expressed as [112]:

$$P(f) = \sum_{l=-(K-1)}^{K-1} V_l \frac{\sin\left(\pi(f-\frac{l}{MK})MK\right)}{MK\,\sin\left(\pi(f-\frac{l}{MK})\right)} \tag{3.24}$$

where the weights of frequency response verify the following equation:

$$\frac{1}{K}\sum_{l=-(K-1)}^{K-1} V_l = 1 \tag{3.25}$$

The term *K* is the overlapping factor between adjacent subchannels, where the continuous frequency field is denoted by *f*, while the V_l term represents the coefficients of PHYDYAS prototype filter $P(f)$ at certain frequencies.

At the output of IFFT processing block, the impulse response of PHYDYAS filter can be given as:

$$P[k] = 1 + 2\sum_{l=1}^{K-1} V_l \cos\left(\frac{2\pi}{MK}k\right) \tag{3.26}$$

where the weights V_l are tabulated in Table 3.3.

Table 3.3. Mirabbasi-Martin filter coefficients [128]-[129]

K	k_1	k_2	k_3	k_4	k_5	k_6	k_7	k_8
2	1	$-\sqrt{2}/2$						
3	1	0.911437	0.411437					
4	1	0.971959	0.707106	-0.235146				
5	1	0.991841	0.865416	-0.501053	0.127478			
6	1	-0.997227	0.941367	-0.707106	0.337383	-0.744167		
8	1	-0.999883	0.993155	-0.927080	0.707106	-0.374861	0.116802	-0.152384

For the Isotropic Orthogonal Transform Algorithm (IOTA) function, which is defined as an algorithm that basically takes the Gaussian function and provides orthogonality in both frequency and time domain. The orthogonalization term O_a corresponding to a given function *x(t)* can be calculated as follows [130]:

$$O_{\tau_0}\{x(t)\} = \frac{x(t)}{\sqrt{\left|\tau_0 \sum_{i=-\infty}^{\infty} \sqrt{x(t-\tau_0 i)}\right|^2}} \tag{3.27}$$

The orthogonalization operator O_a with *a* equal to τ_0 or v_0, leads to orthogonalize *x(t)* along the frequency axis, which can be expressed on the ambiguity function as:

$$Am_y(0, \frac{m}{\tau_0}) = 0, \ \forall\ \mathrm{m} \neq 0, \text{ where } Am_y(0,0) = 1 \tag{3.28}$$

where $y(t) = O_{\tau_0} x(t)$ being the orthogonalization on continuous function. Thus, orthogonalizing $x(t)$ along the time axis requires to apply the orthogonality operation to a frequency domain signal $X(f)$ which is the FT of $x(t)$.

$$y(f) = O_{v_0} X(f) \tag{3.29}$$

Therefore, to perform orthogonalization on $x(t)$, it should be converted first into the frequency domain by taking the *FT*, then it is applied to the orthogonalization operation. Afterwards, it goes back to the time domain by taking the inverse *FT* (*FT*$^{-1}$).

$$y(t) = FT^{-1}\ O_{\tau_0} x(t)\ FT \tag{3.30}$$

where

$$Am_y(\frac{n}{v_0}, 0) = 0,\ \forall\ \mathrm{n} \neq 0, \text{ where } Am_y(0,0) = 1 \tag{3.31}$$

Consequently, the continuous representation of the IOTA pulse function is:

$$P(t) = O_{\tau_0} FT^{-1}\ O_{v_0}\ g_\alpha(t)\ FT_\alpha \tag{3.32}$$

where $g_\alpha(t)$ being the Gaussian function, and α is a spreading factor term. It must be emphasized on the IOTA prototype filter, which is a special case from the Extended Gaussian Function (EGF). The EGF protype filter based on the closed form expression, can be formulated as [130]-[132]:

$$Z_{\alpha,v_0,\tau_0}(t) = 0.5\left[\sum_{k=0}^{\infty} d_{k,\alpha,v_0}\left[g_\alpha(t+\frac{k}{v_0}) + g_\alpha(t-\frac{k}{v_0})\right]\right] \times \sum_{l=0}^{\infty} d_{l,\frac{1}{\alpha},\tau_0} \cos(2\pi l \frac{t}{\tau_0}) \tag{3.33}$$

The spreading factor α being a real positive number with range of $0.528v_0^{\ 2} \le \alpha \le 7.568v_0^{\ 2}$ [133], where the Gaussian function can be expressed as:

$$g_\alpha(t) = (2\alpha)^{0.25} e^{-\pi t^2 \alpha} \tag{3.34}$$

The coefficients d_{k,α,v_0} represents the real valued that can be expressed as [131]:

$$d_{k,\alpha,v_0} = \sum_{l=0}^{\infty} a_{k,I}\ e^{-\left(\frac{\pi I}{2v_0^{\ 2}}\right)\alpha},\ 0 \le k \le \infty \tag{3.35}$$

However, in practice, the expression should be limited to a finite number, due to the fact that is a fastly reducing function. Therefore, $\bar{d}_{k,\alpha,v_0}$ term refers to the coefficients of limited number of *K*.

$$\bar{d}_{k,\alpha,v_0} = \sum_{j=0}^{jk} b_{k,j}\ e^{-\left(\frac{\pi\alpha}{2v_0^{\ 2}}\right)(2j+k)},\ 0 \le k \le K \tag{3.36}$$

where

$$j_k = \left\lfloor \frac{(K-k)}{2} \right\rfloor \tag{3.37}$$

The j_k term is a positive integer number that is identified according to *K*. In Table 3.4, the accuracy of 0.79×10^{-19} is reported based on a list of $b_{k,j}$ coefficients with *K*=14 and α = 1.

Table 3.4. $b_{k,j}$ coefficients of the EGF profile[131].

K	j=0	j=1	j=2	j=3	j=4	j=5	j=6	j=7
0	1	$\frac{3}{4}$	$\frac{105}{64}$	$\frac{675}{256}$	$\frac{76233}{16384}$	$\frac{457107}{65536}$	$\frac{12097169}{1048576}$	$\frac{7054315}{4194304}$
1	-1	$-\frac{15}{8}$	$-\frac{219}{64}$	$-\frac{6055}{1024}$	$-\frac{161925}{16384}$	$-\frac{2067909}{1301072}$	$-\frac{26060847}{1048576}$	
2	$\frac{3}{4}$	$\frac{19}{16}$	$\frac{1545}{512}$	$\frac{9765}{2048}$	$\frac{596277}{65536}$	$\frac{3679941}{262144}$	$\frac{394159701}{16777216}$	
3	$-\frac{5}{8}$	$-\frac{123}{128}$	$-\frac{2289}{1024}$	$-\frac{34871}{8192}$	$-\frac{969375}{131072}$	$-\frac{51182445}{4194304}$		
4	$\frac{35}{64}$	$\frac{213}{256}$	$\frac{7797}{4096}$	$\frac{34871}{8192}$	$\frac{13861065}{2097152}$	$\frac{87185895}{8388608}$		
5	$-\frac{63}{128}$	$-\frac{763}{1024}$	$-\frac{13875}{8192}$	$\frac{790815}{262144}$	$-\frac{23600537}{4194304}$			
6	$\frac{213}{512}$	$\frac{1395}{2048}$	$\frac{202281}{131072}$	$\frac{1434705}{524288}$	$\frac{85037895}{16777216}$			
7	$-\frac{429}{1024}$	$\frac{20691}{32768}$	$-\frac{374325}{262144}$	$-\frac{5297445}{2097152}$				
8	$\frac{6435}{16384}$	$\frac{38753}{65536}$	$\frac{1400487}{1048576}$	$\frac{989593}{4194304}$				
9	$-\frac{12155}{32768}$	$-\frac{146289}{262144}$	$-\frac{2641197}{2097152}$					
10	$\frac{46189}{131072}$	$\frac{277797}{524288}$	$\frac{20050485}{16777216}$					
11	$-\frac{88179}{262144}$	$-\frac{2120495}{4194304}$						
12	$\frac{676039}{2097152}$	$\frac{4063017}{8388608}$						
13	$-\frac{1300075}{4194304}$							
14	$\frac{5014575}{16777216}$							

3.7. Conclusions

In this section, the future multicarrier waveforms of FBCM-OQAM, UFMC and GFDM are evaluated to select the optimum modulation format in order to fulfil the next generation requirements and applications. FBMC based on TMUX configuration shows as a solid framework over other future modulation-waveforms. Consequently, we provide the schematic processing blocks for FBMC-OQAM transmitter/receiver based on the polyphase representations.

This chapter also reviews the most known well time-frequency localized prototype filter that can be employed in FBMC system, i.e. PHYDYAS and IOTA filters. Besides, the impact of intrinsic imaginary interference is analysed, and the special reference symbols of interference approximation sequence is systematically investigated to minimize the induced residual interference which inherent with the retrieved FBMC signals.

Chapter 4. Analysis of a Truncated and Non-shortening Flip-FBMC Models over Indoor LOS and Multipath Propagation-links

"If you don't do the best with what you have, you could never have done better with what you could have had.".

– Ernest Rutherford

This chapter describes the polyphase implementation of the biorthogonal Flip-FBMC-based TMUX configuration as a good alternative to the traditional Flip-CP-OFDM technique for indoor VLC system. The proposed design is tested over several overlapping factors and prototype filters-based figures of merit. Furthermore, the possibility to enhance the system performance in terms of TMUX-latency and system spectral efficiency is investigated using a tail-shortening mechanism with different filter lengths. This chapter also presents the comprehensive theoretical and experimental outcomes of deploying IAM-R and IAM-C types and their influences in Flip-FBMC system. Besides, the impact of inherent interference is investigated with low to high channel delays profile, also based on a single and multitap equalization technique. The throughput rate for truncated and non-shortening Flip-FBMC models based on realistic experimental parameters is provided. Moreover, the chapter also includes the role of flipping technique in FBMC modulation for the sake of avoiding the residual interference. Concretely, the impact of induced imaginary interference outside the first order zone has been investigated and compared to DCO-FBMC scheme, since such zone cannot be covered by using IAM preamble.

4.1. Flipping-based FBMC modulation

The OFDM-OQAM (FBMC) modulation format based on flipping technique will be investigated to overcome the limited dynamic range of the employed LEDs, which is constrained by the signal amplitudes of the optical transmission burst. The LED-restricted dynamic range is considered as one of the major drawbacks in real transmission time for indoor VLC system. Furthermore, as detailed in chapter 2, to overcome the penalty of high hardware complexity in employing ACO technique. Also, to avoid using layer technique which has the main implication of transmitting multiple layers of optical bursts simultaneously, due to such system is required an iterative decoding and high computational loads, Hence, the OFDM-OQAM based on flipping technique will be employed to provide a unipolar format in the IM/DD communication. Moreover, for the first time to the author´s knowledge, this chapter presents the analysis and theoretical results of Flip-FBMC signals transmission over different links of indoor optical wireless communication systems.

4.2. Flip-FBMC based TMUX configuration.

The OFDM-OQAM with TMUX configuration represents a biorthogonal scheme to provide the sufficient flexibility in design requirements, due to either the FFT or IFFT processing blocks can be deployed at the receiver (RX) side [133]-[135]. Such designs, both RX_1 or RX_2 models, respectively, share the same performance results. The core of the FBMC system is its TMUX configuration with the fundamental processing blocks of OQAM pre-processing and the SFB blocks that combines sub-band signals into a single filtered signal. Whereas the AFB includes matching receiver filters, and OQAM post-processing contribute to retrieve the complex input message successfully at the RX side.

A schematic diagram of Flip-FBMC based on a biorthogonal form for a VLC system is depicted in Figure 4.1, which shows the flexibility at the RX side, where either RX_1 or RX_2 is needed to retrieve the complex input message. The bipolar-FBMC signal *X(k)* at the transmitter (TX) side, can be expressed according to equation (3.6). From equations (3.1) and (3.2), the real adjacent symbols ($A_{m,2n}$ and $A_{m,2n+1}$) with a *T*/2 relative time offset to carry the quadrature and in-phase information of the input-complex QAM are obtained using $C2R_{m,n}$ conversion block. Hence, the staggering process results in up-sampling by a factor of 2.

The real successive symbols $A_{m,n}$ are π/2 phase-shifted using $\varphi_{m,n}$ to preserve their orthogonality, where the term $\varphi_{m,n}$ can be calculated in accordance to equations (3.3) and (3.4). To obtain a bipolar-real signal in the FBMC-TMUX transmitter side, the orthogonal-complex symbols with their corresponding phase-shift of β_m must satisfy Hermitian symmetry conditions, as presented in Table 4.1, where the total number of required subchannels is $(2\times(M/2-1)+2)$ in the filter bank, due to the Hermitian symmetry provided in Table 4.1.

Assume that Hermitian symmetry is satisfied between the incoming signal and its transpose-conjugate feeding the IFFT processing block. Hence, a bipolar-real signal is processed convolutionally by a bank of *M* uniform-shifted replicas of a prototype filter, which are symmetric real-valued and delayed by $((M\times K+1)-1)/2$ samples to provide the required causality. The filter

length of ($M\times K+1$) is selected below, with several overlapping factors that determine the number of symbols, which overlap in time domain.

Table 4.1. Hermitian symmetry of input signal in Flip-FBMC based TMUX configuration.

		Symbol Number			
		1	**2**	**...**	**2N**
Subcarrier Number	1	0	0	0	0
	2	$\mathrm{Re}(A_{2,1})\ \beta_2$	$j \times \mathrm{Im}(A_{2,2})\ \beta_2$	...	$\varphi_{2,2N} \times \mathrm{Im}(A_{2,2N})\ \beta_2$
	3	$j \times \mathrm{Im}(A_{3,1})\ \beta_3$	$-1 \times \mathrm{Re}(A_{3,2})\ \beta_3$	...	.....
	4	$-1 \times \mathrm{Re}(A_{4,1})\ \beta_4$	$-j \times \mathrm{Im}(A_{4,2})\ \beta_4$	...	.....
	5	$-j \times \mathrm{Im}(A_{5,1})\ \beta_5$	$\mathrm{Re}(A_{5,2})\ \beta_5$	...	.....
	.....	.....	.....	...	.....
	M/2+1	0	0	0	0
	.....	.....	.....	...	.....
	M -1	$(j \times \mathrm{Im}(A_{3,1})\ \beta_3)^*$	$(-1 \times \mathrm{Im}(A_{3,2})\ \beta_3)^*$	...	.....
	M	$(\mathrm{Re}\ (A_{2,1})\ \beta_2)^*$	$(j \times \mathrm{Im}(A_{2,2})\ \beta_2)^*$	...	$(\varphi_{2,2N} \times \mathrm{Im}(A_{2,2N})\ \beta_2)^*$

The biorthogonal system refers to the possibility of retrieving the transmitted signal either with an IFFT-based AFB at the first receiver (RX_1) by using type-1 polyphase decomposition (Po-De) as shown in Figure 4.1 (a) or with an FFT-based AFB by employing type-2 Po-De filters at the second receiver (RX_2), as shown in Figure 4.1 (b). The synthesis filters represent the m^{th} shifted version of prototype filter *P[k]* of L_p length at the transmitter side, while $f_m(k)$ is the m^{th} analysis filter at the receiver.

Through type-2 Po-De, the $f_m(k)$ term represents as a complex-conjugated and time-reversed model of a synthesis filter $g_m(k)$ [114], which can be expressed according to the equations (3.5) and (3.7). It is worth mentioning that AFB design with IFFT processing blocks is very straightforward to implement, since no further flipping process is required as occurs in a type-2 Po-De. Nevertheless, for the sake of better backward compatibility with OFDM system, the configuration of FBMC-TMUX scheme is practically designed with AFB based on FFT blocks [125] and [117].

The FBMC signal $X(k)$ of bipolar form is achieved by up-sampling with a ratio of $M/2$ to compensate the loss rate , due to the $T/2$ relative time offset for OQAM mapping, followed by parallel-to-serial (P/S) conversion, where in such process the sub-band signals are combined into a single real filtered signal. The filtered signal is converted into to a unipolar format using flipping processing technique that are juxtaposed in consecutive FBMC subframes as $X^+(k)$ and $X^-(k)$ to be employed for IM of the LED, that can be calculated according to equation (2.26).

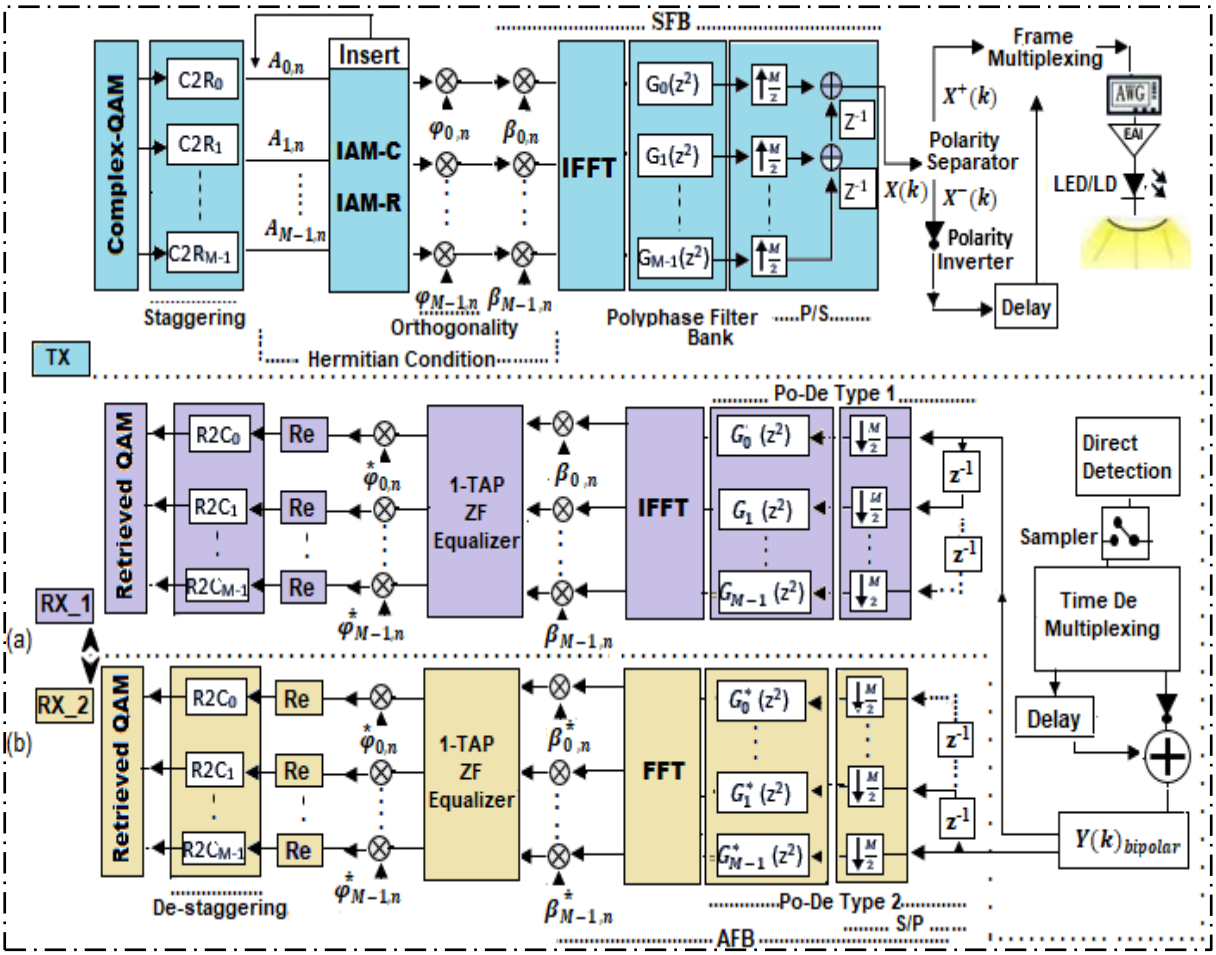

Figure 4.1. Polyphase implementation of the biorthogonal Flip-FBMC-based TMUX configuration at indoor optical wireless communication system for reconstructing the input-complex QAM signal by using either (a) an IFFT-based RX_1 or (b) an FFT-based RX_2.

The successively received FBMC subframes $Y^{+}(k)$ and $Y^{-}(k)$ are subtracted to regenerate the bipolar form as:

$$Y(k)_{\text{Bipolar packet}} = \left(Y^{+}(k)\right) - \left(Y^{-}(k)\right)$$

$$Y(k)_{\text{FBMC\_bipolar}} = \underbrace{X^{+}(k) \otimes h^{+}(l) + Z^{+}(k)}_{Y^{+}(k)} - \underbrace{(X^{-}(k) \otimes -h^{-}(l) + Z^{-}(k))}_{Y^{-}(k)} \tag{4.1}$$

where ⊗ represents convolution, *h(l)* is an optical channel impulse response with *l* taps, and *Z* represents noise samples of AWGN.

The n^{th} non-equalized received symbols of m^{th} subcarriers can be achieved by demodulating the received signal given as [21] and [136]:

$$R_{m,n} = \sum_{k=-\infty}^{\infty} Y(k) P_{m,n}[k]^{*}$$

$$R_{m,n} = H_{m,n}A_{m,n} + j \times \underbrace{\sum_{m0,n0 \in \Omega} H_{m0,n0}A_{m0,n0} \left\langle P_{m,n}[k], P_{m0,n0}[k]^{*} \right\rangle}_{\text{Intrinsic interference}} + \underbrace{\sum_{k=-\infty}^{\infty} Z(k) P_{m,n}[k]^{*}}_{z_{m,n}} \tag{4.2}$$

Finally, the input complex QAM symbol can be recovered by using $R2C_{m,n}$ processing block see equation (3.15).

4.3. Analysis of the optical FBMC structure based on flipping technique over a direct indoor LOS VLC channel.

The most common choices of filter lengths are $IFFT_{Size} \times K$, $IFFT_{Size} \times K-1$, and $IFFT_{Size} \times K+1$, where $IFFT_{Size}$ represents one block of M subcarriers (one symbol = 1 block of M samples). The use of shorter or longer than those filter values give rise to a degradation in system performance, as stated in chapter 2. Therefore, the proposed Flip-FBMC system is tested by using a filter length of $IFFT_{Size} \times K+1$ because it represents the optimum length choice for the reconstruction quality as given in [118].

The impact of flipping technique on FBMC modulation format, where the information burst samples conveyed over the modulation bandwidth of the blue Micro-LED can be given by:

$$\text{Flip-FBMC}_{\text{burst length}} = 2\times\left(IFFT_{\text{Size}} \times (N + K + 0.5)\right) \tag{4.3}$$

As expressed in equation (4.3), there is a penalty of $2\times(K+0.5)$ overhead-blocks based on ($M\times K$ +1) employed filter length, due to the inherent tail of (K+0.5) symbols at both sides of bipolar FBMC burst, which is doubled at transmitter stage because of flipping process. Note that the length of the Flip-OFDM transmitted burst with no CPs or guard bands is only $2\times$ ($N \times IFFT_{Size}$) samples. Thus, Flip-OFDM system exhibits a higher spectral efficiency than the proposed scheme. However, compared to DCO-OFDM signal, a superior gain in the spectral efficiency based on DCO-FBMC signal is reported, since extra CPs and guard bands blocks are required in the OFDM structure to combat ISI impact.

On the other hand, as detailed in chapter 2, several overlapping factors can be utilized in designing the prototype filter in FBMC modulation. Thereby, the spectral efficiency of Flip-FBMC system based on employed several overlapping factors such as: ($K = 3$, $K = 4$ and $K= 5$) with Mirabbasi-Martin prototype filter is tested on a low to high constellation mapping to evaluate the impact of throughput rate for each overlapping factor.

Figure 4.2 shows the comparison of Flip-OFDM with no CP and a Flip-FBMC system based on different overlapping factors using Mirabbasi-Martin filters. It can be observed that the spectral efficiency of the proposed approach is higher for lower overlapping factors and larger frame durations, where a limited packet length shows a significant drop in the information rate from the influence of redundancy tails at both sides of packet data transmission. Consequently, a tail shortening process is an essential procedure in Flip-FBMC signals to enhance the gain in its spectral efficiency, especially for short-packet transmission, as will be detailed in section 4.5.

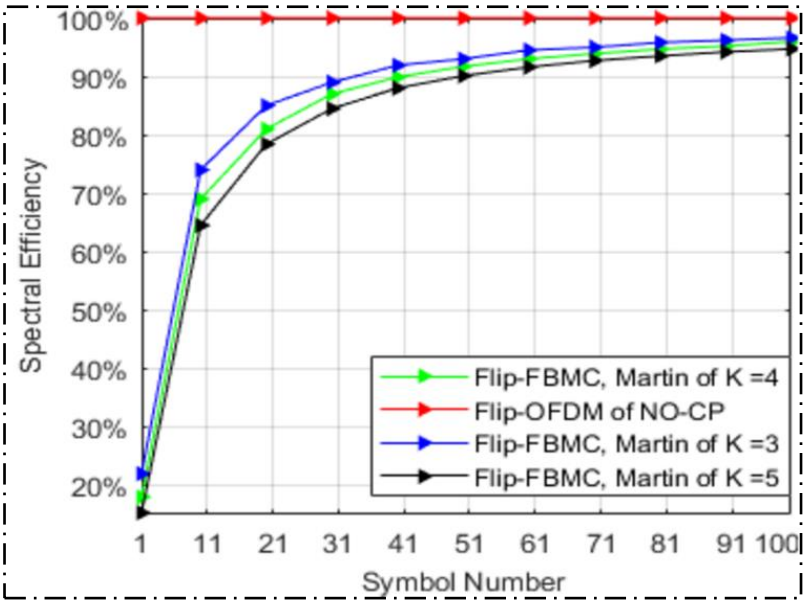

Figure 4.2. Spectral efficiency based in several overlapping factors comparison.

Furthermore, to evaluate the impact of each overlapping factor, the performances of the novel Flip-FBMC-based TMUX configuration and the conventional Flip-OFDM system are assessed in terms of the symbol error rate (SER) vs. electrical SNR, by using the simulation experimental setup of the LOS optical wireless link that is tabulated in Table 4.2. The channel DC gain of the LOS optical wireless link is calculated according to equations (2.6) to (2.9). In the following work, the parameters employed to estimate the LOS channel gain are based on [51], where a blue Micro-LED having a peak wavelength of 450 nm is deployed, and the influences of shot and thermal noise are modeled as AWGN.

Table 4.2. Simulation system parameters.

Parameters	**Value**	
Utilized technique	Flip-FBMC	Flip OFDM
Field of view (FOV)	60°	
Propagation Link	LOS	
Gain of an optical filter	1.0	
Responsivity of PIN 1601FS-AC	0.2 A/W @ 450 nm	
Lens refractive index	1.5	
Transmitted power	4.5 mW	
Area of PD	0.125 mm^2	
AWGN	Shot & thermal noise	
IFFT size (M)	64 samples	
Constellation mapping	Low-high	
Prototype filter	Martin & IOTA	Rectangular
Overlapping factor (*K*)	3, 4 & 5	Non
Number of transmitted symbols	1-100	

The simulation results in sections 4.4 and 4.5 are obtained by assuming the optical channel state information is known at the receiver.

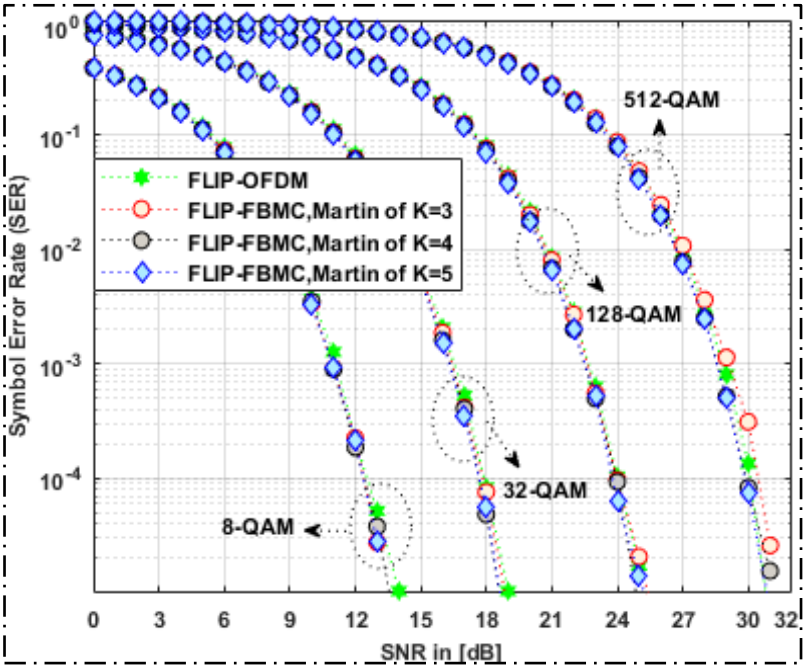

Figure 4.3. Performance comparison between the Flip-FBMC schemes of various overlapping factors over different M-QAM modulation formats in the VLC LOS channel.

Figure 4.3 shows the overlapping factor of 3 presents higher SER values than the conventional optical OFDM technique for higher constellation orders and SNR values higher than 26 dB. Regarding the overlapping factor of 4, it performs as the optimum choice, due to a slightly improved error performance over Flip-OFDM system. Although the choice of K = 5 introduces an almost identical error to K = 4, the boost in computational complexity, filter latency, and gain reduction in spectral efficiency are the most significant drawbacks in employing the overlapping factor of 5.

Nevertheless, the most significant drawback in the FBMC mechanism is its computational complexity [137]. However, regarding [138], FBMC-TMUX-based polyphase systems present less complexity than the one proposed in [139] due to the avoidance of unnecessary operations in frequency spreading. For the sake of comparison, the complexity of the multiplication (M_{com}) and addition (A_{com}) terms required to transmit one block of symbols for both techniques using an FFT Split-Radix algorithm, which can be calculated based on [140] as:

$$M_{\text{com Flip-FBMC}} = \underset{\text{OQAM}}{2} \times \left(\underbrace{2IFFT_{\text{Size}}}_{\beta} + \underbrace{\left(IFFT_{\text{Size}} \left(\log_2\left(IFFT_{\text{Size}}\right)-3\right)+4\right)}_{IFFT} + \underset{SFB}{2L_P} \right) \tag{4.4}$$

$$A_{\text{com Flip-FBMC}} = 2\left(3IFFT_{\text{Size}} \left(\log_2 IFFT_{\text{Size}} -1\right)+4\right)+2IFFT_{\text{Size}} +4\left(L_P - IFFT_{\text{Size}}\right) \tag{4.5}$$

$$M_{\text{com Flip-OFDM}} = \underbrace{\text{IFFT}_{\text{Size}} \left(\log_2\left(IFFT_{\text{Size}} -3\right)+4\right)}_{IFFT} \tag{4.6}$$

$$A_{\text{com Flip-OFDM}} = 3IFFT_{\text{Size}} \left(\log_2 IFFT_{\text{Size}}\right) - 3IFFT_{\text{Size}} + 4 \tag{4.7}$$

As presented in the equations above, Flip-OFDM system offers much less hardware complexity than the proposed one because of an extra β term and M branch for each AFB and SFB processing blocks for a given filter length. It can also be seen that the hardware complexity of optical FBMC signal with flipping technique is slightly reduced by using lower overlap factors such as: K=3. Moreover, the short filter length of ($IFFT_{Size} \times K-1$) is the preferable choice in terms of complexity since the influence of β can be neglected.

Regarding to OOB radiation, the power spectral density of the proposed scheme is examined through an evaluation of the out-of-band emission with respect to the classic Flip-OFDM system. The major feature of the FBMC is its low OOB radiation, which allows more efficient spectrum sharing between users.

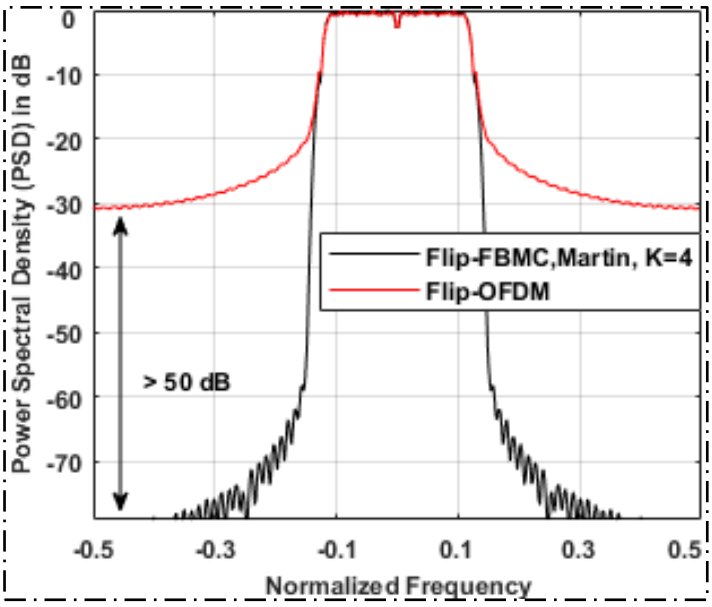

Figure 4.4. Power spectral density of Flip-FBMC vs Flip-OFDM.

Consequently, as presented in Figure 4.4, the capability of the Flip-FBMC scheme to reject the Flip-OFDM energy leakage of up to 50 dB is obtained by using Martin profile with overlapping factor of 4, which also contributes to minimizing the synchronization errors.

4.4. Analysis of the overhead tails based on a hard truncation process.

From equation (4.3), the redundancy symbol-blocks lead to inherently tails at both sides of the transmitted Flip-FBMC signals, Thereby, further spectral analysis is required to optimize the bandwidth efficiency of the proposed system. Consequently, to gain better insight into the implications of overhead tails at both ends of the bipolar packet, a transmission of short data-packet is considered to identify the redundancy blocks in the tail, as illustrated in Figure 4.5. A transmission based on Flip-FBMC technique is considered as bandwidth-limited because of the long filter impulse response, which imposes a ramp-up (initial transition) of 1.5 symbols, and a ramp-down (final transition) of 2.5 symbols at the beginning and end of the bipolar FBMC burst while, an essential half-symbol tail is considered as an inherent and non-removable symbol in the Flip-FBMC mechanism.

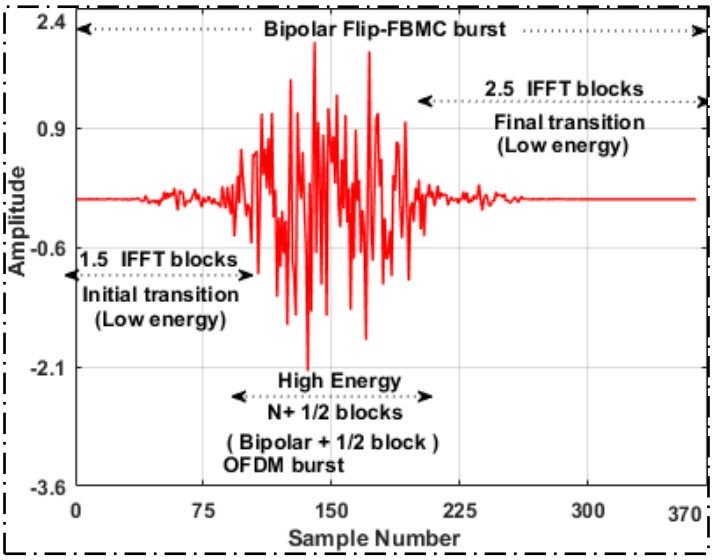

Figure 4.5. Bipolar FBMC burst of a short packet (1 conveyed symbol-block).

These overhead blocks, which are doubled due to the flipping process, yield to a gain reduction penalty in spectral efficiency. Therefore, based on ($IFFT_{Size}$ × K+1) filter length and K= 4, a shortening technique is a fundamental process to avoid the imposed penalty of $2\times(K+0.5)$ extra blocks compared to the transmission of Flip-OFDM burst with no CP.

Hence, it is noteworthy mentioning that most redundancy blocks (1.5 and 2.5 blocks, respectively, at left and right sides of bipolar burst) are truncated with considerable consequences, as shown in (Figure 4.6), where the resulting truncation shows a significant influence on the quality of the retrieved signal.

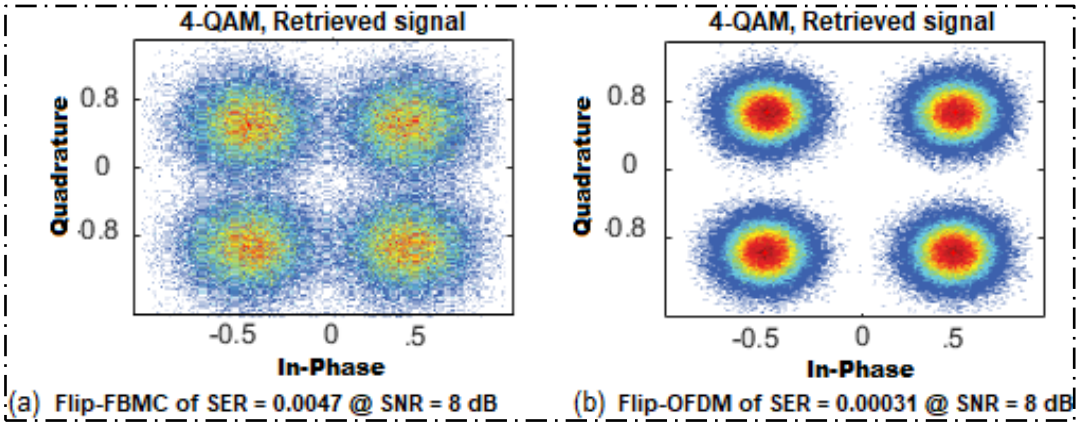

Figure 4.6. Constellations of 4-QAM retrieved signals over a long data burst (100 transmitted symbols) to show (a) the degradation of the Flip-FBMC performance through a hard truncation of the lowest energy parts (1.5 symbols at the beginning of the packet and 2.5 symbols at the end of the data burst) of the tail compared with the classic Flip-OFDM in (b).

For such scenario, further analysis to optimize the transmission quality based on such truncation approach is performed, thereby several truncation-values of the overhead tails have been tested to obtain the optimum shortening values at both ends of bipolar data-packet. In order to limit the interference level of Figure 4.6, the novel shortening values are achieved by leaving part of the redundancy tail (IFFT blocks of low powers), where 1.5 IFFT blocks at the beginning and 1.75

IFFT blocks for the end of a bipolar-FBMC packet is truncated. Notable, where other truncated values drive to degrade the system performance.

To evaluate the implications of chosen shortening values, different prototype filters are considered such as: IOTA and Mirabbasi-Martin (PHYDYAS with K=4) functions, where the assumed truncated values are only valid with an even overlapping factor, i.e. K=4 and a filter length of $IFFT_{Size} \times K+1$.

With regard to the distributed energy of overhead tails, although IOTA filter offers lower tail energy at both ends of a data packet than PHYDYAS pulse function, the truncated power of overhead blocks is further minimized with PHYDYAS filter, as presented in Figure 4.7. Thereby, the transmission power based on the tail-shortened signal is optimum with PHYDYAS profile.

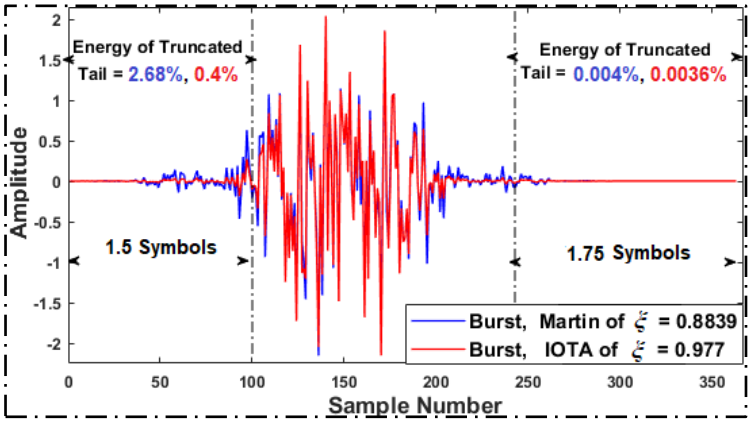

Figure 4.7. Optimal shortening values for the hard truncation method of 1.5 and 1.75 IFFT-blocks at both ends of a bipolar burst based on IOTA and PHYDYAS filters and their localization factors.

The improved spectral efficiency of the truncated packet is presented in Figure 4.8, where the resulting length of FLIP-FBMC burst in samples can be determined according to equation (4.8).

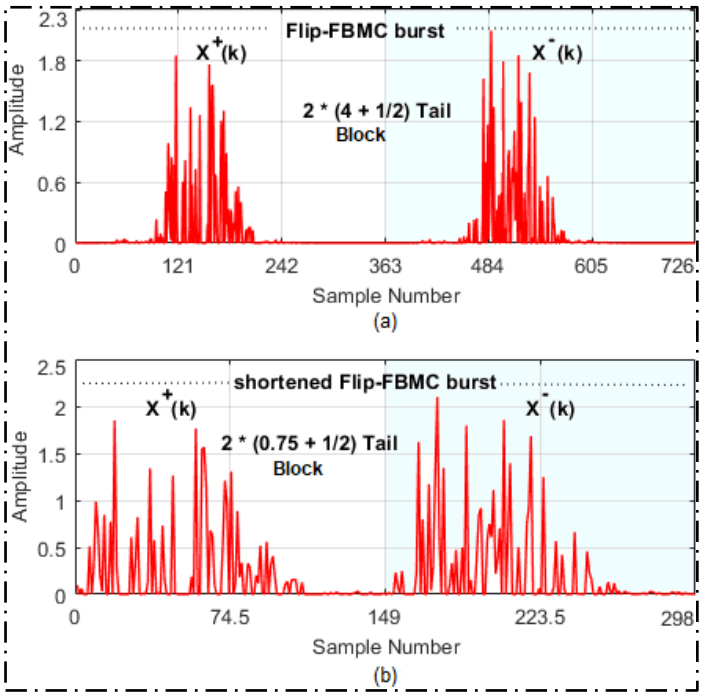

Figure 4.8. Consecutive subframes of a single Flip-FBMC burst for (a), and (b) the truncated version of a Flip-FBMC packet.

$$\text{Truncated Flip-FBMC}_{(\text{lenght of even K})} = 2\times\left(IFFT_{\text{Size}}\times\left(N+K-2.75\right)\right) \tag{4.8}$$

As depicted in Figure 4.8(a), the successive subframes ($X^{+}(k)$ and $X^{-}(k)$) of Flip-FBMC signal, impose a penalty of 2× (4) extra IFFT blocks and 2× (0.5) blocks of an inherent tail. These 9 overhead blocks (penalty) are minimized according to equation (4.8) to only 2.5 extra symbols more than the Flip-OFDM packet, as observed in Figure 4.8(b).

Consequently, the impact of truncation process contributes to promote the information rate, as can be observed in Figure 4.9, where the throughputs of Flip-FBMC are highly dependent on the packet size (data blocks), and the gain in spectral efficiency is significantly improved specifically at low numbers of IFFT blocks.

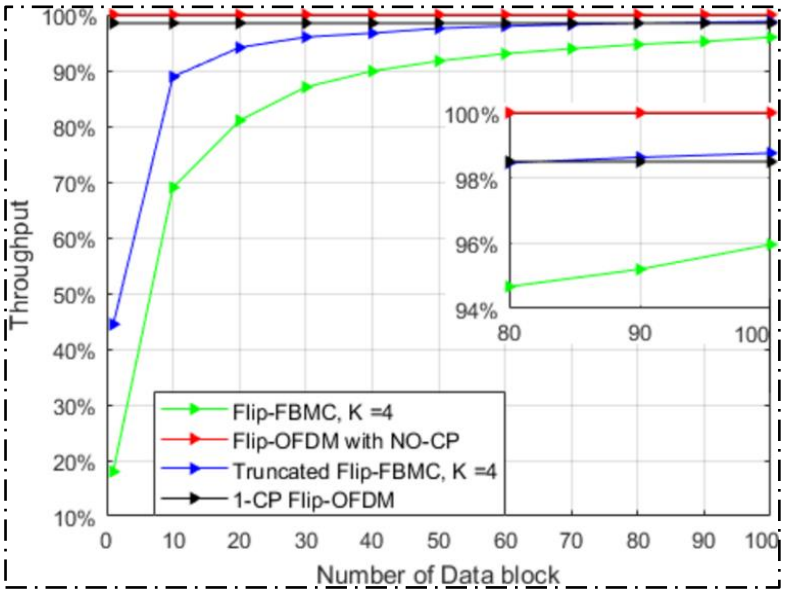

Figure 4.9. Hard truncation impact on spectral efficiency.

Moreover, such truncation also contributes to reduce TMUX-latency in the reconstructed signal presented in equation (3.14) and results as follows:

$$\underbrace{\Delta\Upsilon_{\underbrace{(IFFT_{\text{size}}\times K+1)}_{Length}}}_{\text{at shortening model}} = \frac{2}{IFFT_{\text{Size}}}\left(L_p - 1 - 1.5\,IFFT_{\text{Size}} + \Delta\delta\right) \tag{4.9}$$

where the $1.5\times IFFT_{Size}$ term is derived and added to satisfy the shortening of the data packet transmission. Therefore, the reconstructed delay is reduced from $2K$ to $2K$-3 factor at the AFB output.

According to [141], employing a prototype filter with Heisenberg factor close to 1 ($\xi \approx 1$) leads to the optimum time-frequency pulse localization. Therefore, as presented in Figure 4.7, up to a certain extent, the impact of the localization parameter of a low value, which is remarkable in the performance of the Martin filter with compared to IOTA profile, drives to a higher tail-powers. Therefore, the tail-powers can be reduced by employing a filter with low time and frequency spreading (high value of ξ), i.e. IOTA prototype filter with a near-optimum value of ξ.

The exact ξ of the corresponding work using Martin and IOTA filters of length $IFFT_{Size}\times K+1$ can be measured as follows:

$$\xi = 1/4\pi\Delta W\Delta T \tag{4.10}$$

where

$$0 \le \xi \le 1 \tag{4.11}$$

The localization factor ξ is determined by the dispersion product of ΔW and ΔT, where the synthesis filters $g_m(k)$ have the same frequency dispersion (ΔW) and time dispersion (ΔT). The dispersion values can be calculated as:

$$\Delta W = \sqrt{\int_{-\infty}^{\infty} f^2 \,|P(f)|^2 \, df} \tag{4.12}$$

and

$$\Delta T = \sqrt{\int_{-\infty}^{\infty} t^2 \,|P(t)|^2 \, dt} \tag{4.13}$$

where the $P(t)$ term is the prototype pulse function and $P(f)$ is its Fourier transform. To analyze the impact of localization factor, the tail-shortened signal with PHYDYAS and IOTA filters is transmitted over a flat VLC link.

As depicted in Figure 4.10, the truncation burst using Martin filter causes a remarkable degradation in system performance over a long data burst (100 symbols) and high modulation orders (≥ 64-QAM), while it exhibits an identical SER performance to that of the Flip-OFDM technique over lower order mapping.

On the other hand, the IOTA filter with a localization factor of 0.977 (close to 1) yields to concentrate the signal energy according to an envelope function around its center, which leads to lower energy loss than that of a Martin filter having ξ = 0.8839, as shown in Figure 4.7. Consequently, the truncated packet using an IOTA filter exhibits an identical SER performance to that of the Flip-OFDM technique and a superior performance over the shortening burst based on the Martin filter at high constellation mapping and over a flat VLC channel, as observed in Figure 4.10.

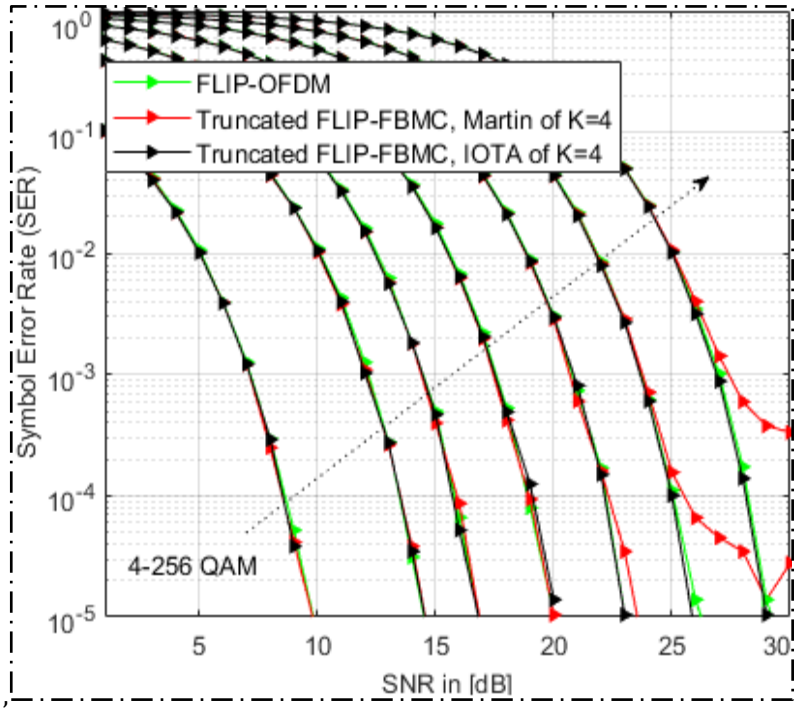

Figure 4.10. Symbol error rate vs SNR over a long data burst of 100 symbol-blocks for Flip-OFDM and Flip-FBMC systems employing IOTA and Martin filters, and for the proposed truncation values of 1.5 ,and 1.75 symbols at both ends of a bipolar burst in a flat VLC channel.

4.5. Analysis performance of the deterministic structure of IAM preamble.

In this section, several preamble structures presented in chapter 3, i.e. IAM-C and IAM-R, are employed to analyse the performance of channel estimation while the system parameters are detailed in Table 4.3, and the LOS channel gain has been considered as the one calculated in chapter 3. In such comparison, the system performance with shortening and non-truncated Flip-FBMC models are compared with Flip-CP-OFDM format. For optical OFDM, only 1 point CP is required to overcome the ISI impact, and a single tap zero forcing equalizer with a single complex block of training symbol is deployed for signal estimation, as detailed in Table 4.3.

Table 4.3. The system parameters for channel estimation.

Parameters	**Value**	
Utilized technique	Flip FBMC	Flip OFDM
IFFT size	64 samples	
Pilot duration in symbols	1.5	1
Constellation mapping	4-QAM	
Prototype filter	IOTA	Rectangular
Channel tap gain	1-Direct LOS	
CP size	0	1
Overlapping factor (*K*)	4	None
Equalization size	1-Tap based CE of IAM-R/C	1-Tap
Number of transmitted symbols	80 symbols	

As can be observed in Figures 4.11(a) and (b), the estimation process to combat the inherent interference with Flip-FBMC mechanism is evaluated based on two types of IAM structure, i.e. IAM-R and IAM-C with 1.5 complex-block duration, where the configurations of such sequential pilots are detailed in chapter 3. The first and third zero blocks T_{m_0,n_0-1} and T_{m_0,n_0+1} are deployed to avoid the interference from the previous frame and from the payload data, respectively. The middle block of IAM sequence T_{m_0,n_0} is loaded with the maximum value to suppress the IMI impact, where the -

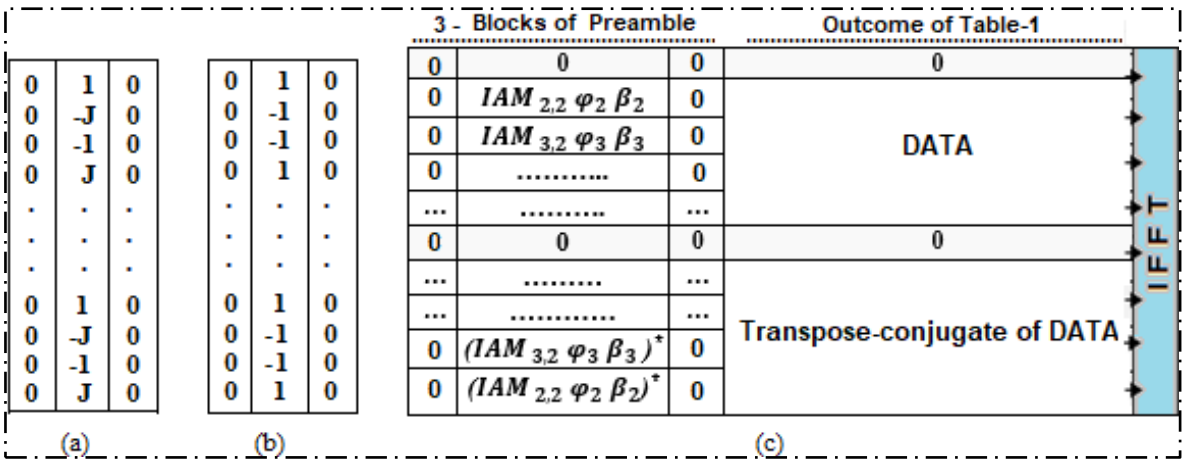

Figure 4.11. Preamble structures for the (a) IAM-C and (b) IAM-R sequence and (c) the frame configuration for the optical FBMC- based TMUX configuration for VLC system.

channel frequency response of estimating the transmitted Flip-FBMC signal with IAM, can be calculated from equations (3.19) and (3.20).

We have assumed 80 baseband data blocks to be conveyed over indoor LOS of VLC system. This assumption drives to an overhead of 1.55% residual tail, based on the tail-shortened signal, and almost identical throughput to CP of one sample for Flip-OFDM system. Whereas it offers approximately 5.7% overhead blocks for a nontruncated data-packet, as observed above in Figure 4.9. In real time transmission, it is noteworthy mentioning that the achievable high data-rate is restricted by LED, due to the 3 dB modulation bandwidth of commercially available LEDs is only several MHz [142]. For such reason, the LED-limited modulation bandwidth can be extended using pre- and post-equalization techniques [143].

In addition, based on a Monte Carlo algorithm and with respect to a traditional Flip-CP-OFDM system, the SNR/SER performance of each nontruncated and truncated Flip-FBMC technique has been evaluated by using IAM-R and IAM-C preamble sequence in estimating the signal quality. Besides, a single tap ZF equalizer is deployed to nullify the effect of LOS channel at the output of the AFB, which can be determined according to [141] as follows:

$$A_{m,n}^{\text{estimated}} = \text{Re}\left\{ \left(\underbrace{\left\langle Y(k), f_{m,n}(k) \right\rangle \downarrow_{\frac{M}{2}}}_{\text{AFB\_output}} \hat{H}_{m,n}^{-1} \right) \underbrace{e^{-j\frac{\pi}{2}(m+n)}}_{\varphi_{m,n}^{*}} \right\} \tag{4.14}$$

As presented in Figure 4.12, the non-shortened/truncated Flip-FBMC designs with IOTA profile of K = 4, and the conventional Flip-CP-OFDM are evaluated in terms of SNR vs. SER with 4-QAM modulation order. The IAM-C type based on Flip-FBMC system delivers 1.7 dB SNR gain over the IAM-R at 10^{-3} of SER region, and 1.8 dB SNR gain with compared to Flip-CP-OFDM system at 10^{-5} of SER. It is worth mentioning that the Heisenberg factor application in shortening tails has not been demonstrated before. Hence, the tail-shortened of Flip-FBMC signal using IAM-C type offers a superior SNR gain of approximately 1.5 dB at SER= 10^{-3}, which decreases with increasing SNR values to reach 1 dB at 10^{-5} SER compared to optical OFDM format results.

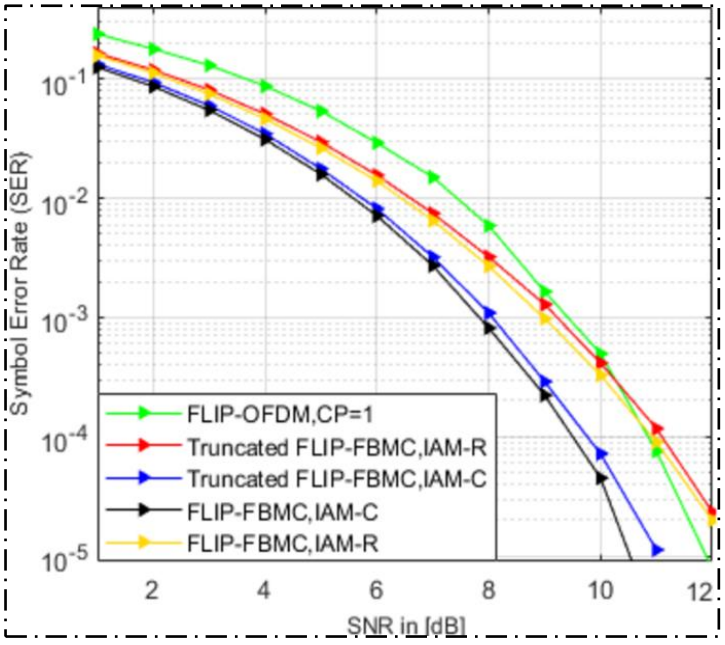

Figure 4.12. SER comparison between the truncated Flip-FBMC scheme and Flip-FBMC using CE-based IAM-R/IAM-C compared with Flip-OFDM of 1-CP in LOS VLC-channel.

However, the superior error performance of IAM-C preamble belongs to the high power of pseudo-pilot $T_{m_0,n_0} + jT_{m_0,n_0}^{\text{Pilot imaginary interference}}$, where the interference weights $jT_{m_0,n_0}^{\text{Pilot imaginary interference}}$ are computed in advance and saved at the receiver with the aid of equations (3.21) to (3.23) for the interference coefficients FBMC, that drives to increase the estimating accuracy of received message. Moreover, the degradation performance based on the deterministic preamble sequence of IAM-R compared to that in IAM-C is due to the required pseudo-pilots in the IAM-C, which have a larger magnitude than those in IAM-R and hence effectively mitigate the impact of IMI and the added Gaussian noise. Consequently, the transmission quality is promoted further with the preamble pilots-based IAM-C sequence.

On the other hand, the analysis reveals that the preamble pilots-based IAM-C is slightly impacted by the hard truncation of a transmitted burst in contrast to the nontruncated version, while a shortened version for estimating the received signal by using IAM-R exhibits an almost-identical SER performance to a nontruncated model using IAM-R because the lower magnitude of pseudo-pilots with compared to the magnitude of IAM-C reference symbols.

Therefore, such performance demonstrates our proposed approach as a promising alternative technique to optical OFDM for VLC systems. Thereby, the presented design can efficiently support signal transmission over free space link-based LED, indoor optical wireless communications and can be broadly deployed in next generation optical applications to enhance IM/DD passive optical network (PON) systems.

4.6. Analysis of Flip-FBMC structure based on *M*×*K* filter length.

Although the Flip-FBMC based *M*×*K*+1 filter length offers a promising solution for indoor IM/DD communication links, the property of low latency is a crucial feature in several emerging services such as the Tactile Internet (the next evolution of the Internet of Things) [144]. Therefore, the Flip-FBMC signals will be investigated based on a shorter prototype pulse function length of *M*×*K*, and identify its implications in terms of the TMUX response and system throughput rate.

The length of transmitted FLIP-FBMC data-packet when a (*M* × *K*) long filter is employed can be given as:

$$\text{Flip-FBMC}_{\underbrace{(\text{M}\times\text{K})}_{\text{Length}}} = 2\left(IFFT_{\text{Size}}\left(N + K - 0.5\right)\right) \tag{4.15}$$

Regarding to the spectral efficiency, as stated in equation (4.15), the imposed system penalty is minimized to (*K* - 0.5) redundancy blocks, which is doubled to (2× (*K* - 0.5)) overhead IFFT-blocks due to the flipping stage, and with respect to the length of Flip-OFDM burst. Whereas the reconstructed delay with the associated (*M* × *K*) filter length can be expressed as:

$$\Delta\Upsilon_{\underbrace{(\text{M}\times K)}_{Length}} = \frac{2}{IFFT_{\text{Size}}}\left(M \times K - IFFT_{\text{Size}}\right) \tag{4.16}$$

Compared to optical FBMC with (*M* × *K*+1) filter length, the spectral efficiency and system latency are significantly minimized, where the TMUX response is reduced (2*K* to 2*K* – 2) by two factors at the output of AFB processing blocks. Whereas the spectral efficiency is enhanced by (2×IFFT) blocks (the penalty reduction at the flipping stage is satisfied as a result of transmitting 7 overhead blocks instead of 9 redundancy symbols).

For such reason, to minimize the implications of overhead blocks at both ends of the bipolar-FBMC
burst of 7 overhead blocks (tails-penalty of 2×3.5 extra), a tail-shortening approach based on hard truncation mechanism is applied at both ends of data packet to support next generation networks requirements of high data-rate transmission and low latency application systems. Hence, based on ($M \times K$) pulse length, novel shortening values are delivered by discarding 1 and 1.5 IFFT-symbols at the inception and termination sides, respectively, of data packet. Thereby, the bipolar-truncated burst can be given as:

$$\underset{\text{Bipolar signal}}{X[k]} = \begin{cases} X[k], & M < k < M \times \left(N + K - 0.5\right) - 1.5M \\ 0, & \text{otherwise} \end{cases} \tag{4.17}$$

The truncated bipolar-signal with residue-overhead tails is doubled by the flipping process at transmission stage. Thus, the length of truncated FLIP-FBMC packet with the associated latency is formulated as:

$$\text{Trun.Flip-FBMC}_{\underbrace{(\text{M}\times\text{K})}_{\text{Length}}} = 2\left(IFFT_{\text{Size}}\left(N + K - 3\right)\right) \tag{4.18}$$

and

$$\underbrace{\Delta\Upsilon_{\underbrace{(\text{M}\times K)}_{Length}}}_{\text{at shortening model}} = \frac{2}{IFFT_{\text{Size}}}\left(M \times K - 2IFFT_{\text{Size}}\right) \tag{4.19}$$

As detailed in equations above, with respect to the nontruncated model, the resulting shortening version of the proposed system improves the transmission capacity by 5 symbol blocks and diminishes the reconstructed delay to $2K - 4$ factors. Besides, the chosen values limit the system penalty to only (2×IFFT) blocks at the conveyed Flip-FBMC subframes.

Overall, with compared to non-truncated model of $M \times K+1$ filter length, the use of $M \times K$ length-based Flip-FBMC enhances its latency by a factor of 2, and the spectral efficiency with 2 symbol-blocks. Whereas the use of $M \times K$ length-based tail-shortened Flip-FBMC signal enhances the TMUX-latency by 1 factor, and the spectral efficiency with 0.5 symbol-block compared to $M \times K+1$ filter length.

Regarding to select the optimum prototype pulse function based on the most popular filter, the characteristics of IOTA and PHYDYAS profiles have been assessed in terms of their figures of merit. The resulted lower redundancy tails with IOTA filter can also be interpreted according to the smaller sidelobe of IOTA impulse response (see Figure 4.13(b)), thereby it has a significant impact regarding to tail truncation process especially at high constellation mapping.

Nevertheless, PHYDYAS prototype filter, as presented in Figure 4.13(a), offers a sharpest spectrum delay, and the smallest sidelobe relative to main-lobe level, which leads to reduce the implications of ISI error and the spectral leakage. Thereby, the interference level in adjacent bands based on PHYDYAS filter is minimized by 5.6 dB compared to frequency response of IOTA filter. Thus, the increment in the main to side lobe ratio (MSLR) are determined as follows:

$$\Delta\text{MSLR} = \left(|P(e^{jw})|^2 - |P(e^{j0})|^2\right)_{PHYDYAS} - \left(|P(e^{jw})|^2 - |P(e^{j0})|^2\right)_{IOTA} \tag{4.20}$$

where $|P(e^{jw})|^2$ term is referred to the maximum level of sidelobe power, and $|P(e^{j0})|^2$ is the acronym for the main peck power. Whereas the ratio of main to side lobe is indicated for MSLR term.

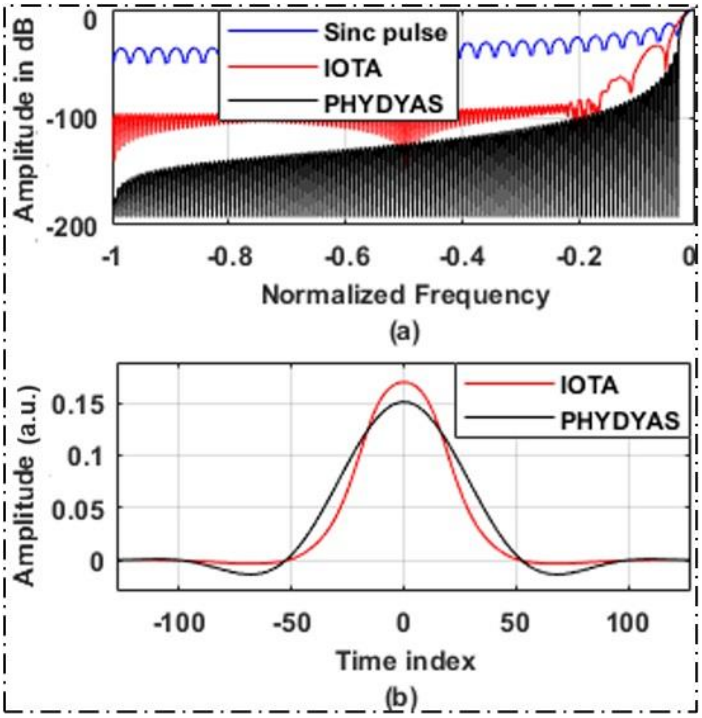

Figure 4.13. Energy distribution of Sinc pulse, IOTA and PHYDYAS filters for (a), and (b) Impulse response for IOTA and PHYDYAS prototypes filters.

Figure 4.13(a) shows the energy distribution for different subcarriers where a higher OOB emission belongs to the Sinc profile-OFDM, compared to the low OOB for IOTA and PHYDYAS profiles. Consequently, Martin filter profile offers a solid performance for various figures of merit, and represents an attractive choice for rejecting the leakage energy and thus, to obtain a reliable signal-to-interference ratio.

4.7. The value of flipping technique with FBMC modulation compared to DCO-FBMC system.

To verify the importance of using flipping technique on FBMC modulation, DCO-FBMC system is investigated over the level of induced imaginary interference for outside the first order zone. For the conventional DCO-FBMC/DCO-OFDM signals, a suitable DC bias is required to produce the non-negative signals, where the rest of negative amplitudes are clipped to zero, as given in equation (4.21):

$$SNR_{effecive} = \frac{\text{Fbmc signal power}}{\sigma_n^2 + \sigma_{upper}^2 + \sigma_{lower}^2} \tag{4.21}$$

where σ_{upper}^2 and σ_{lower}^2 noise components as the result of clipping the upper and lower signal peaks, respectively. For such scenario, the resulting clipping noise component based on DCO-FBMC data-packet has an influence in increasing the intrinsic interference level outside the first order neighbour zone, where signal estimation based on such zone is out of control the IAM preamble**,** as demonstrated below.

Hence, let $\delta_{m,n}^{m_0,n_0} = \sum_{k=-\infty}^{\infty} P_{m,n}[k]\, P_{m_0,n_0}^{*}[k]$ be an interference for outside 1-tap neighborhood symbols ((m_0, n_0) $\notin \Omega^{*}_{(1,1)}$), where $\Omega^{*}(1,1)$ term indicates to $\Omega_{(1,1)}$ - (0,0) zone. Extra attention is required to emphasize that in case of an optical FBMC signal is introduced based on a well localized prototype filter, the 98% of imaginary interference emerges from the first order zone, where the rest of interference values are normally neglected, since such zone cannot be covered using IAM sequence. Thus, the induced interference for outside $\Omega_{(1,1)}$ - (0,0) zone, is investigated over addition of several DC bias values to evaluate the level of interference $\Im$, as follows:

$$\{\Im\}_{B_{DC}} = \frac{\sum_{(m_0,n_0)\notin\Omega_{(1,1)}} |\delta_{m,n}^{m_0,n_0}|^2}{\sum_{(m_0,n_0)\notin\Omega_{(1,1)}} |\delta_{m,n}^{m_0,n_0}|^2 + \sum_{(m_0,n_0)\in\Omega_{(1,1)}-(0,0)} |\sum_{k=-\infty}^{\infty} P_{m,n}[k]\, P_{m_0,n_0}^{*}[k]|^2} \times 100\% \qquad (4.22)$$

According to equations (4.20) and (4.22), at a low addition of B_{DC} level, the noise component resulting from clipping the lower peaks is increased further, which drives to degrade the transmission quality. In such a perspective, a degradation in the quality of estimating signal is not only due to increasing the noise term arisen from clipping the σ^2_{lower}, but also leads to increase the interference level for (m_0, n_0) $\notin \Omega^{*}_{(1,1)}$ zone, which cannot be controlled by using IAM sequence.

Although such induced interference can be reduced by increasing the addition level of B_{DC} values, as illustrated in Figure 4.14, an inefficient system in terms of high optical power results for a given scenario. Consequently, an extra drawback with the unipolar FBMC signal using DCO technique is imposed, with respect to a negligible $\delta_{m,n}^{m_0,n_0}$ impact for Flip-OFDM and Flip-FBMC packets, since the latter has $\sigma^2_{lower} = 0$.

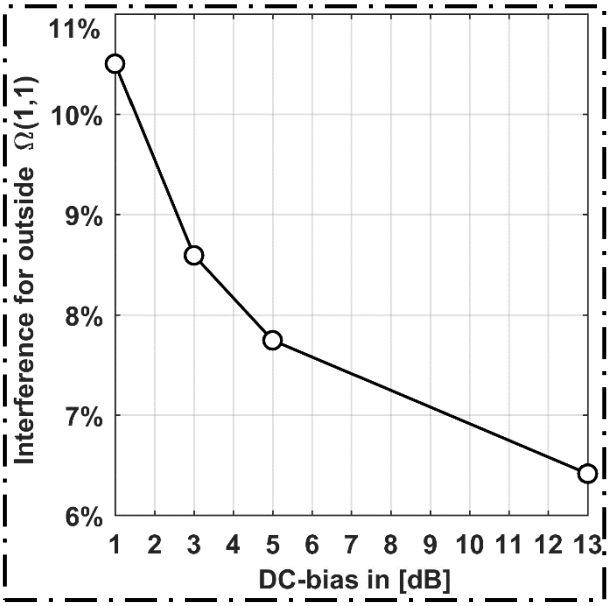

Figure 4.14. Imaginary interference level for outside the first order zone of transmitting only A_{m_0,n_0} =1 through PHYDYAS filter, vs DC bias levels for DCO-FBMC signal.

Consequently, with compared to DCO-FBMC format, where a significant reduction in estimating level is captured. Since such zone is induced with an uncontrollable interference by IAM

sequence, it must be emphasized on the value of deploying flipping process with FBMC modulation to avoid the impairment of induced imaginary interference outside the first tap neighborhood zone.

4.8. The function of multitap equalization to minimize the implications of IMI.

In section 4.6, the proposed design was simulated using a low constellation mapping of 4-QAM order and short delays propagation links for the sake of minimizing the IMI effects, where only 1 point length of CP is required to combat ISI influence. Therefore, such evaluation is not sufficient to assess the implications of imaginary interference, due to IMI impact that has been considered as one of the main drawbacks in FBMC signals dominates at high modulation orders over propagation-links with high delays profile, as detailed in chapter 3.

For such reason, the system comparison will be run over a channel with high delays profile, and three-taps equalizer that can be required to suppress the interference effect. Thus, the receiver side of Flip-FBMC scheme is updated by employing multitap equalization process, as shown in Figure 4.15.

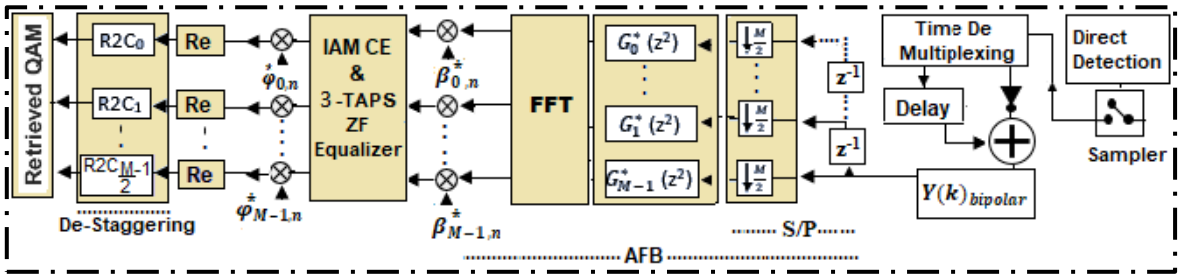

Figure 4.15. TMUX structure of received optical FBMC based on 3-taps system equalization.

In OFDM signals, if a delay spread of the imposed channel within the duration of transmitted symbol and the feasible synchronization error, the channel equalization can be done by deploying subcarrier-wise multiplication by a complex coefficient value (single tap equalizer). Such technique can be directly carried out in FBMC system in case of a channel with flat fading impact.

However, a multitap based subcarrier-wise equalizers could be required to compensate the resulted interference of the not-well time localization of the filter bank waveforms. Before taking the real part of the subchannel signals, the equalizer can perform equalization at several frequency points. For example, if the equalizer is a 3-tap complex FIR filter, three-frequency points within the subchannel can be perfectly equalized, using the zero-forcing (ZF) technique.

As presented in Figure 4.16, the transfer function of a 3-taps finite-impulse response (FIR) equalizers of subchannel *m* and time *n* can be given as:

$$H_{Equalization}(\square) = C_{m,n}^{(-1)}\square + C_{m,n}^{(0)} + C_{m,n}^{(+1)}\square^{-1} \tag{4.23}$$

The weights of filter $C_{m,n}^{(s)}$ that belong to s = {−1, 0, 1}, can be determined by assessing the transfer function, which is set to the desired response, at the selected frequency points. The value of +1 refers to the upper sub-band edge, while s = -1 denotes the lower sub-band edge and, the center of sub-band is referred by s=0. Hence, the target values can be expressed as follows [145]:

$$X_{m,n}^{(s)} = \varpi \frac{\left(H_{m,n}^{(s)}\right)^*}{\left|H_{m,n}^{(s)}\right|^2 + \wp} \tag{4.24}$$

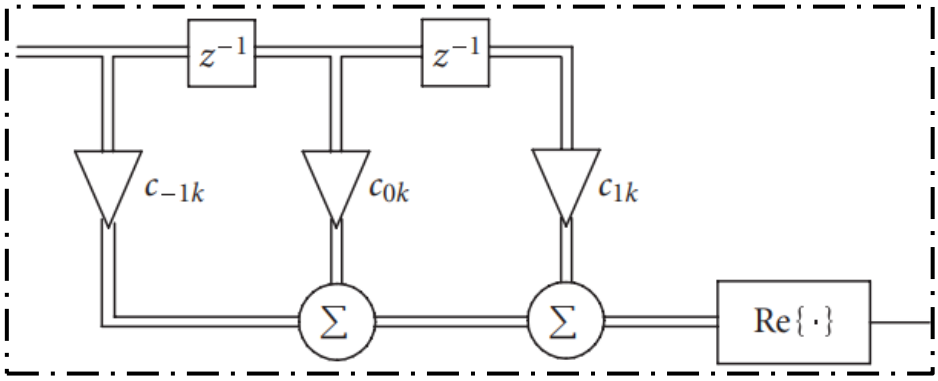

Figure 4.16. Diagram of three taps subcarrier equalizer based on FIR filter [146].

The $H_{m,n}^{(s)}$ term being the estimated channel frequency response of subchannel *m* and time *n*, while ϖ and $\wp$ terms are scaling factors with values of 1 and 0, respectively, in ZF equalizer. Therefore, from the target points of equation (4.24), the filter weights can be computed as follows [145]:

$$C_{m,n}^{(-1)} = \frac{X_{m,n}^{(0)} \square^{-2} - X_{m,n}^{(1)} \square^{-1}(\square^{-1}+1) + X_{m,n}^{(2)} \square^{-1}}{1-\square^{-1}-\square^{-2}+\square^{-3}} \tag{4.25}$$

$$C_{m,n}^{(1)} = \frac{X_{m,n}^{(0)} \square^{-1} - X_{m,n}^{(1)} \square^{-1}(\square^{-1}+1) + X_{m,n}^{(-2)} \square^{-2}}{1-\square^{-1}-\square^{-2}+\square^{-3}} \tag{4.26}$$

$$C_{m,n}^{(0)} = \frac{-X_{m,n}^{(0)} \square^{-1} + X_{m,n}^{(1)}(\square^{-2}+1) - X_{m,n}^{(2)} \square^{-1}}{\left(-1+\square^{-1}\right)^2} \tag{4.27}$$

The term $\square = e^{(jW_c)}$ with $-W_c$ and W_c being the lower and upper sub-band edge frequencies. Consequently, to enhance the interference power using ZF approach, the filter weights are set such that the achieved equalizer response compensates the channel response precisely at the prearranged frequency points.

The system simulation values are stated in Table 4.4, where a cubic room with (5.0m, 5.0m, 3.0m) (length, width, height) is considered with a LED located at the center of ceiling, i.e. coordinates

(2.5m, 2.5m, 3m) and a PD located at (5.0m,1.0m, 0.0m) coordinates at the floor-corner and other simulation parameters are adopted according to [147].

Table 4.4. Simulation system parameters

Parameters	Value	
Utilized technique	Flip-FBMC	Flip-OFDM
modelled as AWGN	Influences of shot & thermal noise	
Lens refractive index	1.5	
Constellation mapping	4-QAM	
Area of PD	1 cm^2	
Propagation Model	LOS and Multipath	
IFFT size (*M*)	256 samples	
Constellation mapping	4-QAM	
Prototype filter	PHYDYAS	Rectangular
Equalization size	1 and 3-Taps	1-Tap
Overlapping factor (*K*)	4	...
Filter length	$M \times K$	...
Guard band	0	5 samples
Pilot blocks	1.5 (IAM-C)	1
CP size	0	40 samples
Baseband data blocks (*N*)	30	

As illustrated in Figure 4.17, the gain of the first three non-LOS channel is given as: 0.467×10^{-6}, 0.211×10^{-6} and 0.107×10^{-6}, respectively, where the LOS propagation scenario leads to 1.232×10^{-6} amplitude impulse response.

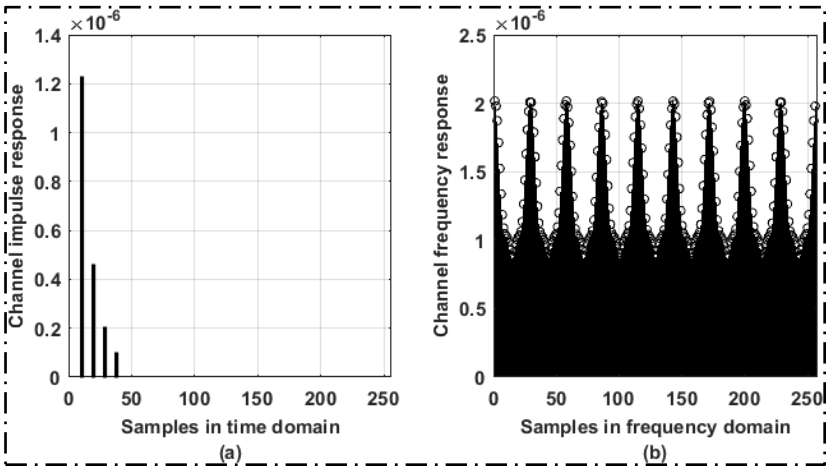

Figure 4.17. (a) Impulse response, and (b) frequency response for a channel of multipath propagations

Increasing ISI level leads to induce the impact of IMI on the retrieved FBMC signal, where the influence of such assumption can be interpreted according to the following scenarios. The channel impulse response of Figure 4.17 (a) corresponds to the transmitted-symbol time lower than the delay spread. In Figure 4.17 (b) the channel frequency response corresponds to a bandwidth (BW) of transmitted-symbol larger than the Channel coherence bandwidth.

As detailed in Table 4.4, numerical simulations are executed based on the realistic experimental parameters of [21], where 40 samples of CPs (to suppress the ISI influence), 5 guard-band samples and a single training reference block are employed for optical OFDM signal, whereas a 1.5 complex training pilots of IAM-C with three-taps equalizer based on PHYDYAS profile are deployed in Flip-FBMC system. In such simulation, the conventional Flip-CP-OFDM and Flip-FBMC systems are assessed in terms of SNR vs. SER, where a baseband of 30 data blocks, 256 samples of IFFT length and a single block for synchronization purposes are deployed to evaluate the transmission quality.

Thereby, for such realistic-experimental values, the increment in flow rate for the non-truncated model of Flip-FBMC signals with $M\times K$ PHYDYAS length is limited to only ≈ 4% with respect to Flip-OFDM of 40 samples of CP. On the other hand, the tail-shortened version, as a result of the hard truncation of the minimum tails-energy, offers ≈ 11% increment in the spectral efficiency with compared to Flip-CP-OFDM.

Based on a single tap equalizer, as observed in Figure 4.18, although Flip-CP-OFDM scheme shows enhanced performance over Flip-FBMC system at SER of 10^{-4} as a result of the added CP samples, the proposed design outperforms the optical OFDM format at low SNR zones, due to the role for high amplitude power of $T_{m_0,n_0} + jT_{m_0,n_0}^{\text{Pilot imaginary interference}}$ term in minimizing the noise effect, over LOS and multipath propagation links. For such scenario, the system degradation at high SNR region is due to the influence of inherent interference, where the constrained condition of channel maximum delay, $\mathrm{Re}\{I_{m,n}\} \cong 0$, is violated.

Thereby, on a sub-carrier basis, the equalization based on a single tap is not sufficient to suppress the IMI over a channel with high delays profile.

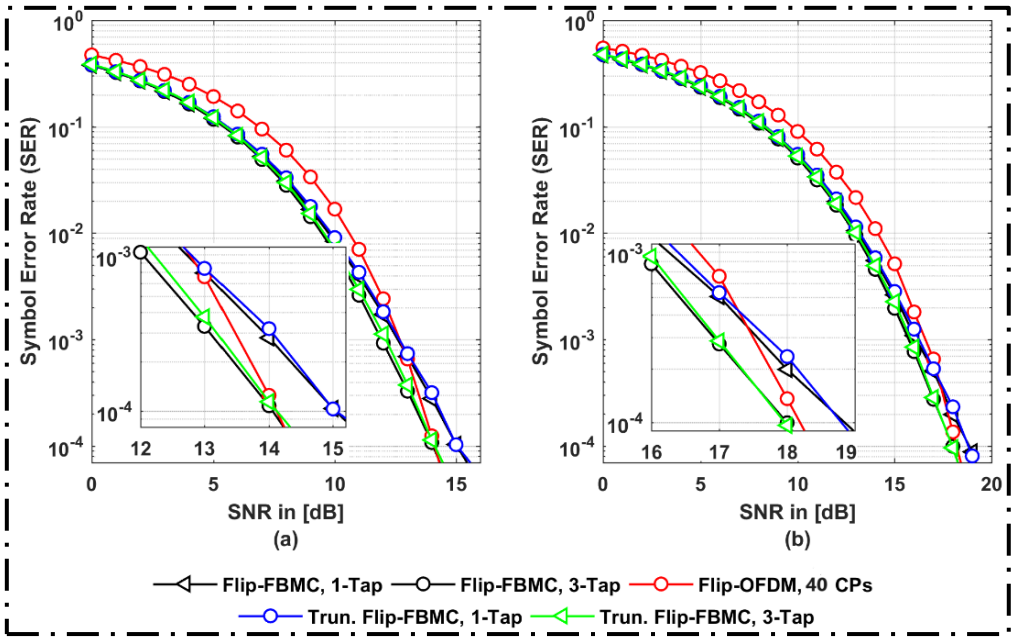

Figure 4.18. SER vs. SNR for the original Flip-FBMC and the tail-shortened signal with PHYDYAS filter by using 1 and 3-taps equalization compared with optical OFDM of 40 samples for various transmission scenarios: a) LOS and b) multipath propagations.

On the other hand, a design of multitap equalization plays a crucial role in mitigating the IMI implications over different propagation links, as demonstrated in Figure 4.18. from equations (4.24) - (4.27), the Flip-FBMC signal with IAM-C preamble is estimated by deploying three-taps equalizer and interpolation, where such design shows a significant ability in mitigating the SNR gains and combating the influence of intrinsic interference. In such performance, and in contrast with the conventional unipolar OFDM performance, the Flip-FBMC model with multitap equalization offers 0.7 dB SNR gain at 10^{-3} of SER. Whereas at high SNR zone, an identical error is satisfied for both systems at LOS/multipath environments, as shown in Figure 4.18. Furthermore, with compared to Flip-FBCM design of a single tap equalizer, the 3-taps equalizer for estimating optical FBMC signal delivers 1 dB SNR gain at 10^{-4} of SER for LOS and multipath propagation-links.

From the obtained outcomes, and with respect to the tail-shortened Flip-FBMC model, the simulation results validate the proposed shortening version, and depict almost identical SNR/SER performance to non-truncated model (see Figure 4.18).

4.9. Conclusions

This chapter presents the design of a Flip-FBMC scheme with a biorthogonal form to provide sufficient flexibility for future indoor networks. The optical FBMC signal employs different prototype filters, i.e. IOTA and PHYDYAS profiles, based on several overlapping factors and ($M \times K$) and ($M \times K+1$) filter lengths. Regarding to a length of ($M \times K+1$), the analysis revealed that the spectral efficiency of the proposed design suffers from the ramp-up and the ramp-down at the beginning and the end, respectively, of the data packet. Thereby, the Flip-FBMC signal imposed a penalty of 9 extra transmitted symbols compared to the Flip-OFDM burst besides, the ($2\times K$) factors in TMUX-latency. Consequently, the possibility to maximize the throughput rate and minimize latency has been investigated for the first time through a tail shortening approach.

Hence, the simulation analysis using IAM-C type over LOS VLC link under low delays profile presented 1.5 dB SNR gain at 10^{-3} SER over IAM-R type, and 1.0 dB SNR gain at 10^{-5} SER compared to Flip-OFDM format with a single point CP. Although the obtained results confirmed the effectiveness of truncation process in limiting the spectral efficiency and reconstructed delays to only 2.5 extra IFFT blocks and ($2K$ - 3) factors, respectively, the estimating signal with Flip-FBMC based on IAM-C preamble only shows a slight impact by the truncated burst compared to the nontruncated model.

On the other hand, for the sake of improving the transmission performance, the proposed system has been investigated with ($M \times K$) filter length. In such scenario, with compared to non-truncated model of $M\times K+1$ filter length, the use of $M\times K$ length enhanced the TMUX-latency by 2 factors and increased the throughput rate with 2 IFFT blocks. Furthermore, the use of the truncated-tail burst contributed to improve the spectral efficiency with 0.5 symbol-block, and minimized the TMUX-response by 1 factor, compared to a transmission with packet of $M\times K+1$ filter length.

To assess the impact of inherent interference, a channel with high delays profile has been considered. Compared to Flip-OFDM with 40 samples of CPs, the Flip-FBMC system showed a degradation performance at high SNR region, where the violation in the constrained condition of channel maximum delay $\mathrm{Re}\{I_{m,n}\} \cong 0$ is held. Therefore, the signal equalization based on a single

tap is not sufficient to suppress the IMI impact over several LOS and multipath links of high delays profile.

For such implications, the designed system has been updated by using three-taps equalizer to optimize the estimation accuracy. At low SNR regions and compared to Flip-CP-OFDM scheme, the Flip-FBMC system with 3-taps equalizer offered 0.7 dB SNR gain. While 1 dB SNR gain and identical error with respect to Flip-FBMC with 1-tap equalizer and unipolar OFDM, respectively, are delivered over different propagation links.

Based on real experimental parameters, the possibility to improve the transmission performance has been reported, where the increment of ≈ 4% in throughput rate has been optimized to ≈ 11% using a tail-shortening mechanism. The multitap equalization for a tail-shortened signal exhibited almost identical performance to non-truncated model, and hence verified the optimum redundancy blocks that have been discarded at both ends of residual tails.

Moreover, extra attention is required to emphasize the value of flipping technique with FBMC modulation to avoid the interference implications outside the first order zone. Hence, the first theoretical analysis for estimating the impact of induced imaginary interference outside the first order zone has been introduced with compared to DCO-FBMC system. Thus, such investigation revealed a serious degradation in estimating accuracy, which is more evident when reduced values of the added DC-bias since that zone cannot be covered using IAM preamble.

Chapter 5. Advanced techniques for optical FBMC signals transmission

You cannot force ideas. Successful ideas are the result of slow growth. Ideas do not reach perfection in a day, no matter how much study is put upon them.

– Alexander Graham Bell

This chapter proposes to exploit the well time-frequency localization property of extended Gaussian function in non-coherent optical systems, such as indoor VLC links. This chapter presents the first theoretical analysis of the impact of several spreading factors over low to high constellation mapping and LOS/multipath propagation links. Such investigation is performed based on a trade-off between the optimal reconstruction of signal quality and spectral features to assess the Flip-FBMC robustness against the influence of residual interference, compared to Flip-CP-OFDM system performance. Moreover, this chapter identifies the maximum allowable spreading parameter in retrieving the transmitted optical FBMC signals accurately based on the localization property and MSLR level. Additionally, the implication of tuning the spreading parameters in terms of the confinement level of interference power at the first order neighborhood blocks is also included in this section. In addition, the section presents the implications of high peak power using IAM preamble over the illumination purposes and the restricted dynamic range of LED, compared to another advanced FBMC system, i.e. Flip- FBMC signal based on frame repetition model. Besides, the level of estimation accuracy based on the metric of clipping distortion and induced imaginary interference outside the first order zone is also included in this section.

5.1. Role of pseudo pilot-values in enhancing the transmission accuracy based on the IAM-C sequence.

The transmission quality of multicarrier modulation based on FBMC signals essentially depends on the employed envelope function. Hence, as detailed in previous section, the main goal is to disclose the optimum structure of IAM preamble that yields the overall powers of complex pseudo pilots $T_{m_0,n_0} + jT_{m_0,n_0}^{\text{Pilot imaginary interference}}$ sufficiently high to promote the estimation quality of the retrieved signal.

Thus, different well-localized prototype functions in time and frequency domains are desirable in FBMC mechanism, such as PHYDYAS, IOTA, EGF and Hermite filters are considered in this chapter. The Hermite pulse function is primary proposed by Haas [148], where it represents the linear combination of Hermite Gaussian functions that verify the Nyquist-I criterion. Therefore, the coefficients of such pulse can be provided by polynomials of Hermite filter, where the impulse response of Hermite prototype filter can be defined as:

$$p(t)_{\text{Hermite}} = \left(1/\sqrt{T_0}\right) \exp\left(-2\pi(t/T_0)^2\right) \times \sum_{i=\{0,\ 4,\ 8,\ 12,\ 16,\ 20\}} A_i H_i(2\sqrt{\pi}(t/T_0)) \tag{5.1}$$

To evaluate the imaginary intrinsic interference at $\Omega_{(1,1)}$ - (0,0) neighborhood zone that emerge from transmitting a signal of A_{m_0,n_0} = 1 over a noiseless channel effect, several pulse shaping filters are deployed to assess the most powerful interference that is integrated in the first tap neighborhood block zone, as detailed in Table 5.1. From such zone, as high as possible interference powers at $\Omega_{(1,1)}$ - (0,0) of blue region (limiting the interference Impact over the 1-tap neighbourhood symbols), better estimation can be delivered with the use of pseudo pilots based IAM preamble, as demonstrated below.

Table 5.1. Amplitudes of residual interference by only transmitting A_{m_0,n_0} = 1 in Flip-FBMC system using IOTA, PHYDYAS and Hermite filters, and based on $M\times K+1$ filter length of K = 4 with n_0 even time-index

IOTA filter	n_0-1	n_0	n_0+1
m_0-1	$-0.2173j$	$-0.4585j$	$-0.2173j$
m_0	$0.4378j$	1	$-0.4378j$
m_0+1	$-0.2173j$	$0.4585j$	$-0.2173j$
PHYDYAS filter	n_0-1	n_0	n_0+1
m_0-1	$-0.2058j$	$-0.2393j$	$-0.2058j$
m_0	$0.5644j$	1	$-0.5644j$
m_0+1	$-0.2058j$	$0.2393j$	$-0.2058j$
Hermite filter	n_0-1	n_0	n_0+1
m_0-1	$-0.2281j$	$-0.4491j$	$-0.2281j$
m_0	$0.4369j$	1	$-0.4369j$
m_0+1	$-0.2281j$	$0.4491j$	$-0.2281j$

According to Table 5.1, the total power of pure imaginary interference (shaded values) using Hermite filter (2.40276) that confined in the 1-tap neighbourhood zone is much higher than the interference power based on PHYDYAS function (2.1809), while the intrinsic interference power-based IOTA filter (2.36307) is slightly lower with compared to Hermite filter, where such interference-levels are evaluated based on equation (5.2).

$$\sum_{\Omega_{(1,1)}-(0,0)} \left|\zeta_{m_0,n_0}^{m,n}\right|^2_{\text{Hermite}} > \sum_{\Omega_{(1,1)}-(0,0)} \left|\zeta_{m_0,n_0}^{m,n}\right|^2_{\text{IOTA}} > \sum_{\Omega_{(1,1)}-(0,0)} \left|\zeta_{m_0,n_0}^{m,n}\right|^2_{\text{PHYDYAS}} \tag{5.2}$$

The incrementing power in such confined interference drives to increase the level of complex pseudo pilots ($PLT_{m_0,n_0}^{\text{Hermite}} > PLT_{m_0,n_0}^{\text{IOTA}} > PLT_{m_0,n_0}^{\text{PHYDYAS}}$), which leads to enhance the estimation accuracy, as observed in Figure 5.1.

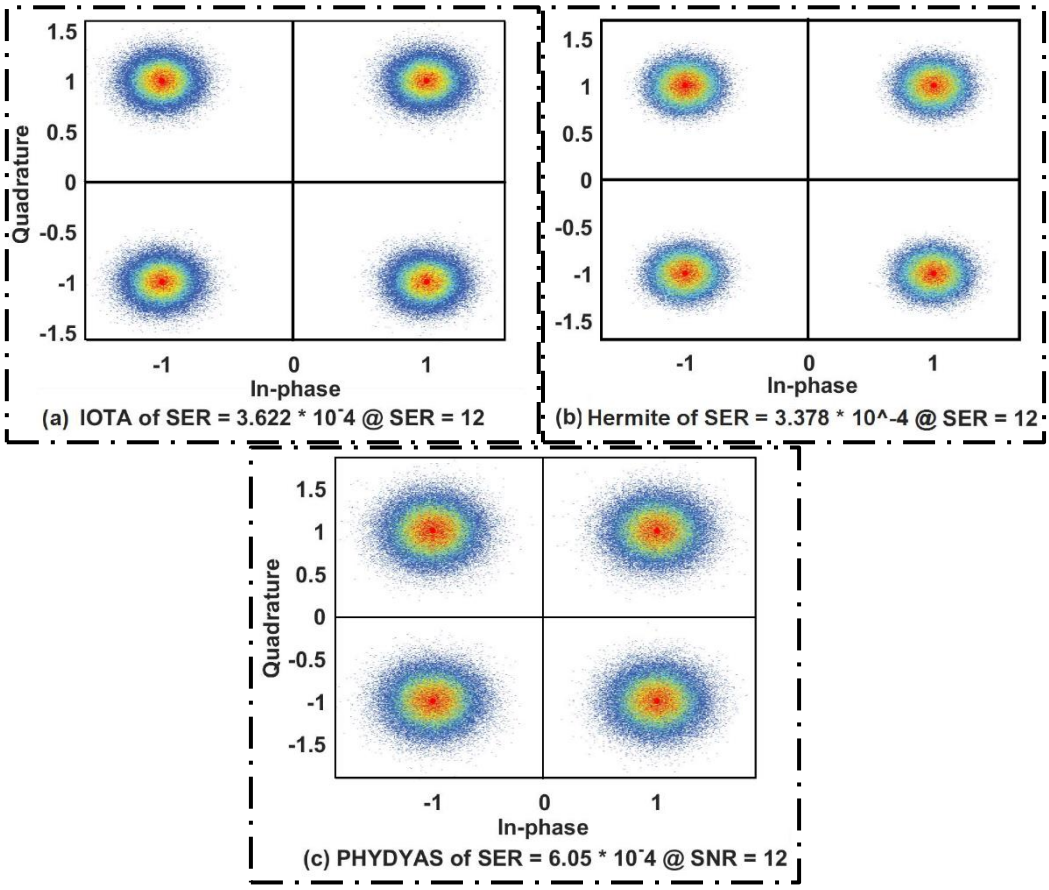

Figure 5.1. Constellations of 4-QAM of retrieved signals based on AWGN link and by using IAM-C preamble to show (a) the performance of IOTA filter, and (b) Hermite SNR/SER gain with compared to PHYDYAS function in (c).

As exhibited in Figure 5.1, the impact of confining high interference power (blue zone) leads to increase the accuracy of estimating Flip-FBMC signals by using Hermite pulse function over other used filters. A slightly enhanced performance using Hermite filter than IOTA profile belongs to the Hermite impulse response, which can confine higher power (high powers of pseudo pilots). While concentrating the low energy according to an envelope function around its center of PHYDYAS pulse, which drives to reduce the accuracy with compared to IOTA and Hermite profiles based on Flip-FBMC signal (higher sidelobe impulse function increases the interference power outside the first tap zone), as shown in Figure 5.2. Furthermore, lower side-lobe power in the impulse responses of Hermite and IOTA filters, with compared to PHYDYAS profile, leads to

enhance the truncation process mechanism (reducing the truncated power), as detailed in the next section.

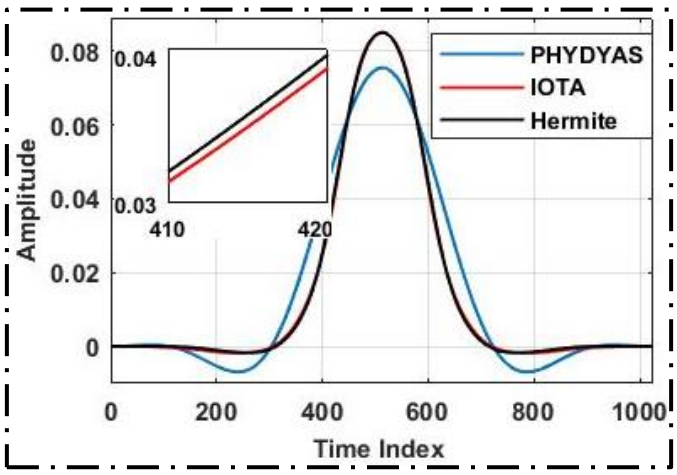

Figure 5.2. Impulse response for different filters of Hermite, IOTA and PHYDYAS profiles.

Consequently, IOTA and Hermite prototype filters represent an optimum choice for AWGN (a link with low delays profile) over a filter with low confinement power at 1-tap neighborhood symbols, such as PHYDYAS filter.

5.2. Analysis of Extended Gaussian function filter with Flip-FBMC signals.

The slightly enhanced performance using Hermite profile compared to optical FBMC using IOTA filter, is not sufficient to overcome the intrinsic interference over a link of long delays profile. IOTA filter is a special case of EGF pulse function with the frequency splitting between two consecutive sub-bands and the signaling interval time are chosen to have a value of $\frac{1}{\sqrt{2}}$ with $\alpha = 1$, where IOTA function can be determined as:

$$Z_{\mathrm{IOTA}}(t) = Z_{1,\ 1/\sqrt{2},\ 1/\sqrt{2}}(t) \tag{5.3}$$

Therebefore, another well localized time frequency prototype filter. i.e. EGF filter, is proposed for the non-coherent optical systems, where the time-domain expression of such pulse function can be calculated by equation (3.32).

The coefficients d_{k,α,v_0} with EGF function see equations (3.32) to (3.34), which based on limited values of *K*, can be determined according to Table 3.4. Regarding to a positive-real value of α, the spreading parameter plays a crucial role in determining the estimation accuracy, due to range of the spreading factor can be tuned with a range of $0.528v_0^2 \le \alpha \le 7.568v_0^2$ (see section 3.6).

The influence of such tuning contributes to control the shaping of the selected filter profile. Hence, as presented in Figure 5.2, the power within the main lobe of designed impulse response can be significantly increased with incrementing the value of α. Whereas, with a low value of tuning factor, such as $\alpha = 0.5$, the amplitude of sidelobe-impulse response is increased further. However, higher confinement powers within the main lobe drive to limit the intrinsic interference at the first order neighbourhood zone, where the mechanism of deterministic preamble, i.e. IAM-C sequence, can be efficiently deployed to minimize the interference impact, and hence an improvement in the level of estimation accuracy is verified in such transmission scenario.

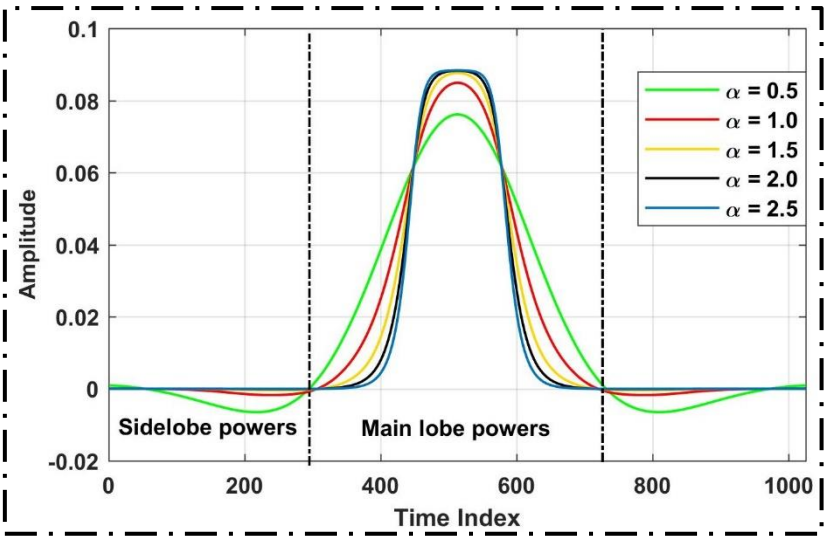

Figure 5.3. Impulse response for different spreading factor based on EGF profile.

To assess the accuracy level based on estimation process by using IAM-C preamble, the influence of restricting the most powerful inherit interference for $\Omega_{(1,1)}$ - (0,0) zone, as shown in Figure 5.3, is investigated. Thus, the optical FBMC based on tuning the spreading parameters of EGF pulse function is compared to Flip-OFDM signals over an AWGN channel and different QAM-constellation mapping, i.e. 4-QAM and 16-QAM orders.

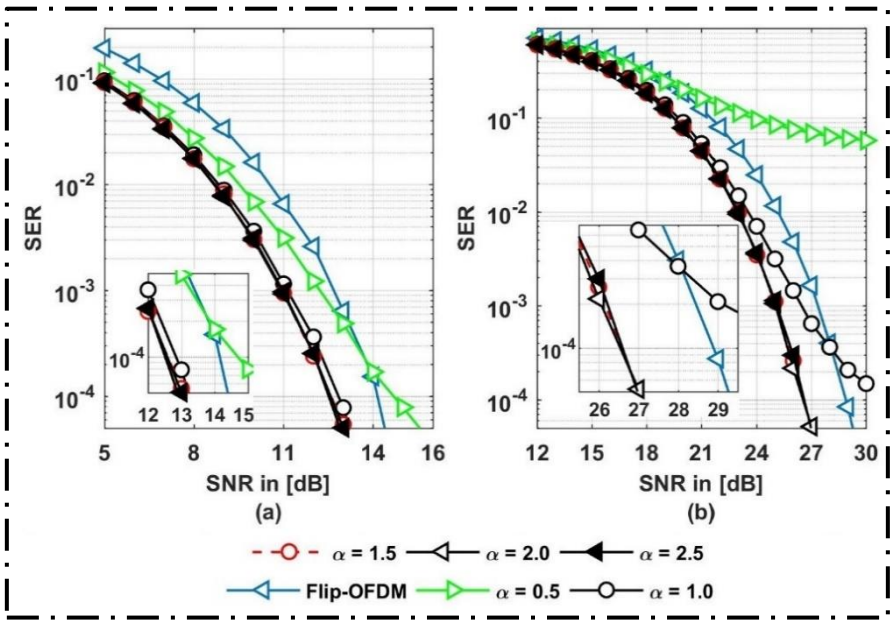

Figure 5.4, SER vs. SNR for the several profiles of spreading factors with EGF filter and Flip-OFDM system over: (a) 4-QAM order, (b) 64-constellation mapping.

Form the presented results, the performance drops with EGF of $\alpha = 0.5$ can be interpreted according to the spectral analysis of Figure 5.3, where the impulse response with high sidelobe powers drive to leak the interference out the $\Omega_{(1,1)}$ - (0,0) zone, Thereby, higher amplitude levels of intrinsic interference are spreading out the first order region, which cannot be covered using IAM-C training pilots, i.e. $\alpha = 0.5$, compared to high powers of pseudo pilots with other spreading factors. Thus, the highest degree of α, i.e. $\alpha = 2.5$, based on EGF profile shows a

superior performance over Flip-OFDM system. Hence, the significant role of PLT_{m_0,n_0} is reported, at high constellation mapping (64-QAM) in Figure 5.4(b), to supress the noise effect, where 2.2 dB SNR gain is achieved at SER of 10^{-4}, compared to a transmission based on OFDM technique. Extra attention is needed to emphasize that the degradation with IOTA filter ($\mathrm{EGF\ of}\ \alpha = 1.0$) at 64-QAM order because of the interference effect, confirms on the ability of EGF filter to supress the interference. Although such investigation offered a remarkable promoted performance with compared to other optical multicarrier systems, the influence of IMI appears with a minimum level in case of AWGN link. Besides, such analysis is only concentrated on the level of powerful $\zeta_{m_0,n_0}^{m,n}$ at $\Omega_{(1,1)}$ - (0,0) zone. Consequently, further spectral analysis based on several figures of merit is needed to verify the impact of tuning the spreading factor on the system performance using different degrees of channel delays. Therefore, the impact of noise floor between sub-bands, frequency response, maximum level of $\zeta_{m_0,n_0}^{m,n}$ at $\Omega_{(1,1)}$ - (0,0) region and Heisenberg uncertainty inequality (localization factor) are considered to identify the optimum spreading factor. Regarding to the implications of interference power p_{int} between sub-bands and, due to the lack of orthogonality between the subchannel, the impact response of noise floor is induced, and it can be calculated as given in [149]:

$$\mathrm{Noise}_{\mathrm{floor}} = 2p_{\mathrm{int}} \tag{5.4}$$

and

$$p_{\mathrm{int}} = 2\int_{-1/2M}^{1/2M} |G(f)|^2 \left(\sum_{m=1}^{M/2} \left| G(f + \frac{2m}{M}) \right|^2 \right) df \tag{5.5}$$

The frequency response of EGF filter is denoted by $G(f)$. From the above equations, by calibrating α using EGF profile, the p_{int} between different indices of sub-bands can be controlled, as captured in Figure 5.5. Consequently, in such analysis, an increment of the degree of α in the range $1 \le \alpha \le 3$

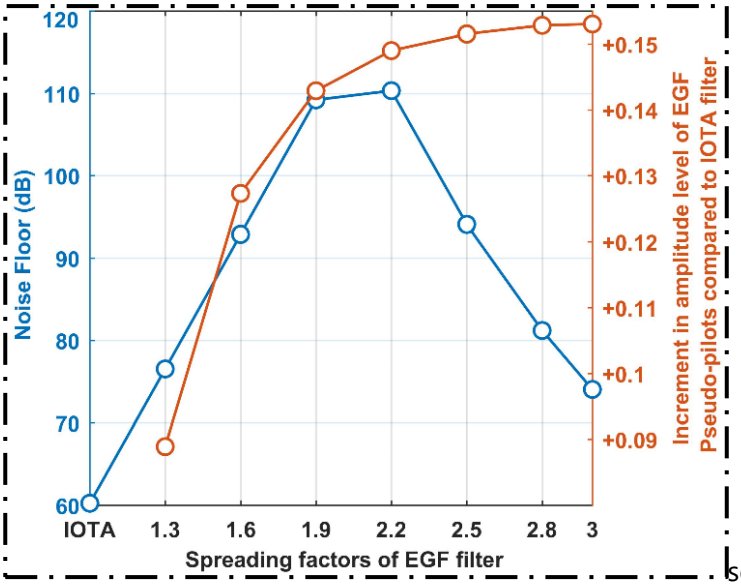

see

Figure 5.5. Absolute noise floor due to interference levels between subchannels (left axis) and increase in amplitudes of pseudo-pilots (right axis) for various spreading factors of EGF filter with respect to EGF of α = 1 (IOTA filter).

that observed in Figure 5.5, where high confining interference powers at the first order zone, and thus, an increase of the magnitude level of pseudo-pilots. Besides, the level of interference power between sub-bands can be limited further, where a maximum reduction of 110 dB is delivered by using $\alpha = 2.2$. Moreover, the estimation accuracy is enhanced further based on boosting α level beyond 60 dB compared to $\alpha = 1.0$ profile (IOTA filter).

5.3. Analysis performance of incrementing the spreading factor over several channel delays profiles.

The degradation in the quality of the retrieved signals over links with high delay profiles and/or high constellation mapping belongs to the IMI impact that is induced and inherent in FBMC mechanisms. To evaluate such assumption, the EGF filter with several spreading parameters is considered. An empty room with length = 3.0 m, width = 3.0 m and height = 3.0 m dimensions is considered. The spacing between the LED light source and two reflective walls are 2 m and 1.5 m, respectively. While the distance between PD surface and the bounce points are 1.6 m and 2.5 m. The responsivity of the PD (PIN 1601FS-AC) equals to 0.2 A/W @ 450 nm, and a value of 0.125 mm^2 for the PD area and other simulation parameters employed in [150].

Numerical simulations deploy the CPs of 12.5% samples to supress the ISI in unipolar OFDM signals, which are compared to Flip-FBMC with several EGF profiles over different propagation links, and low to high constellation mapping. In the following simulation, a single block for synchronizing purpose, the 100 blocks of baseband message and 256 samples of IFFT length are deployed in such analysis. From the observed SER vs. SNR comparison of the insets in Figure 5.6, the choice of $\alpha = 1.6$, at SER of 10^{-4} and high modulation order of 64-QAM, delivers SNR gains of 2 dB and 1 dB, respectively, with compared to $\alpha = 1.0$ (IOTA pulse) with Flip-FBMC signals. Besides, a superior performance gain is obtained by using the spreading factor of 1.6, at 4 and 16-QAM orders, with compared to Flip-CP-OFDM system.

Consequently, in such comparison scenario, the cancelation condition of residual IMI is satisfied, $\left(\mathrm{Re}\left\{I_{m_0,n_0}\right\} \approx 0\right)$, according to equation (5.6), due to the noise influence that is inversely proportional to the high amplitude levels of $PLT_{m_0,n_0}^{\alpha=1.6}$, and limiting the subchannel interference with high spreading factor, such as $\alpha = 1.6$ (higher $PLT_{m_0,n_0}^{\alpha=1.6}$ mitigates the noise impact, and hence enhancing the estimation accuracy).

$$A_{m_0,n_0}^{\text{estimated}} = A_{m_0,n_0} + \mathrm{Re}\left\{I_{m_0,n_0}\right\} \tag{5.6}$$

On the contrary, the Flip-CP-OFDM scheme outperforms the performance of unipolar FBMC with EGF filter, at high QAM modulation orders, i.e. 64-QAM, due to the multiple bounces that drives to spread the retrieved duration of propagation message. In such scenario, the restricted approximation assumption, $\left(\mathrm{Re}\left\{I_{m_0,n_0}\right\} \approx 0\right)$ based on IAM-C type, is violated, and no longer validated, due to the impact of residual interference that dominates in such indoor VLC-interference links, as shown in Figure 5.6(b and c).

However, it is worth noting that the ability to mitigating the IMI effect is more evident with IOTA filter compared to other values of spreading factor at high channel delays profile and QAM order, as presented in Figure 5.6(c), where the increment in SNR value does not subject with mitigation the IMI influence, i.e. a degradation of the quality of retrieved signal is obtained by $\alpha = 2.5$ EGF profile.

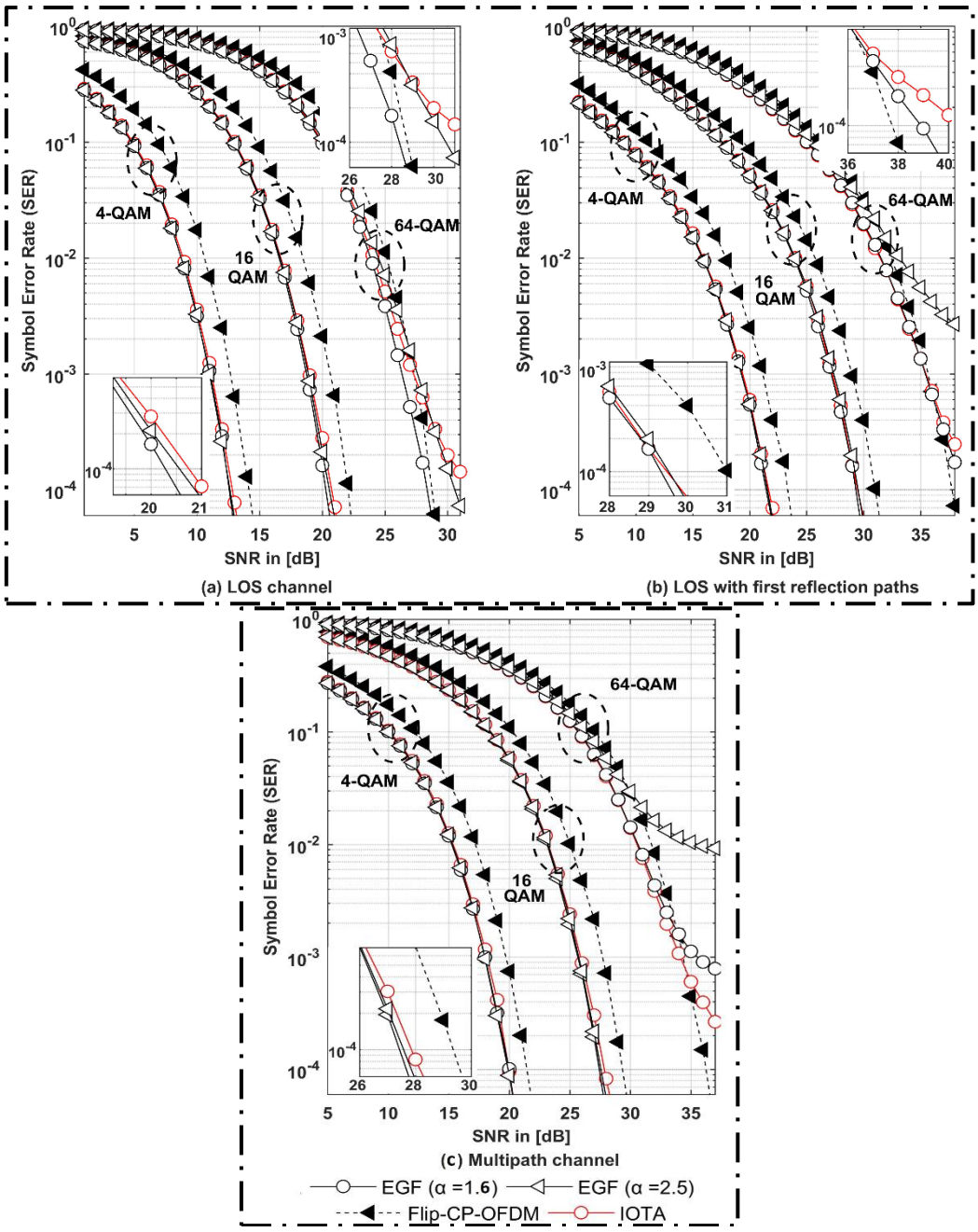

Figure. 5.6. SER vs. SNR for the proposed Flip-FBMC scheme using EGF filters with different spreading factors and Flip-CP-OFDM over different propagation links: a) LOS, b) LOS with first reflection paths and, multipath channel (LOS link with the first and second reflection paths) for (c).

On the other hand, extra attention is required to emphasize that based on the spectral analysis of Figure 5.5, higher spreading parameters, i.e. $\alpha = 1.6$ and $\alpha = 2.5$, offers a lower impact of noise floor, and a higher pseudo pilots than the IOTA filter $(\text{EGF of } \alpha = 1.0)$ performance. However, such analysis results are reflected with the SER vs. SNR simulation results, i.e. when the Flip-FBMC signals are conveyed over a channel of high delays profile and high constellation mapping, as revealed in Figure 5.6(c).

Therefore, further spectral analysis, i.e. the localization feature of filter profile and the interference level in adjacent bands, is required to analyse the IOTA performance with respect to other spreading parameters of EGF filter (see Figures 5.5 and 5.7). As detailed in section 5.2, the associated residual interference of equation (5.6) is mitigated further in case of using a well time-

frequency localized pulse function, such as the prototype filter with a localization parameter close to one ($\xi \approx 1$). From the equations (4.10 to 4.13), the optimum well-localized profile is achieved by using IOTA filter, where $\xi \approx 0.977$ is delivered, with compared to low values of $\xi \approx 0.9264$ and $\xi \approx 0.8155$, respectively, for $\alpha = 1.6$ and $\alpha = 2.5$ of EGF profiles.

Regarding the frequency response analysis that identifies the interference level in adjacent bands, as revealed in Figure 5.7, the lowest MSLR level of ≈ -33.9 dB is achieved by IOTA filter, followed by $\alpha = 1.6, \alpha = 2.5$ and $\alpha = 2.9$ of EGF profiles, respectively, of ≈ -24.3 dB, ≈ -19.1 dB and ≈ -17.9 dB MSLR levels. Furthermore, the worst MSLR level of ≈ -17.7 dB, which increases the interference level by 16.2 dB in adjacent bands, is obtained with $\alpha = 3.0$ with respect to IOTA-MSLR level. Consequently, from the obtained analysis results, the IOTA profile tends to be the optimum localized pulse function with the lowest MSLR level that has a significant impact for minimizing the IMI implications with the received signals under highly time spreading links, and high modulation order of 64, as presented in Figure 5.6(c).

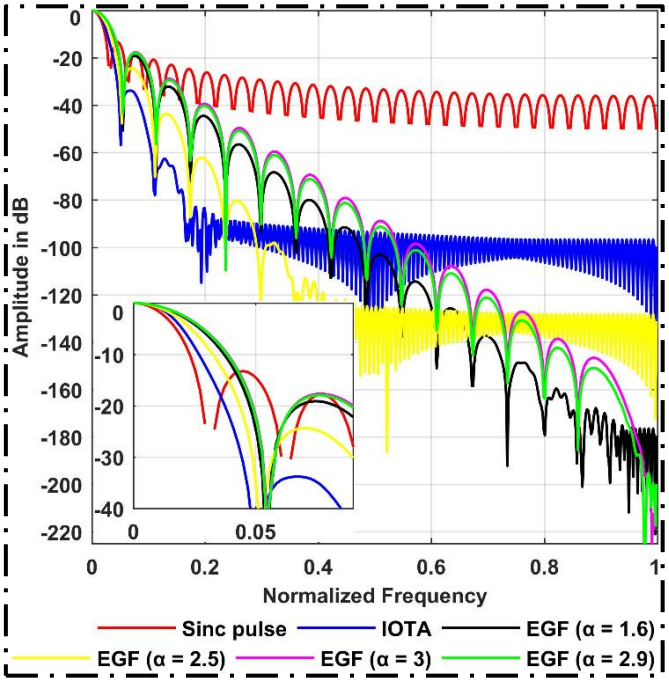

Figure 5.7. Frequency response of the EGF filter with several spreading factors compared to the distribution energy of OFDM signal.

Although higher α caused a degradation in MSLR level and the localized property, higher confining power of residual interference within the first order zone, it drives to increase the amplitude level of pseudo pilots and reducing the interference degree between adjacent subchannels. In such analysis scenario, the quality of system performance mainly depends on the link delay and QAM-order.

Therefore, regarding to Figure 5.1, over a link with minimum delay profile (ideal channel), where the performance quality is highly correlated with the increment value of spreading factor. Thereby, according to Table 5.2, EGF filter with (α = 2.9) performs the maximum allowable profile that can retrieve the transmitted signal successfully. On the other hand, the recovery of transmitted blocks using EGF filter of (α = 3.0), which degrades the MSLR level to beyond -17 dB, fails in retrieving the accurate values, such as a transmission of A_{m_0,n_0} = 1 with $\boldsymbol{n_0}$ even time-index, is retrieved as a noisy signal of 0.99994 (a.u.), as tabulated in Table 5.2.

Table 5.2. Intrinsic interference only transmitting A_{m_0,n_0} = 1 in Flip-FBMC system using EGF filter with $\alpha = 2.9$ and $\alpha = 3.0$ profiles, and based on $M \times k+1$ length of K = 4 with n_0 even time-index

For α = 2.9	$n_0 - 1$	n_0	$n_0 + 1$
$m_0 - 1$	$-0.0710\,j$	$-0.6924\,j$	$-0.0710\,j$
m_0	$0.1025\,j$	1	$-0.1025\,j$
$m_0 + 1$	$-0.0710\,j$	$0.6924\,j$	$-0.0710\,j$
For α = 3.0	$n_0 - 1$	n_0	$n_0 + 1$
$m_0 - 1$	$-0.0658\,j$	$-0.6945\,j$	$-0.0658\,j$
m_0	$0.0948\,j$	0.99994	$-0.0948\,j$
$m_0 + 1$	$-0.0658\,j$	$0.6945\,j$	$-0.0658\,j$

Moreover, another aspect regarding the use of high spreading parameter, which drives to concentrate the signal power around the envelope centre of used profile, as revealed in the analysis impulse response of Figure 5.3. Thereby, such perspective contributes to minimizing the power of redundancy blocks, and hence the transmission quality for tail-shortening applications can be supported further. Moreover, as presented in Figure 5.7, higher value of α using EGF filter drives to increase the system OOB emission, although it still offers better features in terms of rejecting the leakage energy compared to OFDM-Sinc profile.

However, it is worthy to highlight a significant drawback in using the deterministic preamble sequence of IAM-C type, where the resulting high peak power over the data load with using preamble blocks, which is further boosted with high α, is classified as a main penalty of Flip-FBMC signals. Such implication is restricted with deploying IAM-preamble for estimating the unipolar FBMC burst, while any arbitrarily training block can be deployed in estimating the OFDM data packet. Therefore, such perspective is a problem in particular VLC condition of illumination purpose, such as in dimming applications. Besides, at realistic transmission scenario, such impediment implies a serious implication for the restricted dynamic range of LED, where signal clipping and magnitude distortion are, as detailed in the next section.

Another crucial indication is related to the performance of Hermite prototype filter, which slightly outperforms the quality of retrieved optical FBMC signal based IOTA pulse function, as exhibited in Figure 5.1. However, such scenario is only valid over ideal channel (when the delay spread of propagation link is low) as the Hermite pseudo pilots is slightly higher than the one with EGF filter of α = 1.0. Nevertheless, the positive unipolar FBMC signal with IOTA function still provides an enhanced MSLR by almost 1 dB, with respect to the interference level in adjacent bands of Hermite profile.

Overall, in the following section, the tuning spreading factor of EGF profile with optical FBMC signal performs as a promising solution for inherent interference with several communication links. In such scenario, the increment in the amplitude of pseudo-pilots with the corresponding reduction of noise floor contribute to satisfy the IMI suppression over low-high constellation mapping and a link of low delay profile. Furthermore, the isotropic property of IOTA pulse (EGF with α = 1.0) with localization parameter factor of ≈ 1, and the lowest MSLR level of ≈ -33.9 dB provide a mitigation of the residual interference when the conveyed Flip-FBMC burst is propagated over higher constellations and over a channel profile of high delays.

5.4. Analysis of IAM preamble in realistic transmission scenario

In realistic transmission scenario, the high amplitude for the deterministic preamble sequence of IAM is refereed as the fundamental impairment for the restricted dynamic range of LED of indoor VLC system, since the peak power of such preambles are much higher than the data load as demonstrated below.

However, LED dynamic range constraint is considered as a fundamental impediment in IM/DD optical system, the use of flipping technique with unipolar FBMC signals has a significant value to avoid the component impact of noise as a consequence of clipping the lower peaks. Therefore, the baseband transmitted signal for Flip-FBMC data packet is updated by employing only the upper clipping level (saturation point) of a commercial LED, since in such conveyed burst the $\sigma^2_{\text{lower}} = 0$ as given blow:

$$\underbrace{X^{+}[k]}_{\text{Positive part}} = \begin{cases} X[k], & 0 \le X[k] \le C_U \\ C_U, & X[k] > C_U \\ 0, & \text{otherwise} \end{cases}$$

$$X^{-}[k] = \begin{cases} -X[k], & -C_U \le X[k] < 0 \\ C_U, & X[k] < 0 \;\&\; X[k] - C_U \\ 0, & \text{otherwise} \end{cases} \qquad (5.7)$$

$$\text{Negative part}$$

where the C_U term denotes the upper maximum value (the maximum current and the optical saturation point) of high power LED (OSRAM, SFH 4230), where beyond than C_U level, signal clipping and amplitude distortion are prevailing. From this perspective, the high power of modulated IAM preamble based on IAM-R and IAM-C types are systematically analysed regarding to the nonlinear transfer characteristics of LED for the sake of evaluating the transmission quality. Thereby, based on [27], the maximum permissible voltage of the upper-bound equals to 0.5 voltage that is adopted according to LED manufacturer data sheet, and the turn-on-voltage is zero due to the use of Flip-FBMC structure.

From the impulse response analysis for Figures (5.2 and 5.3), the IOTA and PHYDYAS profiles tend to be an attractive solution for mitigating the clipping distortion that restricts the usage of high constellation mapping and SNR.

The influence of clipping data packet is investigated using DCO-FBMC and unipolar FBMC with signal fillping. As observed in Figure 8, in case of using DCO technique, a first insight points out that the bipolar FBMC packet with a level of high amplitude is more evident with IOTA pulse function based on IAM-C preamble, due to the signal energy that concentrates around its center profile. Therefore, a minimized clipping signal can be delivered using PHYDYAS profile with IAM-R sequence according to the distribution powers of the main-lobe/sidelobe impulse response. In such scenario, Flip-FBMC signals with IOTA pulse based on IAM-C/IAM-R types expose to a severe clipping for the lower pecks for the sake of providing the non-negative burst. In other words, the implication of such amplitude is required to add higher B_{DC} level compared to PHYDYAS-B_{DC} level in order to achieve the unipolar format $\left(\left(B_{DC}\right)_{PHYDYAS} \square \left(B_{DC}\right)_{IOTA}\right)$, thereby resulting a system of an inefficient power.

Hence, a unipolar FBMC signal is considered with flipping technique to avoid the addition of excessive B_{DC} level. Under upper clipping level of Flip-FBMS signals, the deterministic preamble sequence of IAM-C type with convergent levels of high power can be exposed to a repeated truncation due to flipping the negative pecks, where such clipping is taken place at the inception of each FBMC subframe for the sake of fitting the clipped data packet within the operation LED bounds. For such assumption, the $SNR_{effective}$ of equation (4.21) is notably limited and a degradation in transmission quality is dominated, due to increasing the noise component level $\left(\sigma^2_{upper}\right)_{\uparrow}$.

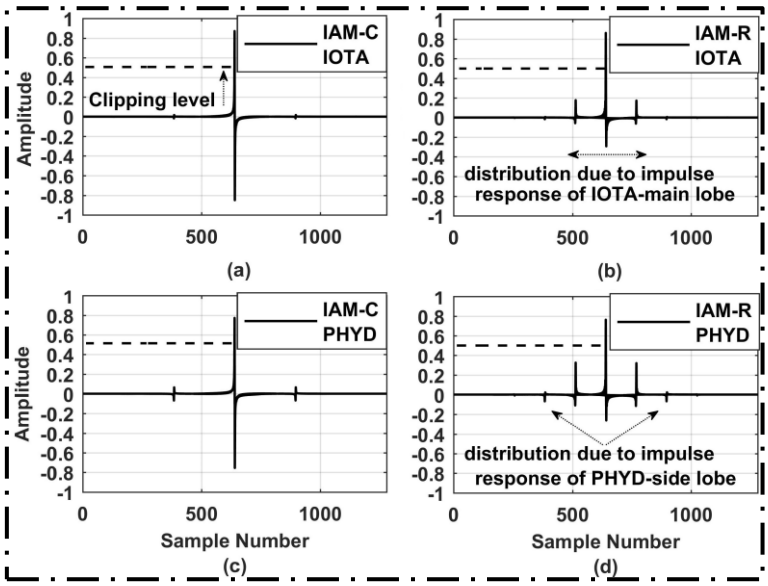

Figure 5.8. Energy configuration for optical modulated preambles of IAM-C/IAM-R types-based IOTA and PHYDYAS filters with bipolar-FBMC signals.

On the contrary, as revealed in Figure 5.8, it must be emphasized on the crucial role of PHYDYAS profile with IAM-R type in mitigating the nonlinear distortion of restricted-LED bounds, thereby it performs as an attractive choice for IM/DD optical systems. However, compared to randomly reference signals with unipolar OFDM structure, the signal estimation with FBMC mechanism is limited only with high power of IAM preamble, where the average optical power $Popt_{\text{Flip-FBMC}} = E\left[X_{\text{Flip-FBM}}(t)\right]$ of such scenario that restricted with the LED-transfer characteristics of [$C_L = 0$ Volts, $C_U = 0.5$ Volts] tends to conflict with various targets of dimming levels (*TD*), which can be defined as:

$$TD_{\text{Flip-FBM}} = \frac{E\left[X_{\text{Flip-FBM}}(t)\right]}{\left(\ell_b\left(C_U - C_L\right)\right)} \tag{5.8}$$

where C_L term stands for the minimum permissible voltage, and the brightness factor is denoted by ℓ_b. Compared to a certain target of dimming level of $TD_{Flip-OFDM}$, the level of brightness based on Flip-FBMC power is remarkably affected by the clipping distortion with reduction in the effected SNR. Consequently, advanced FBMC technique that can support the VLC conditions of high throughput rate (communication) with several dimming/brightness levels (illumination),

should be investigated to avoid the implications with the deterministic sequence of IAM preamble.

5.5. Flip-FBMC signals with Frame repetition model

To overcome the implication of high-power level with IAM preamble, an advanced optical FBMC is proposed based on block repetition technique [25]-[26], which is exploited to mitigate the residual imaginary interference using any arbitrary reference signals instead of IAM sequence. Therefore, Flip-FBMC based frame repetition model is proposed and updated to satisfy an identical power budget between the multicarrier optical system.

$$E\left[X_{\text{Flip-FBM}}(t)\right] = E\left[X_{\text{Flip-OFDM}}(t)\right] = E\left[X_{\text{Flip-FBM}_{\text{Frame repetition}}}(t)\right] \tag{5.9}$$

In such design, due to the amplitude symmetry of residual interference around a position of (0,0) (see equations (3.10) to (3.12)), the implication of intrinsic interference, for high QAM orders and bounces of high delays can be mitigated further by sending two copies of data message with (*m*, *n*) and (*m*, 2*N*-1-*n*) time-frequency positions, respectively, in the original and duplicated frames, in place of splitting the input QAM signal into real and imaginary sections. To produce an average power of one (QAM signal with unity power) over the consecutive subframes, a couple of $1/\sqrt{2}$ complex QAM symbols with a *T*/2 relative time offset in the original $A^{O}_{m,n}$ and duplicated $A^{D}_{m,n}$ frames, respectively, as expressed below:

$$\begin{aligned} \left\{A^{O}_{m,n}\right\}^{n\,=\,1,\ldots,\,N}_{m\,=\,1,\ldots,\,(M/2)\,-1} &= \frac{1}{\sqrt{2}}\,QAM_{m,n} \\ \left\{A^{D}_{m,n}\right\}^{n\,=\,N+1,\ldots,\,2N}_{m\,=\,1,\ldots,\,(M/2)\,-1} &= \frac{1}{\sqrt{2}}\,QAM_{m,n} \end{aligned} \tag{5.10}$$

As observed in Figure (5.9), the real unipolar FBMC signals result from using the fundamental processing blocks of TMUX configuration, where the transmitted/received signals are delivered under the use of equations (3.6) and (4.2).

The n^{th} non-equalized received symbols of m^{th} subcarriers based on the frame repetition model is retrieved by demodulating the received signal that can be expressed as follows:

$$\begin{aligned} R^{\text{Repition model}}_{m,n} &= R^{O}_{m_0,n_0} + R^{D}_{m_0,n_0} \\ R^{\text{Repition model}}_{m,n} &= H_{m_0} A^{O}_{m_0,n_0} + \sum_{k=-\infty}^{\infty} \sum_{(m,n)\neq(m_0,n_0)} H_m A^{O}_{m,n} P_{m,n}[k] P^{*}_{m_0,n_0}[k] + Z^{O}_{m_0,n_0} + \\ &\quad H_{m_0} A^{D}_{m_0,n_0} + \sum_{k=-\infty}^{\infty} \sum_{(m,n)\neq(m_0,n_0)} H_m \; A^{D}_{m,n} \; P_{m,2N+1-n}[k] P^{*}_{m_0,2N+1-n_0}[k] + Z^{D}_{m_0,n_0} \end{aligned} \tag{5.11}$$

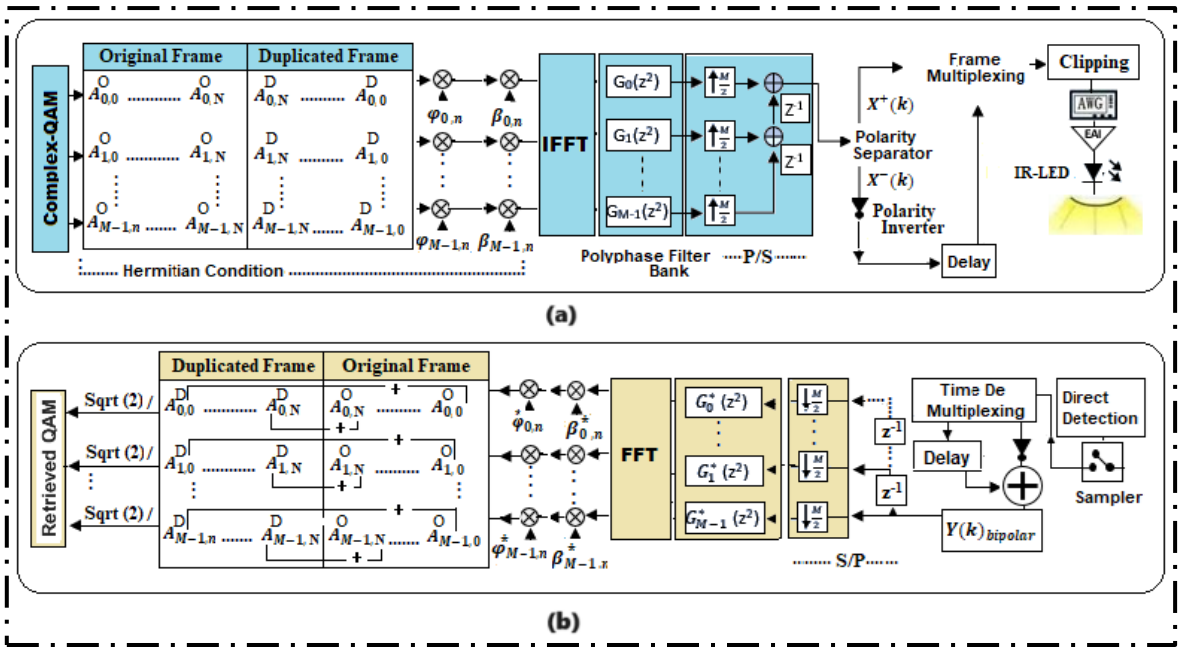

Figure 5.9. Schematic diagram of (a) transmitter and (b) receiver for the proposed Flip-FBMC system-based frame repetition configuration in a VLC system.

As given in equation (5.11), the received message consists of the original $R^{O}_{m_0,n_0}$ and duplicated frames $R^{D}_{m_0,n_0}$ with the associated imaginary interference, where such interferences emerge with identical amplitude and reversed signs around the reference signals with $(m_0,n_0)^{O}$ and $(m_0,n_0)^{D}$ positions, as detailed in Table 5.3, where the transmitted signal is tested with PHYDYAS pulse of *M* × *K* length. The probability, based AWGN of shot and thermal noises with overall σ^2, at any given time instance, X_n takes the value z is determined by:

$$pro(X_n = z) = p(z) = \frac{1}{\sqrt{2\pi\sigma^2}} \exp\ (-\frac{z^2}{2\sigma^2}) \tag{5.12}$$

The choice of PHYDYAS pulse function belongs to the higher distribution energy with its sidelobe that drives to minimize the level of interference by 5.6 dB, with compared to IOTA profile (|MSLR$_{PHYDYAS}$| - |MSLR$_{IOTA}$|).

Table 5.3. Demodulated signal of transmitting only $QAM_{m_0,n_0} = 1$ in optical FBMC, based frame repetition technique with n_0 at even time index, using PHYDYAS profile of *M* × *K* length.

	n_0-2 *original* frame	n_0-1 *original* frame	n_0 *original* frame	n_0 *duplicated* frame	n_0+1 *duplicated* frame	n_0+2 *duplicated* frame
m_0-1	0.0502 - 0.0290j	0.0495 - 0.0286j	0.0205 - 0.0118j	-0.0205 + 0.0118j	-0.0495 + 0.0286j	-0.0502 + 0.0290j
m_0	0.0002 + 0.0472j	0.0001 + 0.3991j	$\sqrt{2}$ /2 + 0.399j	$\sqrt{2}$ /2 - 0.399j	-0.0001 – 0.3991j	-0.0002 - 0.0472j
m_0+1	0.1028 + 0.0594j	-0.2026 - 0.1169j	0.2726 + 0.1574j	-0.2726 - 0.1574j	0.2026 + 0.1169j	-0.1028 - 0.0594j

Consequently, the impact of intrinsic interferences for both original and repeated copies can be vanished for the $\Omega_{(1,1)}$ - (0,0) region and outside the 1-tap neighbourhood zone, as expressed below:

$$I_{m,n}^{O} + I_{m,n}^{D} = \sum_{k=-\infty}^{\infty} \sum_{(m,n)\neq(m_0,n_0)} H_m \; A_{m,n}^{O} \; P_{m,n}[k] P_{m_0,n_0}^{*}[k] + \sum_{k=-\infty}^{\infty} \sum_{(m,n)\neq(m_0,n_0)} H_m \; A_{m,2N+1-n} \; P_{m,2N+1-n}[k] P_{m_0,2N+1-n_0}^{*}[k] \tag{5.13}$$

Thus, the total interference can be suppressed to 0, $I_{m,n}^{O} + I_{m,n}^{D} = 0$, as confirmed by sending a reference signal at ideal transmission of a noise-free link, as confirmed in Table 5.3. Thereby, to cope with derived equation of (5.10) and, since the estimation stage with free $I_{m,n}^{\text{Total interference}}$ implication, the retrieved input complex QAM signal can be obtained by dividing over $\sqrt{2}$, as given below:

$$A_{m,n}^{estimated} = \left(A_{m,n}^{O} \; Z_{m,n}^{O} + A_{m,n}^{D} \; Z_{m,n}^{D} \right) \Big/ \sqrt{2} \times H_m \tag{5.14}$$

Therefore, as given in Table 5.3, the transmission of a reference signal with $QAM_{m_0,n_0} = 1$, is retrieved successfully $\left(\sqrt{2}/2 + \sqrt{2}/2\right)/2$ by using equation (5.14).

As detailed in Table 5.3, the Flip-FBMC signals based frame repetition model experience identical interference with reversed signs, compared to the traditional Flip-FBMC based IAM preamble that only can cover the interference over the $\Omega_{(1,1)}$ - (0,0) zone. From such perspective, the proposed and classical systems are investigated over several clipping ratios γ to assess the interference level for (m_0, n_0) $\notin \Omega_{(1,1)}$. Thus, the $\Im$ over (m_0, n_0) $\notin \Omega_{(1,1)}$ zone of equation (4.22) is updated to determine $\Im$ with several γ :

$$\left\{\Im\right\}_{\gamma} = \frac{\sum_{(m_0,n_0)\notin\Omega_{(1,1)}} |\delta_{m,n}^{m_0,n_0}|^2}{\sum_{(m_0,n_0)\notin\Omega_{(1,1)}} |\delta_{m,n}^{m_0,n_0}|^2 + \sum_{(m_0,n_0)\in\Omega_{(1,1)}-(0,0)} |\sum_{k=-\infty}^{\infty} P_{m,n}[k] \; P_{m_0,n_0}^{*}[k]|^2} \times 100\% \tag{5.15}$$

As illustrated in Figure 5.10, the interference level for (m_0, n_0) $\notin \Omega_{(1,1)}$ zone is significantly high with traditional Flip-FBMC signals, as the residual interference of such zone arises to be out of control the use of IAM preamble.

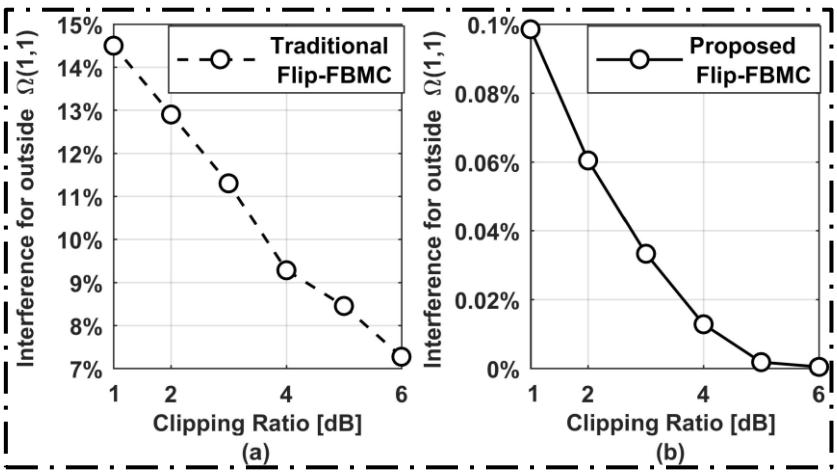

Figure 5.10. Interference level for outside the first order neighbourhood zone for transmitting only $QAM_{m_0,n_0} = 1$ through PHYDYAS filter, vs Clipping ratio for (a) traditional Flip-FBMC based IAM preambles, and (b) Flip-FBMC using frame repetition format.

Therefore, for outside the $\Omega_{(1,1)}$ - (0,0) zone, the $\Im_\gamma$ impact is significantly boosted with increasing the C_U level for Flip-FBMC/IAM system. While a low degree of $\Im_\gamma$ influence is reported with the proposed design, as the effect of $R^O_{m_0,n_0} + R^D_{m_0,n_0}$ verifies the interference suppression $\left(I^O_{m,n} + I^D_{m,n} \right)$, i.e. $\Im^{\text{IAM}}_{\gamma=1\text{ dB}} = 14.5\% >> \Im^{\text{Frame repetition}}_{\gamma=1\text{ dB}} = 0.1\%$.

Therefore, to analyse the clipping distortion with upper bound level of used LED, high reference symbol-power is assigned for estimating the quality of received message. Such pilot-amplitude is designed to evaluate the power distribution of main-lobe/sidelobe PHYDYAS profile by the use frame repetition technique, for the sake of a fair comparison with high power of IAM preamble. Besides, the use of high reference symbol-powers over the payload data in the major literature contribute also to determine the minimum required SNR with high estimation accuracy, where such scenario could experience a nonlinear distortion due to the restricted C_U level.

Consequently, two configurations of reference symbols are exploited for estimating purpose and avoiding the high pilot powers over the data load. For such scenario, the power allocation for the first type of *M*/2-1 training pilots is arranged at the first and 2*N* blocks, respectively, for the original and repeated frames, such as $Pilot_{m,1} = Pilot_{m,2N} = 0.707\ (-1)^m \times 0.707\, j$. While the second configuration of pilot blocks is given as $Pilot_{m,1} = Pilot_{m,2N} = (j)^m$. It is worthy to highlight that the use of such training pilots in FBMC modulation could be slightly affected (shifted up or down) by the payload data, compared. However, the levels of optical multicarrier schemes in Figure 5.11 are obtained based on numerous Montel Carlo simulations.

Furthermore, the training pilots are required only a single complex block for estimating the retrieved signal, while a duration of 1.5 complex blocks of IAM preamble are exploited for the estimation process. Hence, due to the processing of flipping technique, the spectral efficiency with Flip-FBMC based on frame repetition model is enhance by a single block over the Flip-FBMC with IAM preamble. The channel estimation of retrieved FBMC signal with frame repetition model is expressed as:

$$\hat{H_m} = \frac{\overbrace{(R^O_m + R^D_m)/\sqrt{2}}^{total\ \text{received}\ pilots}}{Pilot_m} \tag{5.16}$$

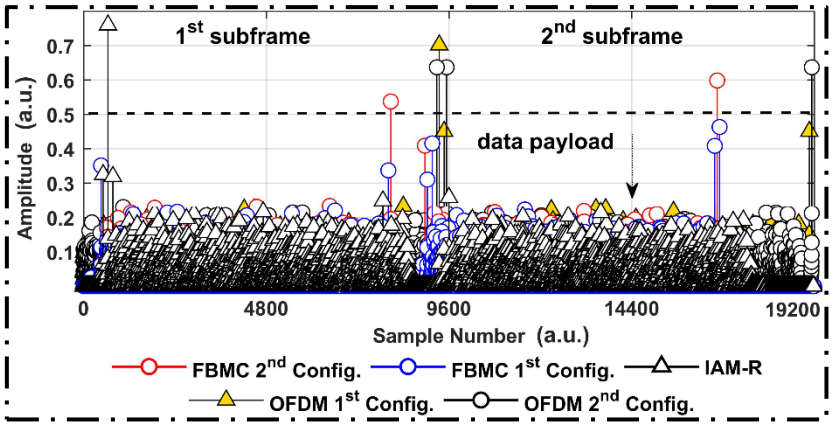

Figure 5.11. Clipping level at transmitted subframes of Flip-FBMC-based frame repetition format, Flip-FBMC with IAM-R using PHYDYAS filter, and Flip-CP-OFDM format based on different configurations of training symbols.

According to Figure 5.11, a first insight points out that even with the use the IAM-R type that has a lower amplitude with respect to IAM-C type, the Flip-FBMC/IAM system exposes a severe clipping distortion compared to other optical multicarrier system. The power allocation for reference symbols depends on the main lobe/sidelobe of PHYDYAS function, which leads to low amplitude-levels of successive FBMC subframes by using frame repetition technique, thereby, the minimum implication of clipping distortion is reported with the proposed system, as expressed below:

$$\underbrace{\int_{C_u=0.5}^{\infty}(z-C_u)^2\,p(z)dz}_{\sigma^2_{\text{Clip-Flip FBMC/IAM-R}}} > \underbrace{\int_{C_u=0.5}^{\infty}(z-C_u)^2\,p(z)dz}_{\sigma^2_{\text{Clip-Flip OFDM}}} >> \underbrace{\int_{C_u=0.5}^{\infty}(z-C_u)^2\,p(z)dz}_{\sigma^2_{\text{Clip-proposed FBMC}}} \tag{5.17}$$

Thereby, the overall noise power ($\sigma^2_{\text{clip}} + \sigma^2_{\text{thermal+shot}}$) is kept minimum, and as a consequence, an enhanced $\text{SNR}_{\text{proposed-FBMC}}$ level is captured over the $\text{SNR}_{\text{Flip-FBMC/IAM}}$ and $\text{SNR}_{\text{Flip-OFDM}}$ values. In other words, such enhancement can be also interpreted as increasing the allowable injected power. Thus, it is also can be seen as a key factor in promoting the upper level of limited dynamic range, as given below:

$$C_{u\_new} = C_u + |\,\Delta X[k]_{\text{Flip-OFDM}} - \Delta X[k]_{\text{Flip-FBMC}}\,| \tag{5.18}$$

where

$$\Delta X[k] = X[k] - X[k]_{\text{clipping}} \tag{5.19}$$

The term of C_{u_new} is referred to the enhanced upper clipping level over C_u with high power LED manufacturer data sheet.

However, the promising features of using Flip-FBMC with frame repetition technique comes at the expense of high hardware complexity.

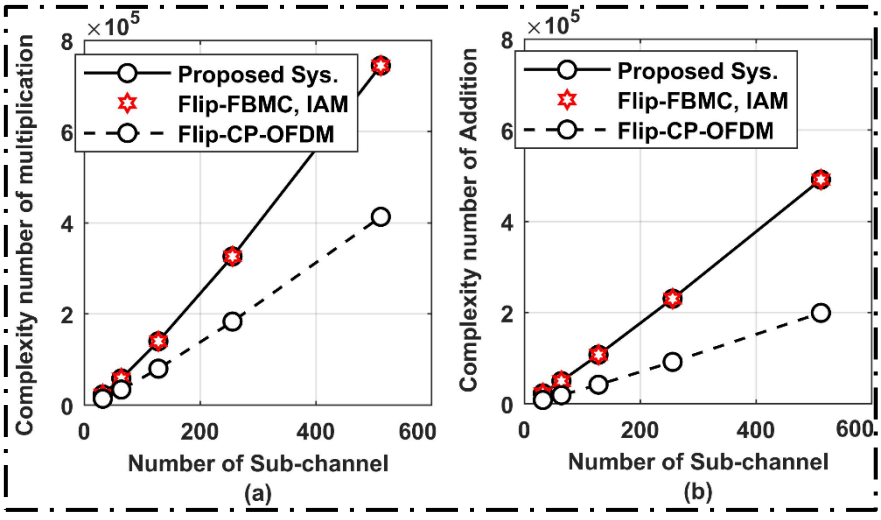

Figure 5.12. The implementation complexity comparison between several optical multicarrier systems based on the number of multiplications for (a), and additions for (b).

As revealed in Figure 5.12, identical hardware complexity is shared for both Flip-FBMC/IAM and the proposed design, thereby, such high complexity tends to be as one of the main drawbacks in FBMC mechanism, compared to the minimized one in unipolar OFDM signals.

5.6. The performance analysis of Flip-FBMC signals based on frame repetition characteristics.

In order to induce the intrinsic interference further, which is predominant even at low constellation mapping of 4-QAM order and over the propagation links with high delay spreads, we adopt the simulation system parameters detailed in Table 4.9. From the Monte Carlo simulation results, the impact of reducing the imaginary interference is confirmed by using the frame repetition model. Thus, the proposed design presents an enhanced SNR gain over Flip-FBMC/IAM model, and as a consequence, an almost identical performance for both the Flip-FBMC/ frame repetition and Flip-CP-OFDM systems is delivered, as presented in Figure 5.13. Moreover, the enhanced performance is more evident with Flip-FBMC based IAM-C type compared to one with IAM-R type, due to the higher powers of pseudo pilots, such as pseudo pilots/IAM-C $\{E\,|T_{m_0,n_0}|^2\}_{m\,=\,2:M/2} = 2.176$ and, 1.23 with IAM-R.

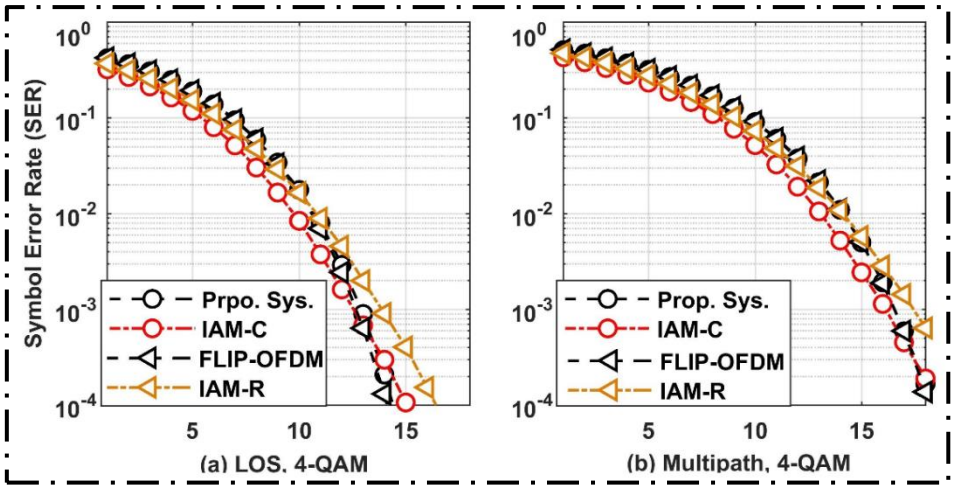

Figure 5.13. SER vs. SNR for Flip-FBMC system-based frame repetition, optical FBMC using IAM preambles and Flip-CP-OFDM over 4-QAM at different propagation scenarios of VLC system.

As observed in Figure 5.14, over high constellation mapping of 16-QAM order and at SER of 10^{-4}, the Flip-CP-OFDM outperforms the performance of each Flip-FBMC/IAM and the proposed system, where the degradation in latter is due to violating the interference cancellation assumption, i.e. $\left(I^{O}_{m,n} + I^{D}_{m,n} \neq 0\right)$, since the intrinsic interference from adjacent blocks is induced at a link with high delay spread or/and QAM orders. Moreover, the interference implication based on Flip-FBMC/IAM system dominates in such scenario, where the resulting drop of its performance refers to the interference mitigation cannot comply with SNR increment, thereby, the condition of reliable estimation is violated, i.e. $\mathrm{Re}\{I_{m,n}\} \neq 0$.

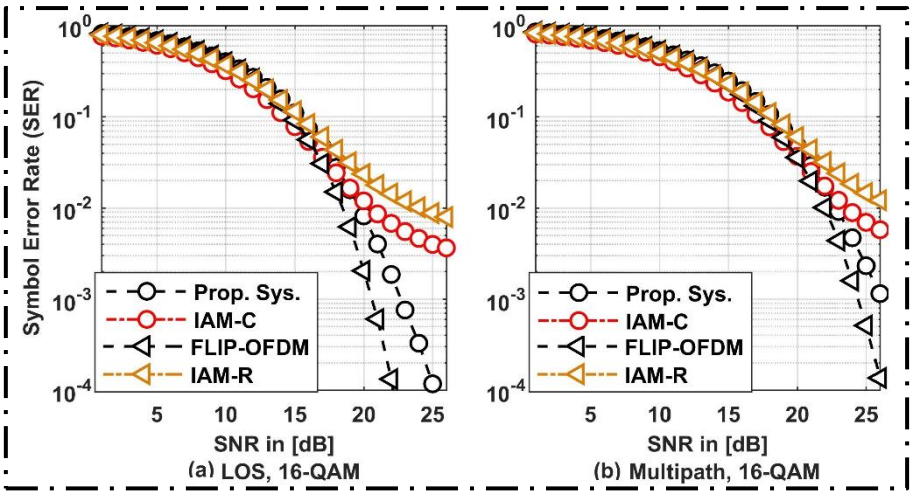

Figure 5.14. Performance comparison between optical FBMC/IAM preambles, Flip-CP-OFDM and Flip-FBMC system-based frame repetition, over 16-QAM orders at different propagation scenarios of VLC system.

On the other hand, over a realistic transmission scenario, where the influence of nonlinear distortion is analysed in term of imposing the LED-maximum permissible level, as illustrated in Figure 5.15. In such scenario, the Flip-FBMC using frame repetition model exhibits a superior performance over other IM/DD multicarrier systems, where the use of PHYDYAS profile with the proposed design has a crucial aspect in mitigating the implications with clipping distortion, where high clipping ratio leads to increase $\sigma^2_{\text{clip/Flip-OFDM}}$ level, and as a consequence, a low transmission quality of optical OFDM is resulted. Therefore, compared to Flip-CP-OFDM, the Flip-FBMC/frame repetition delivers better SNR gains, i.e. 1.6 dB and 2.7 dB SNR gains, respectively, by using the first configuration model of reference symbols, as observed in Figure 5.15(a and c).

Regarding to the level of allowable injected power, from equations (5.18 to 5.19), the level of amplitude distortion with unipolar OFDM based C_u bound is taken as a metric of expanding the upper clipping bound to a level where a higher pilot power can be injected in, i.e. the value of $C_{u\text{-new}}$ is $(C_{u\_\text{LED}} + \Delta X[k])$ and $(C_{u\_\text{LED}} + \Delta X[k])$ based on the first and second pilot typologies, respectively, with respect to C_{u_LED} manufacturer data sheet.

On the other hand, according to equation (5.8), and based on high power training references over the payload data, several targets of brightness/dimming levels can be supported by using the proposed design, compared to implications with IAM sequence, and pilot symbols with Flip-CP-OFDM system, owing to main lobe/sidelobe in the impulse response of PHYDYAS profile in Flip-FBMC/frame repetition model, due to decreasing the clipping distortion over a linear operation range of LED.

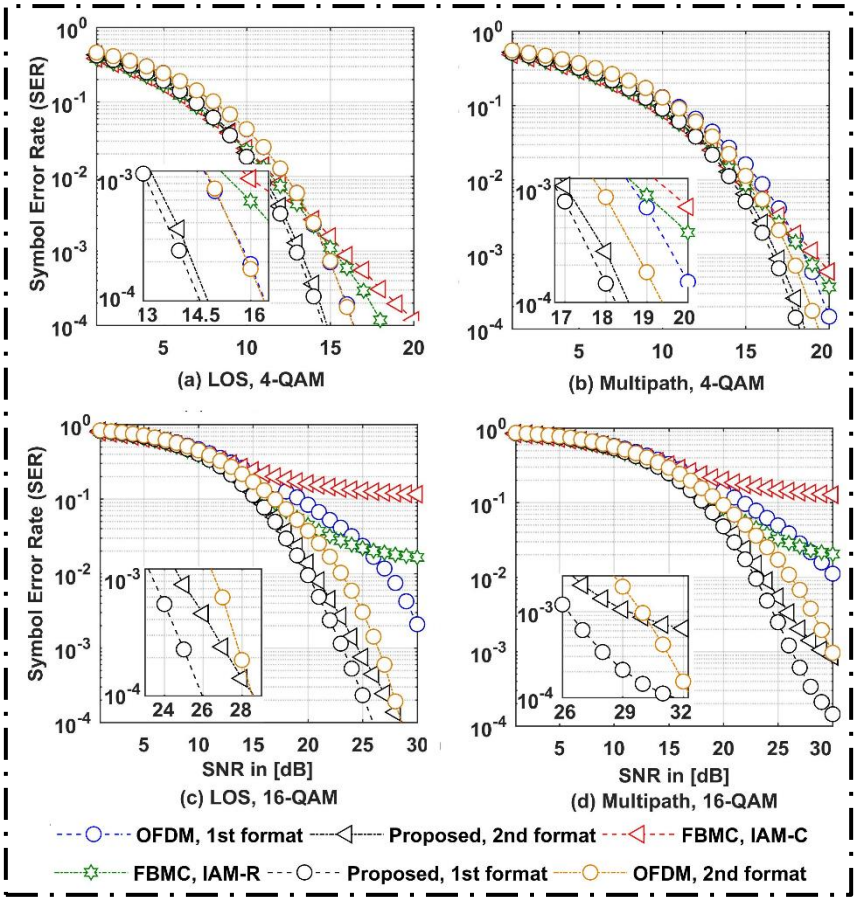

Figure 5.15. The impact of imposing the maximum permissible level for SER vs. SNR of the proposed scheme, optical FBMC/IAM systems and Flip-CP-OFDM based the first and second pilot typologies over (a) LOS/4-QAM and LOS/16-QAM for (c); whereas multipath propagation scenarios of 4-QAM and 16-QAM for (b) and (d), respectively.

Moreover, the performance failure with traditional Flip-FBMC can be interpreted as the high power of IAM sequence is exposed to severe clipping, which in turn causes to spread the power confinement outside the first order neighborhood zone, as the $\Omega_{(1,1)}$ - (0,0) zone, cannot be controlled by IAM sequence, Thereby, a reduction in estimation level is obtained, as detailed in Figure 5.10. Furthermore, the estimation process based IAM-C/ IAM-R sequence over the realistic transmission manner conflicts with the systematic analysis of IAM-C/ IAM-R performance, as shown in Figure 5.14, as the energy confinement within the first order zone is higher with the use of IAM-C type, thereby, the $\sigma^2_{clip/IAM\text{-}C} >> \sigma^2_{clip/IAM\text{-}R}$ contributes to include more signal amplitudes beyond the linear dynamic range for LED.

Consequently, for indoor optical wireless communications systems, the high-speed data transmission with a superior performance over Flip-CP-OFDM signals is delivered by using the proposed design, which can be effectively employed in next generation VLC-application systems, such as the indoor robotic control-based VLC links [151], and virtual and augmented reality systems [152].

5.7. Conclusions

In this chapter, the first theoretical analysis of time-frequency localization (TFL) property for the EGF filter with several profiles of spreading factor has been proposed in non-coherent optical

systems, i.e. indoor VLC-interference link based on FBMC data packet. The designed system is exploited for the sake of mitigating the impact of residual interference with FBMC structure. In order to emphasize on the energy level of pseudo pilots, different prototype filters and several spreading factors based on EGF filter have been systematically analyzed to evaluate the retrieved signal quality. From such perspective, the analysis revealed that a low value of spreading factor, I.e. EGF profile with $\alpha = 0.5$, leads to an inherent interference that has been spread out the first order of neighborhood blocks, which drove to decrease the amplitude level of pseudo pilots. Hence, the degradation in estimating accuracy is obtained, due to the predominant interference in optical FBMC system.

On the other hand, such performance can be promoted using high spreading factor. However, to identify the optimum spreading factor, further spectral analysis, such as the impact of noise floor, localization property and MSLR level, have been considered to analyze the influence of tuning α, compared to IOTA filter over low to high QAM-orders and different propagation links, i.e. LOS and multipath channels.

From the obtained results, the comprehensive investigation revealed that the suppression impact of inherent residual interference in received Flip-FBMC signals can be delivered by reducing the noise floor beyond 60 dB, and maximizing the amplitude level of pseudo-pilots. Consequently, due to the promising property of high spreading parameters based EGF profiles, the proposed system offered a superior SNR gain to Flip-FBMC based IOTA filter of α=1.6 over different channels of low delays and higher constellations, .Besides, the performance of proposed system outperforms the one with Flip-CP-OFDM scheme.

However, the main drawback of increasing the spreading factor has been reported as the severe degradation in the localization property and MSLR level of $\approx$ -17.7 dB, i.e. a noisy retrieved signals is resulted even at a noiseless channel impact using $\alpha = 3.0$. From such perspective, the spreading factor of $\alpha = 2.9$ has been represented as the maximum allowable tuning parameter that able to recovering the transmitted burst accurately. On the contrary, over high delay spread paths with higher constellations mapping, the enhancement in system robustness against the interference implication is more evident for the isotropic property of $\alpha = 1.0$ (IOTA) with Heisenberg factor ($\approx$ 1).

Although increasing the spreading factor leads to integrate more useful information in an envelope function around its center which enhancing the tail-shortening applications (reducing the truncated power), the accuracy of channel estimation process has only been restricted with the use of high power of IAM preamble. Thereby, the violation for VLC condition with dimming application, and the restricted dynamic range with maximum saturation point of LED have been reported.

Consequently, to avoid the impact of high power IAM preamble over the payload data, the Flip-FBMC with frame repetition model has been proposed with different prototype profiles. In such design model, the minimum IMI influence with the retrieved data packet results by sending two copies of the input complex message in successive subframes with a $T/2$ relative time offset.

Moreover, the metric of clipping distortion has been analyzed using Flip-FBMC/IAM and Flip-FBMC/frame repetition systems, from this perspective, such analysis revealed that the impact of intrinsic interference outside the first order neighborhood zone, is induced further with Flip-FBMC signals based IAM preamble, and as a consequence, a severe degradation in estimating

accuracy is captured as such zone cannot be covered using IAM preamble. On the contrary, the minimum interference from such zone resulting by using frame repetition technique, due to the interferences experience identical amplitudes with reversed signs within the original and duplicated copies of received FBMC signals.

Over a realistic transmission scenario, the crucial aspect of PHYDYAS profile in minimizing the high pilot powers over the payload is delivered, thereby, the unipolar FBMC/frame repetition model with PHYDYAS pulse function offered superior SNR gains, compared to Flip-CP-OFDM system and over links of high delays profile and higher QAM orders. Hence, the high transmission rate in next generation VLC requirements can be efficiently supported by using such design.

Chapter 6. Conclusions and future work

"Science knows no country, because knowledge belongs to humanity, and is the torch which illuminates the world".

–Louis Pasteur

6.1. Conclusions

This Thesis aims to make a step forward in potential modulation formats to be used in VLC systems as enabling technology in 6G networks, which can verify the ever-growing 6G platform. VLC is a promising technology that has been suggested for future short-range communications in next generation networks, where such networks are expected to offer ultra high-speed connections, low latency, and enhanced characteristics of KPIs with respect to previous wireless communication generations, and cannot be provided with legacy RF platforms. The limited modulation bandwidth and restricted dynamic range of the employed LEDs are the main impairments in VLC systems, since they can impede the multilevel dimming control and high-speed 6G demands. From such perspective, advanced optical modulation models, i.e. Flip-FBMC/IAM preamble and Flip-FBMC/Frame repetition waveforms, are investigated to serve as a potential modulation for 6G communication systems, owing to the employed pulse shaping filter that features low OOB emissions and guard band/CPs free transmission and thus, enhances throughput rate and spectral efficiency with compared to OFDM format.

The analytical formulation of Flip-FBMC with IAM configuration, also based on tail-shortening algorithm, has been analysed to enable the high speed-transmission with low TMUX-latency. The estimation accuracy of such algorithm is highly dependent on the impulse response-based pulse profile, while protype filter lengths and interference confinement power at the first order zone, which is controlled by IAM preamble-type, i.e. the tail-shortening signal with $M\times K+1$ IOTA filter

length with the use of IAM-C preamble type, offer a superior SNR gain of approximately 1.5 dB at SER= 10^{-3} over Flip-CP-OFDM and truncated Flip-FBMC with IAM-R systems, respectively.

However, the proposed design in such analysis was run over a low constellation mapping of 4-QAM order and short propagation-links for the sake of minimizing the IMI effects, where only 1 point length of CP is required to combat ISI influence in OFDM system. Therefore, such evaluation is not sufficient to assess the impact of intrinsic interference, since IMI impact is considered as one of the main drawbacks in FBMC signals and dominates at high modulation orders and/or over propagation-links with high delays profile.

From this perspective, over propagation-links with very high delays profile, an efficient multitap equalization is proposed to compensate the performance failure using a single tap equalization due to the induced interference at retrieved FBMC signals, where the constrained condition of channel maximum delay is no more valid, $\mathrm{Re}\{I_{m,n}\} >> 0$. Also, in such analysis, over a realistic limited modulation bandwidth of the employed LED, the transmission rate and latency metric are optimized through a tail-shortening algorithm with $M \times K$ filter length, i.e. the aggregate transmission rate is extended from 4% to 11% over the throughput rate of Flip-CP-OFDM system.

Furthermore, for the sake of emphasizing the value of Flip-FBMC/IAM technique in avoiding the intrinsic interference, compared to a reduction in the estimating accuracy by using DCO-FBMC/IAM format, where such a downfall performance has been reported because of the induced IMI that spreads out the first neighbourhood symbols, which is more evident when low levels of the added DC-bias are required. Thereby, devoting flipping technique to provide the unipolar FBMC format can be presented as a potential technique for the next-generation optical networks.

This thesis also confirms the role of TFL property in minimizing the interference effect, where the first theoretical analysis has been presented based on the optimal trade-off between the IMI minimization and the spectrum features. At high constellation mapping, comprehensive analysis revealed a superior performance over other optical multicarrier schemes that can be delivered by increasing the spreading factor in EGF function up to its threshold level of 2.9 ($\alpha = 2.9$). Thereby, for α higher than such level, a retrieved noisy signal is captured even at ideal propagation link (noise-free channel). Such scenario leads to the reduction in the localization parameter and degradation of the MSLR level beyond -17 dB, which increases the interference level by 16.2 dB in adjacent bands.

Moreover, over a link with high delays profile and low constellation mapping, the simulation results emphasized that tuning the spreading factor up to 1.6 level ($\alpha = 1.6$) leads to overcome the IOTA-downfall performance and enhance its SNR gain over the conventional Flip-CP-OFDM, owing to minimizing the level of noise floor beyond 60 dB, and confining higher interference power at the first order zone. Nevertheless, the Flip-FBMC/IAM robustness against a predominant residual interference is even more crucial by using Heisenberg parameter with value ≈ 1, i.e. IOTA filter of $\xi \approx 0.977$, in the event of higher constellation mapping and delay spread links.

However, over a realistic transmission scenario of applying the characteristics of LED, the analysis revealed that the use of deterministic preamble sequence with Flip-FBMC signals using IOTA or other EGF profiles lead to place the limitation of linear dynamic range to a level where a severe clipping distortion dominates, which in turn also impedes the dimming/brightness levels requirements, compared to high power reference symbols with Flip-CP-OFDM system at indoor

VLC systems. From such perspective, for the first time, theoretical investigation is performed to analyse the impact of clipping distortion on IMI outside the first order zone that is normally neglected by researchers. Thereby, the outcomes of such implications indicated to a severe reduction in estimating accuracy as a consequence of induced interference outside the 1-tap region, which cannot be covered with the use of IAM sequence.

Consequently, to overcome the implications on Flip-FBMC/IAM systems, this thesis has been oriented toward proposing a sufficient modulation scheme that can support the high-speed transmission and multilevel brightness of VLC conditions, thereby, Flip-FBMC based on Frame repetition technique has been proposed to meet such requirements. Through numerical results, we showed that the estimating accuracy can be significantly improved owing to the IMI effect outside the first order zone is induced with identical levels and reversed signs around the pilot symbols for each original and duplicated subframe of the proposed design, compared to Flip-FBMC/IAM system, i.e. the interference level outside the first order zone with Flip-FBMC/frame repetition model is 1%, compared to 14.5% by using Flip-FBMC/IAM model based on 1dB of clipping distortion level. Additionally, the PHYDYAS profile is presented as a viable candidate to cope with the limited linear range of LED, owing to the role of allocation powers of main lobe/sidelobe impulse response in reducing the impairment of clipping distortion. Therefore, compared to Flip-CP-OFDM, the Flip-FBMC of frame repetition system offered better SNR gains, i.e. 1.6 dB and 2.7 dB SNR gains, over links of high delay profile and constellation orders, which in turn, can be also interpreted as expanding the upper clipping bound to a level where a higher pilot power can be injected and thus, wide range of brightness levels based on high amplitude pilots can be supported. Therefore, such characteristics place Flip-FBMC/frame repetition using PHYDYAS profile a step forward to enabling the VLC-6G network.

6.2. Future works

This Thesis has mainly considered the investigation of advanced filter bank multicarrier waveform schemes to meet the high-speed transmission and low latency demands of VLC-6G networks. The development of Flip-FBMC/Frame repetition system has contributed to cope with the current limitations of indoor VLC modulation systems. Nevertheless, there are various aspects might be further enhanced and, thereby, they are proposed as future work.

Employing Flipping technique to provide the unipolar FBMC signal came at the expense of reducing the throughput rate, thereby, a novel block-coding technique needs to be suggested to overcome such limitation. Moreover, an investigation of joint transmitter/receiver of optical FBMC/frame repetition based on multiple-input and multiple-output OWC channels is required to evaluate the system efficiency against modulation and multi receivers-induced interference.

The hardware complexity of the proposed architecture is very high compared to optical OFDM system. Thereby, as a future work, the hardware implementation of the suggested transmitter/receiver architectures would be beneficial, i.e. FBMC based fast convolution technique. A comprehensive analysis of numerical precision-effect should be taken place, specifically for fix-point implementations. Such design will perform a crucial aspect if Field Programmable Gate Array (FGPA) realization is considered.

To reduce the penalty of duplicated tails in Flip-FBMC data packet, and to minimize the mutual interference from adjacent blocks, ACO-FBMC/frame repetition technique needs to be modified to satisfy the assumption of interference suppression, where the IMI of identical amplitudes and

signs with received FBMC subframes is varied. In other words, clipping the negative part for each original and duplicated frame leads to generate a different interference at each subframes, thereby, a modified frame repetition is required to be investigated in order to overcome such downside.

It will be interesting to analyse the Flip-FBMC based frame repetition model under high order constellation mapping and/or links with larger delays profile to identify the assumption on maximum delay that can be tolerated. Although a significant enhanced performance of Flip-FBMC using EGF/IAM model has been demonstrated over other optical multicarrier systems (optical OFDM and FBMC/IAM based IOTA systems), the impairments of deterministic preamble sequence with IAM preamble require further processing to achieve an efficient optical FBMC system, i.e. reducing the high power over the payload data with IAM preamble. Consequently, the possibility to enhance the estimating accuracy can be provided by the use of optimized-hybrid EGF based IAM sequence with frame repetition model in Flip-FBMC system, since such a prospective vision would be attractive in 6G network. Such investigation can be extended for different propagation distances to serve in the next version of optical wireless standards, i.e. IEEE P802.15.13.

Furthermore, employing FBMC waveform in various optical applications is considered as one of the 6G hot promising topic that has not been experimentally tested yet, i.e. passive optical network-based IM/DD systems to enhance system performance and underwater optical communication [153]-[154]. Notably, the low latency of the proposed design is a crucial feature in the Tactile Internet (the next evolution of the Internet of Things), thereby, it would be interesting to extend such investigation to include such applications.

List of publications

Journals

J.1. **M. S. Bahaaelden**, B. Ortega, R. Pérez-Jiménez and M. Renfors, "Efficiency Analysis of a Truncated Flip-FBMC in Burst Optical Transmission," in IEEE Access, vol. 9, pp. 100558-100569, 2021.

Conference proceedings

C.1. **M. S. B. Bahaaelden**, B. Ortega and R. Perez-Jimenez, "Non-coherent Optical FBMC Signals based on Extended Gaussian Function well Time-Frequency Localized filters," *2023 International Wireless Communications and Mobile Computing (IWCMC)*, Marrakesh, Morocco, pp. 1418-1423, 2023.

C.2. **M. S. B. Bahaaelden,** B. Ortega, R. Perez-Jimenez and V. Almenar, "Optical FBMC Signals using Frame Repetition for Indoor Wireless Communication System," *2023 International Conference on Smart-Green Technology in Electrical and Information Systems (ICSGTEIS)*, Badung, Bali, Indonesia, pp. 235-240, 2023.

C.3. **M. S. B. Bahaaelden,** B. Ortega, R. Perez-Jimenez and V. Almenar, "Enhanced Signal Transmission Performance based on Multitap Equalization in Optical FBMC Burst," *2023 6th International Conference on Advanced Communication Technologies and Networking (CommNet)*, Rabat, Morocco, pp. 1-6, 2023.

.

References

[1] R. W. Burns, “Communications: An international history of the formative years,” IET Publication, vol. 32, no.1, pp.192-196, 2004.
[2] Bell, Alexander Graham. “On the production and reproduction of sound by light.” American Journal of Science, no. 118, pp. 305 – 324, 1980.

[3] D. Karunatilaka, F. Zafar, V. Kalavally and R. Parthiban, "LED Based Indoor Visible Light Communications: State of the Art," in IEEE Communications Surveys & Tutorials, vol. 17, no. 3, pp. 1649-1678, thirdquarter 2015.

[4] He, Cuiwei, and Chen Chen, "A Review of Advanced Transceiver Technologies in Visible Light Communications" Photonics 10, no. 6: 648. 2023. https://doi.org/10.3390/photonics10060648.

[5] A. Şahin, Y. S. Eroğlu, İ. Güvenç, N. Pala and M. Yüksel, "Hybrid 3-D Localization for Visible Light Communication Systems," in Journal of Lightwave Technology, vol. 33, no. 22, pp. 4589-4599, 15 Nov.15, 2015.

[6] H. Li et al., "A Fast and High-Accuracy Real-Time Visible Light Positioning System Based on Single LED Lamp With a Beacon," in IEEE Photonics Journal, vol. 12, no. 6, pp. 1-12, Dec. 2020,

[7] Y. Wang et al., "Meta-Reinforcement Learning for Reliable Communication in THz/VLC Wireless VR Networks," in IEEE Transactions on Wireless Communications, vol. 21, no. 9, pp. 7778-7793, Sept. 2022

[8] Alraih S et al., "Revolution or Evolution? Technical Requirements and Considerations towards 6G Mobile Communications, ". Sensors, no. 3: 762, 2022.

[9] R. Rahman and A. Ashok, "High Throughput Mobile Visible Light Communication," *2020 IEEE International Conference on Pervasive Computing and Communications Workshops (PerCom Workshops)*, Austin, TX, pp. 1-2, USA, 2020.

[10] M. Yu, C. T. Geldard and W. O. Popoola, "Comparison of CAP and OFDM Modulation for LED-based Underwater Optical Wireless Communications," 2022 International Conference on Broadband Communications for Next Generation Networks and Multimedia Applications (CoBCom), Graz, Austria, pp. 1-6, 2022.

[11] R. Rodes et al., “Carrierless amplitude phase modulation of vcsel with 4 bit/s/hz spectral efficiency for use in WDM-PON,” Opt. Exp., vol. 19, no. 27, pp. 26 551–26 556, Dec. 2011.

[12] B. Aly, M. Elamassie, M. Uysal and E. Kınav, "Experimental Evaluation of Unipolar OFDM VLC System on Software Defined Platform," 2019 15th International Conference on Telecommunications (ConTEL), Graz, Austria, pp. 1-6, 2019.

[13] R. Alindra, M. O. Fauzan, R. Ramadhan and S. Rahardjo, "Performance Analysis of DCO-OFDM and ACO-OFDM for Visible Light Communication System," 2018 3rd International Seminar on Sensors, Instrumentation, Measurement and Metrology (ISSIMM), Depok, Indonesia, pp. 84-90, 2018.

[14] M. Bellanger, "Filter banks and OFDM-OQAM for high throughput wireless LAN," 2008 3rd International Symposium on Communications, Control and Signal Processing, Saint Julian's, Malta, pp. 758-761, 2008.

[15] K. K. -C. Lee, "An Intrinsic Interference Mitigation Scheme for FBMC-QAM Systems," in IEEE Access, vol. 7, pp. 51907-51914, 2019,

[16] Liu, T., Li, H., "Carrier frequency offset estimation for OFDM systems with time-varying DC Offset," EURASIP J. Adv. Signal Process. 2012.

[17] Suseela V., Vakamulla V. M., "Impact of STO and STO-estimation in DST-DCO-OFDM-based visible light communication, " ICT Express, 5 Sep. 2022.

[18] F. Hamdar, C. M. G. Gussen, J. Nadal, C. A. Nour and A. Baghdadi, "FBMC/OQAM Transceiver for Future Wireless Communication Systems: Inherent Potentials, Recent Advances, Research Challenges," in IEEE Open Journal of Vehicular Technology, vol. 4, pp. 652-666, 2023

[19] S. Alshami, "Performance Analysis of OFDMA, UFMC, and FBMC for Optical Wireless Communication," 2021 1st International Conference on Emerging Smart Technologies and Applications (eSmarTA), Sana'a, Yemen, pp. 1-4, 2021.

[20] S. Niu, P. Wang, S. Chi, Z. Liu, W. Pang and L. Guo, "Enhanced Optical OFDM/OQAM for Visible Light Communication Systems," in IEEE Wireless Communications Letters, vol. 10, no. 3, pp. 614-618, March 2021.

[21] B. Lin et al., “Experimental demonstration of OFDM/OQAM transmission for visible light communications,” IEEE Photon. J., vol. 8, no. 5, Oct. 2016.

[22] F. Rottenberg, Y. Medjahdi, E. Kofidis and J. Louveaux, "Preamble-based channel estimation in asynchronous FBMC-OQAM distributed MIMO systems," 2015 International Symposium on Wireless Communication Systems (ISWCS), Brussels, Belgium, pp. 566-570, 2015.

[23] A. Aminjavaheri et al., "Impact of timing and frequency offsets on multicarrier waveform candidates for 5G," 2015 IEEE Signal Processing and Signal Processing Education Workshop (SP/SPE), Salt Lake City, UT, USA, pp. 178-183, 2015.

[24] X. Fang, Y. Xu, Z. Chen and F. Zhang, "Frequency-Domain Channel Estimation for Polarization-Division-Multiplexed CO-OFDM/OQAM Systems," in Journal of Lightwave Technology, vol. 33, no. 13, pp. 2743-2750, 1 July1, 2015.

[25] D. Kong, J. Li, K. Luo and T. Jiang, "Reducing Pilot Overhead: Channel Estimation With Symbol Repetition in MIMO-FBMC Systems," in IEEE Transactions on Communications, vol. 68, no. 12, pp. 7634-7646, Dec. 2020.

[26] D. Kong, X. Zheng, Y. Zhang and T. Jiang, "Frame Repetition: A Solution to Imaginary Interference Cancellation in FBMC/OQAM Systems," in IEEE Transactions on Signal Processing, vol. 68, pp. 1259-1273, 2020.

[27] R. Mesleh, H. Elgala and H. Haas, "LED nonlinearity mitigation techniques in optical wireless OFDM communication systems," in Journal of Optical Communications and Networking, vol. 4, no. 11, pp. 865-875, Nov. 2012.

[28] J. -P. M. G. Linnartz, X. Deng and P. Van Voorthuisen, "Impact of Dynamic LED Non-Linearity on DCO-OFDM Optical Wireless Communication," in IEEE Communications Letters, vol. 25, no. 10, pp. 3335-3339, Oct. 2021.

[29] J. Yli-Kaakinen and M. Renfors, "Optimized burst truncation in fast-convolution filter bank based waveform generation," 2015 IEEE 16th International Workshop on Signal Processing Advances in Wireless Communications (SPAWC), Stockholm, Sweden, pp. 71-75, 2015.

[30] M. J. Abdoli, M. Jia and J. Ma, "Weighted circularly convolved filtering in OFDM/OQAM," 2013 IEEE 24th Annual International Symposium on Personal, Indoor, and Mobile Radio Communications (PIMRC), London, UK, pp. 657-661, 2013.

[31] A. Kabir, M. T. Ahammed, C. Das, M. H. Kaium, M. A. Zardar and S. Prathibha, "Light Fidelity (Li-Fi) based Indoor Communication System," 2022 International Conference on Advances in Computing, Communication and Applied Informatics (ACCAI), Chennai, India, pp. 1-5, 2022.

[32] P. Kuppusamy, S. Muthuraj and S. Gopinath, "Survey and challenges of Li-Fi with comparison of Wi-Fi," *2016 International Conference on Wireless Communications, Signal Processing and Networking (WiSPNET)*, Chennai, India, pp. 896-899, 2016.

[33] S. Dimitrov and H. Haas, Principles of LED light communications：towards networked Li-Fi, Cambridge University Press; 1st ed., 2015.

[34] L. E. M. Matheus, A. B. Vieira, L. F. M. Vieira, M. A. M. Vieira and O. Gnawali, "Visible Light Communication: Concepts, Applications and Challenges," in *IEEE Communications Surveys & Tutorials*, vol. 21, no. 4, pp. 3204-3237, Fourthquarter 2019.

[35] N. Chi, Y. Zhou, Y. Wei and F. Hu, "Visible Light Communication in 6G: Advances, Challenges, and Prospects," in *IEEE Vehicular Technology Magazine*, vol. 15, no. 4, pp. 93-102, Dec. 2020.

[36] H. Elgala, R. Mesleh and H. Haas, "An LED Model for Intensity-Modulated Optical Communication Systems," in *IEEE Photonics Technology Letters*, vol. 22, no. 11, pp. 835-837, June1, 2010.

[37] Hu, L., Choi, J., Hwangbo, S. et al., "Flexible micro-LED display and its application in Gbps multi-channel visible light communication," npj Flex Electron 6, Dec. 2022. https://doi.org/10.1038/s41528-022-00234-z.

[38] Z. Rao et al., "10.5 Gbps visible light communication systems based on c-plane freestanding GaN micro-LED," in Journal of Lightwave Technology, 2024.

[39] F. Xu et al., "High Bandwidth Semi-Polar InGaN/GaN Micro-LEDs With Low Current Injection for Visible Light Communication," in IEEE Photonics Journal, vol. 15, no. 1, pp. 1-4, Feb. 2023.

[40] Daniel M. et al., "Hundred-meter Gb/s deep ultraviolet wireless communications using AlGaN micro-LEDs," Opt. Express 30, pp. 46811-46821, 2022.

[41] Y. -H. Chang et al., "4.343-Gbit/s Green Semipolar (20-21) μ-LED for High Speed Visible Light Communication," in IEEE Photonics Journal, vol. 13, no. 4, pp. 1-4, Aug. 2021.

[42] Mohamed Sufyan Islim, Ricardo X. Ferreira, Xiangyu He, Enyuan Xie, Stefan Videv, Shaun Viola, Scott Watson, Nikolaos Bamiedakis, Richard V. Penty, Ian H. White, Anthony E. Kelly, Erdan Gu, Harald Haas, and Martin D. Dawson, "Towards 10 Gb/s orthogonal frequency division

multiplexing-based visible light communication using a GaN violet micro-LED," Photon. Res. 5, A35-A43 (2017).

[43] R. X. G. Ferreira et al., "High Bandwidth GaN-Based Micro-LEDs for Multi-Gb/s Visible Light Communications," in IEEE Photonics Technology Letters, vol. 28, no. 19, pp. 2023-2026, 1 Oct.1, 2016.

[44] H. Chun et al., "Visible Light Communication Using a Blue GaN μ LED and Fluorescent Polymer Color Converter," in IEEE Photonics Technology Letters, vol. 26, no. 20, pp. 2035-2038, 15 Oct.15, 2014.

[45] T. Komine and M. Nakagawa, "Fundamental analysis for visible-light communication system using LED lights," in IEEE Transactions on Consumer Electronics, vol. 50, no. 1, pp. 100-107, Feb. 2004.

[46] X. Liu, D. Zou, N. Huang and S. Zhang, "A Comprehensive Accuracy Analysis of Visible Light Positioning under Shot Noise," 2020 IEEE/CIC International Conference on Communications in China (ICCC Workshops), Chongqing, China, pp. 167-172, 2020.

[44] Pallab K. Choudhury, "Enhanced tolerance against optical background noise in VLC link by using line coded signal with receiver filter," Results in Optics, vol. 1, Nov. 2020. https://doi.org/10.1016/j.rio.2020.100020.

[48] J. M. Kahn and J. R. Barry, "Wireless infrared communications," in Proceedings of the IEEE, vol. 85, no. 2, pp. 265-298, Feb. 1997.

[49] S. Long, M. -A. Khalighi, M. Wolf, Z. Ghassemlooy and S. Bourennane, "Performance of carrier-less amplitude and phase modulation with frequency domain equalization for indoor visible light communications," 2015 4th International Workshop on Optical Wireless Communications (IWOW), Istanbul, Turkey, pp. 16-20, 2015.

[50] T. Komine and M. Nakagawa, "Fundamental analysis for visible-light communication system using LED lights," in *IEEE Transactions on Consumer Electronics*, vol. 50, no. 1, pp. 100-107, Feb. 2004.

[51] M. Ijaz *et al.*, "Optical spatial modulation OFDM using micro LEDs," *2014 48th Asilomar Conference on Signals, Systems and Computers*, Pacific Grove, CA, pp. 1734-1738, 2014.

[52] H. Qian, S. J. Yao, S. Z. Cai and T. Zhou, "Adaptive Postdistortion for Nonlinear LEDs in Visible Light Communications," in IEEE Photonics Journal, vol. 6, no. 4, pp. 1-8, Aug. 2014.

[53] A. Al-Kinani, C. -X. Wang, H. Haas and Y. Yang, "Characterization and Modeling of Visible Light Communication Channels," *2016 IEEE 83rd Vehicular Technology Conference (VTC Spring)*, Nanjing, China, pp. 1-5, 2016.

[54] Shi, Jianyang, Wenqing Niu, Yinaer Ha, Zengyi Xu, Ziwei Li, Shaohua Yu, and Nan Chi, "AI-Enabled Intelligent Visible Light Communications: Challenges, Progress, and Future" Photonics 9, no. 8: 529, 2022.

[55] N. Fujimoto and S. Yamamoto, "The fastest visible light transmissions of 662 Mb/s by a blue LED, 600 Mb/s by a red LED, and 520 Mb/s by a green LED based on simple OOK-NRZ modulation of a commercially available RGB-type white LED using pre-emphasis and post-equalizing techniques," 2014 The European Conference on Optical Communication (ECOC), Cannes, France, pp. 1-3, 2014.

[56] X. Li et al., "Wireless Visible Light Communications Employing Feed-Forward Pre-Equalization and PAM-4 Modulation," in Journal of Lightwave Technology, vol. 34, no. 8, pp. 2049-2055, 15 April15, 201

[57] M. I. Olmedo et al., "Multiband Carrierless Amplitude Phase Modulation for High Capacity Optical Data Links," in Journal of Lightwave Technology, vol. 32, no. 4, pp. 798-804, Feb.15, 2014.

[58] F. M. Wu et al., "Performance Comparison of OFDM Signal and CAP Signal Over High Capacity RGB-LED-Based WDM Visible Light Communication," in IEEE Photonics Journal, vol. 5, no. 4, pp. 7901507-7901507, Aug. 2013.

[59] S. Long, M. -A. Khalighi, M. Wolf, Z. Ghassemlooy and S. Bourennane, "Performance of carrier-less amplitude and phase modulation with frequency domain equalization for indoor visible light communications," 2015 4th International Workshop on Optical Wireless Communications (IWOW), Istanbul, Turkey, pp. 16-20, 2015.

[60] F. Barrami, Y. Le Guennec, E. Novakov and P. Busson, "An optical power efficient asymmetrically companded DCO-OFDM for IM/DD systems," 2014 23rd Wireless and Optical Communication Conference (WOCC), Newark, NJ, USA, pp. 1-6, 2014.

[61] C. He and J. Armstrong, "Clipping Noise Mitigation in Optical OFDM Systems," in IEEE Communications Letters, vol. 21, no. 3, pp. 548-551, March 2017.

[62] R. Islam, P. Choudhury and M. A. Islam, "Analysis of DCO-OFDM and flip-OFDM for IM/DD optical-wireless system," 8th International Conference on Electrical and Computer Engineering, Dhaka, Bangladesh, pp. 32-35, 2014.

[63] B. Ranjha and M. Kavehrad, "Hybrid asymmetrically clipped OFDM-based IM/DD optical wireless system," in Journal of Optical Communications and Networking, vol. 6, no. 4, pp. 387-396, April 2014.

[64] F. Barrami, Y. Le Guennec, E. Novakov and P. Busson, "An optical power efficient asymmetrically companded DCO-OFDM for IM/DD systems," 2014 23rd Wireless and Optical Communication Conference (WOCC), Newark, NJ, USA, pp. 1-6, 2014.

[65] B. Li, W. Xu, Z. Li and Y. Zhou, "Adaptively Biased OFDM for IM/DD-Aided Optical Wireless Communication Systems," in IEEE Wireless Communications Letters, vol. 9, no. 5, pp. 698-701, May 2020.

[66] Darwesh, Laialy, and Natan Kopeika, "Improved Performance in the Detection of ACO-OFDM Modulated Signals Using Deep Learning Modules" Applied Sciences, 2020. https://doi.org/10.3390/app10238380.

[67] B. Aly, M. Elamassie, M. Uysal and E. Kınav, "Experimental Evaluation of Unipolar OFDM VLC System on Software Defined Platform," 2019 15th International Conference on Telecommunications (ConTEL), Graz, Austria pp. 1-6, 2019.

[68] R. S. J. Godwin, K. Veena and D. S. Kumar, "Performance analysis of direct detection Flip-OFDM for VLC system," 2016 International Conference on Emerging Trends in Engineering, Technology and Science (ICETETS), Pudukkottai, India, pp. 1-5, 2016.

[69] N. Fernando, Y. Hong and E. Viterbo, "Flip-OFDM for optical wireless communications," 2011 IEEE Information Theory Workshop, Paraty, Brazil, pp. 5-9, 2011.

[70] Abd Elkarim M, Aly MH, AbdelKader HM, Elsherbini MM. LED nonlinearity mitigation in LACO-OFDM optical communications based on adaptive predistortion and postdistortion techniques. Appl Opt. Aug. 2021.

[71] D. Tsonev and H. Haas, "Avoiding spectral efficiency loss in unipolar OFDM for optical wireless communication," 2014 IEEE International Conference on Communications (ICC), Sydney, NSW, Australia, pp. 3336-3341, 2014.

[72] G. Stepniak, "Minimum Bandwidth Nonnegative Pulses for Optical Transmission," in IEEE Communications Letters, vol. 23, no. 3, pp. 438-441, March 2019.

[73] N. A. Alhaj et al., "Integration of Hybrid Networks, AI, Ultra Massive-MIMO, THz Frequency, and FBMC Modulation Toward 6G Requirements: A Review," in IEEE Access, vol. 12, pp. 483-513, 2024.

[74] M. I. Maulana and M. Suryanegara, "Progress in 6G Technology: A Short Review," *2023 6th International Conference of Computer and Informatics Engineering (IC2IE)*, Lombok, Indonesia, 2023, pp. 36-41

[75] E. Niarchou, A. C. Boucouvalas, Z. Ghassemlooy, L. N. Alves and S. Zvanovec, "Visible Light Communications for 6G Wireless Networks," *2021 Third South American Colloquium on Visible Light Communications (SACVLC)*, Toledo, Brazil, pp. 01-06, 2021.

[76] S. Ariyanti and M. Suryanegara, "Visible Light Communication (VLC) for 6G Technology: The Potency and Research Challenges," 2020 Fourth World Conference on Smart Trends in Systems, Security and Sustainability (WorldS4), London, UK, pp. 490-493, 2020.

[77] F. Hamdar, C. M. G. Gussen, J. Nadal, C. A. Nour and A. Baghdadi, "FBMC/OQAM Transceiver for Future Wireless Communication Systems: Inherent Potentials, Recent Advances, Research Challenges," in IEEE Open Journal of Vehicular Technology, vol. 4, pp. 652-666, 2023.

[78] R. Ahmad, H. Elgala, S. Almajali, H. Bany Salameh and M. Ayyash, "Unified Physical-Layer Learning Framework Toward VLC-Enabled 6G Indoor Flying Networks," in *IEEE Internet of Things Journal*, vol. 11, no. 3, pp. 5545-5557, 1 Feb.1, 2024,

[79] V. Georlette and V. Moeyaert, "Li-Fi and Visible Light Communication for Smart Cities and Industry 4.0: challenges, research & market status in 2023," 2023 23rd International Conference on Transparent Optical Networks (ICTON), Bucharest, Romania, pp. 1-4, 2023.

[80] Aboelala O, Lee IE, Chung GC., "A Survey of Hybrid Free Space Optics (FSO) Communication Networks to Achieve 5G Connectivity for Backhauling," Entropy, no. 11: 1573, 2022.

[81] G.A. Torres Guzmán, D.A. Rodríguez Erazo, M.A. Leguizamón Páez. "LI-FI: current status, advances and future projection" Revista Ingeniería Solidaria, vol. 17, no. 2, 2021.

[82] E. Calvanese Strinati et al., "6G: The Next Frontier: From Holographic Messaging to Artificial Intelligence Using Subterahertz and Visible Light Communication," in IEEE Vehicular Technology Magazine, vol. 14, no. 3, pp. 42-50, Sept. 2019.

[83] H. Qian, S. J. Yao, S. Z. Cai and T. Zhou, "Adaptive Postdistortion for Nonlinear LEDs in Visible Light Communications," in IEEE Photonics Journal, vol. 6, no. 4, pp. 1-8, Aug. 2014,

[84] I. Stefan, H. Elgala, R. Mesleh, D. O'Brien and H. Haas, "Optical Wireless OFDM System on FPGA: Study of LED Nonlinearity Effects," 2011 IEEE 73rd Vehicular Technology Conference (VTC Spring), Budapest, Hungary, pp. 1-5, 2011,

[85] D. Karunatilaka, F. Zafar, V. Kalavally and R. Parthiban, "LED Based Indoor Visible Light Communications: State of the Art," in IEEE Communications Surveys & Tutorials, vol. 17, no. 3, pp. 1649-1678, thirdquarter 2015.

[86] Q. Wang, Z. Wang, L. Dai and J. Quan, "Dimmable Visible Light Communications Based on Multilayer ACO-OFDM," in IEEE Photonics Journal, vol. 8, no. 3, pp. 1-11, June 2016.

[87] L. E. M. Matheus, A. B. Vieira, L. F. M. Vieira, M. A. M. Vieira and O. Gnawali, "Visible Light Communication: Concepts, Applications and Challenges," in IEEE Communications Surveys & Tutorials, vol. 21, no. 4, pp. 3204-3237, Fourthquarter 2019.

[88] Ji, R.; Wang, S.; Liu, Q.; Lu, W. High-Speed Visible Light Communications: Enabling Technologies and State of the Art. Appl. Sci., no. 4: 589, 2018.

[89] A. Khreishah, S. Shao, A. Gharaibeh, M. Ayyash, H. Elgala and N. Ansari, "A Hybrid RF-VLC System for Energy Efficient Wireless Access," in IEEE Transactions on Green Communications and Networking, vol. 2, no. 4, pp. 932-944, Dec. 2018.

[90] Lee, C. C., Chuan Seng Tan, H. Y. Wong and Mazlaini Yahya. "Performance evaluation of hybrid VLC using device cost and power over data throughput criteria." Optics & Photonics - Optical Engineering + Applications (2013).

[91] Z. Xu and B. M. Sadler, "Ultraviolet Communications: Potential and State-Of-The-Art," in IEEE Communications Magazine, vol. 46, no. 5, pp. 67-73, May 2008.

[92] M. B. Rahaim, A. M. Vegni and T. D. C. Little, "A hybrid Radio Frequency and broadcast Visible Light Communication system," 2011 IEEE GLOBECOM Workshops (GC Wkshps), Houston, TX, USA, pp. 792-796, 2011.

[93] H. B. Eldeeb, M. Hosney, H. M. Elsayed, R. I. Badr, M. Uysal and H. A. I. Selmy, "Optimal Resource Allocation and Interference Management for Multi-User Uplink Light Communication Systems With Angular Diversity Technology," in IEEE Access, vol. 8, pp. 203224-203236, 2020.

[94] T. -C. Bui and S. Kiravittaya, "Demonstration of using camera communication based infrared LED for uplink in indoor visible light communication," 2016 IEEE Sixth International Conference on Communications and Electronics (ICCE), Ha-Long, pp. 71-76, Vietnam, 2016.

[95] Z. Zeng, M. D. Soltani, M. Safari and H. Haas, "Angle Diversity Receiver in LiFi Cellular Networks," ICC 2019 - 2019 IEEE International Conference on Communications (ICC), Shanghai, ,pp. 1-6, China, 2019.

[96] M. T. Alresheedi and J. M. H. Elmirghani, "Hologram selection in realistic indoor optical wireless systems with angle diversity receivers," in Journal of Optical Communications and Networking, vol. 7, no. 8, pp. 797-813, August 2015.

[97] He, Cuiwei, and Chen Chen, "A Review of Advanced Transceiver Technologies in Visible Light Communications" Photonics 10, no. 6: 648, 2023.

[98] Soltani, M.D., et al., "Terabit Indoor Laser-Based Wireless Communications: LiFi 2.0 for 6G", arXiv, 2022.

[99] Liu, Y., et al., "High-capacity optical wireless VCSEL array transmitter with uniform coverage. In Free-Space Laser Communications XXXV", SPIE: Paris, France, Volume 12413, pp. 144–150, 2023.

[100] Bao, X., Adjardjah, W., Okine, A.A. et al. A QoE-maximization-based vertical handover scheme for VLC heterogeneous networks. J Wireless Com Network 2018, 269 (2018).

[101] G. Ma, R. Parthiban and N. Karmakar, "A Comparison of IVHO and DVHO in Heterogeneous VLC-RF Networks," 2021 IEEE Region 10 Symposium (TENSYMP), Jeju, Korea, Republic of, pp. 1-7, 2021.

[102] IEEE approves 802.11bb LiFi, converge network digest in 5G/6G/Wi-Fi, July, 2023. https://convergedigest.com/ieee-approves-802-11bb-lifi/.

[103] E. Khorov and I. Levitsky, "Current Status and Challenges of Li-Fi: IEEE 802.11bb," in IEEE Communications Standards Magazine, vol. 6, no. 2, pp. 35-41, June 2022.

[104] M. T. Guneser, A. S. Sahab and C. Seker, "Performance analysis of modulation techniques in 5G communication system," in China Communications, vol. 19, no. 8, pp. 100-114, Aug. 2022.

[105] T. Poornima, K. Dhinesh and R. Sudhakar, "Waveform candidates for 5G mobile communications," 2017 2nd IEEE International Conference on Recent Trends in Electronics, Information & Communication Technology (RTEICT), Bangalore, pp. 856-860, India, 2017.

[106] H. Jebbar, S. E. Hassani and A. E. Abbassi, "Performance study of 5G multicarrier waveforms," 2017 International Conference on Wireless Networks and Mobile Communications (WINCOM), Rabat, Morocco, pp. 1-6, 2017.

[107] Mrinalini and K. Kumar Singh, "A Survey Paper on Multicarrier Modulation Techniques," 2018 5th IEEE Uttar Pradesh Section International Conference on Electrical, Electronics and Computer Engineering (UPCON), Gorakhpur, India, pp. 1-6, 2018.

[108] B. Khan and F. J. Velez, "Multicarrier Waveform Candidates for Beyond 5G," 2020 12th International Symposium on Communication Systems, Networks and Digital Signal Processing (CSNDSP), Porto, Portugal, pp. 1-6, 2020.

[109] Gerzaguet, R., Bartzoudis, N., Baltar, L.G. et al. The 5G candidate waveform race: a comparison of complexity and performance. J Wireless Com Network 2017, 13 (2017).

[110] T. Kebede, Y. Wondie, J. Steinbrunn, H. B. Kassa and K. T. Kornegay, "Multi-Carrier Waveforms and Multiple Access Strategies in Wireless Networks: Performance, Applications, and Challenges," in IEEE Access, vol. 10, pp. 21120-21140, 2022.

[111] J. Chu, M. Gao, X. Liu, M. Bi, H. Huang and G. Shen, "Channel Estimation Based on Complex-Valued Neural Networks in IM/DD FBMC/OQAM Transmission System," in Journal of Lightwave Technology, vol. 40, no. 4, pp. 1055-1063, 15 Feb.15, 2022.

[112] H. M. Abdel-Atty, W. A. Raslan and A. T. Khalil, "Evaluation and Analysis of FBMC/OQAM Systems Based on Pulse Shaping Filters," in IEEE Access, vol. 8, pp. 55750-55772, 2020.

[113] A. Viholainen, T. Ihalainen, T. H. Stitz, M. Renfors and M. Bellanger, "Prototype filter design for filter bank based multicarrier transmission," 2009 17th European Signal Processing Conference, Glasgow, UK, pp. 1359-1363, 2009.

[114] C. Boyd, R. -A. Pitaval, O. Tirkkonen and R. Wichman, "On the time-frequency localisation of 5G candidate waveforms," 2015 IEEE 16th International Workshop on Signal Processing Advances in Wireless Communications (SPAWC), Stockholm, pp. 101-105, Sweden, 2015.

[115] T. Stitz, T. Ihalainen, A. Viholainen et al. "Pilot-Based Synchronization and Equalization in Filter Bank Multicarrier Communications," EURASIP J. Adv. Signal Process. 2010.

[116] M. Aldababseh and A. Jamoos.,"Estimation of FBMC/OQAM fading channels using dual Kalman filters," the Scientific World Journal, 2014, 586403. [Online]. Available: https://doi.org/10.1155/2014/586403

[117] INFSO-ICT-211887 Project PHYDYAS, Deliverable 5.1: Prototype filter and structure optimization, Jan. 2009. [Online]. Available: http://www.ict-phydyas.org/delivrables/PHYDYAS-D5-1.pdf/view.

[118] D. William, M.Guerra and T. Abrão, "Efficient multitap equalization for FBMC-OQAM systems," Trans Emerg Telecommun Technol, vol. 30, no. 12, 2019.

[119] D. Kong, D. Chen, D. Qu and T. Jiang, "Preamble optimization based on frequency domain averaging for channel estimation in OQAM-OFDM systems," 2015 International Conference on Wireless Communications & Signal Processing (WCSP), Nanjing, pp. 1-6, China, 2015.

[120] H. Lin, C. Lele and P. Siohan, "Equalization with Interference Cancellation for Hermitian Symmetric OFDM/OQAM systems," 2008 IEEE International Symposium on Power Line Communications and Its Applications, Jeju, Korea (South), pp. 363-368, 2008.

[121] E. Kofidis, "Preamble-Based Estimation of Highly Frequency Selective Channels in FBMC/OQAM Systems," in IEEE Transactions on Signal Processing, vol. 65, no. 7, pp. 1855-1868, 1 April1, 2017.

[122] G. Srikanth, S. L. Nisha and S. G. S. Prasad, "Performance of FBMC for 5G Communication," 2018 3rd IEEE International Conference on Recent Trends in Electronics, Information & Communication Technology (RTEICT), Bangalore, India, pp. 828-832, 2018.

[123] E. Kofidis, D. Katselis, A. Rontogiannis, S. Theodoridis, "Preamble-based Channel Estimation in OFDM/OQAM Systems: A Review," Signal Processing, vol. 93, pp. 2038-2054, July 2013.

[124] R. Kobayashi, A. Mussi and T. Abrão, "Near-perfect reconstruction short length pulses for FBMC systems: re-optimising OFDP design via semi-definite programming", IET Signal Processing, October 2019.

[125] P. Siohan, C. Siclet and N. Lacaille, "Analysis and design of OFDM/OQAM systems based on filterbank theory," in IEEE Transactions on Signal Processing, vol. 50, no. 5, pp. 1170-1183, May 2002.

[126] W. Cui, D. Qu, T. Jiang and B. Farhang-Boroujeny, "Coded Auxiliary Pilots for Channel Estimation in FBMC-OQAM Systems," in IEEE Transactions on Vehicular Technology, vol. 65, no. 5, pp. 2936-2946, May 2016.

[127] C. Lele, P. Siohan, R. Legouable and J. . -P. Javaudin, "Preamble-based channel estimation techniques for OFDM/OQAM over the powerline," 2007 IEEE International Symposium on Power Line Communications and Its Applications, Pisa, pp. 59-64, Italy, 2007.

[128] M. G. Bellanger, "Specification and design of a prototype filter for filter bank based multicarrier transmission," 2001 IEEE International Conference on Acoustics, Speech, and Signal Processing. Proceedings (Cat. No.01CH37221), Salt Lake City, UT, USA, vol.4, pp. 2417-2420, 2001.

[129] K. W. Martin, "Small side-lobe filter design for multitone data-communication applications," in IEEE Transactions on Circuits and Systems II: Analog and Digital Signal Processing, vol. 45, no. 8, pp. 1155-1161, Aug. 1998.

[130] P. Siohan and C. Roche, "Derivation of extended Gaussian functions based on the Zak transform," in IEEE Signal Processing Letters, vol. 11, no. 3, pp. 401-403, March 2004.

[131] P. Siohan and C. Roche, "Cosine-modulated filterbanks based on extended Gaussian functions," in IEEE Transactions on Signal Processing, vol. 48, no. 11, pp. 3052-3061, Nov. 2000.

[132] A. Sahin, I. Guvenc and H. Arslan, "A Survey on Multicarrier Communications: Prototype Filters, Lattice Structures, and Implementation Aspects," in IEEE Communications Surveys & Tutorials, vol. 16, no. 3, pp. 1312-1338, Third Quarter 2013.

[133] Jinfeng Du and Svant Signell, "Time frequency localization of pulse shaping filters in OFD/OQAM systems," 2007 6th International Conference on Information, Communications & Signal Processing, Singapore, pp. 1-5, 2007.

[134] P.P. Vaidyanathan: *Multirate Systems and Filter Banks*. Prentice-Hall, Englewood Cliffs, NJ, USA; 1993.

[135] T. Stitz, T. Ihalainen, A. Viholainen *et al.* "Pilot-Based Synchronization and Equalization in Filter Bank Multicarrier Communications," *EURASIP J. Adv. Signal Process.* 2010.

[136] J. Shi, J. He, R. Zhang and Rui Deng, "Experimental demonstration of blind equalization for OFDM/ OQAM-VLC system," *Optical engineering*, vol. 58, Jun. 2019.

[137] S. Taheri, M. Ghoraishi, P. Xiao and L. Zhang, "Efficient Implementation of Filter Bank Multicarrier Systems Using Circular Fast Convolution," in IEEE Access, vol. 5, pp. 2855-2869, 2017.

[138] A. Husam and Z. Kollár, "Complexity Comparison of Filter Bank Multicarrier Transmitter Schemes," 2018 11th International Symposium on Communication Systems, Networks & Digital Signal Processing (CSNDSP), Budapest, pp. 1-4, 2018.

[139] R. Chen, K. -H. Park, C. Shen, T. Khee Ng, B. S. Ooi and M. -S. Alouini, "Visible light communication using DC-biased optical filter bank multi-carrier modulation," *2018 Global LIFI Congress (GLC)*, Paris, France, pp. 1-6, 2018.

[140] A. -a. Husam and Z. Kollár, "Complexity Comparison of Filter Bank Multicarrier Transmitter Schemes," *2018 11th International Symposium on Communication Systems, Networks & Digital Signal Processing (CSNDSP)*, Budapest, Hungary, pp. 1-4, 2018.

[141] R. T. Kobayashi and T. Abrão, "FBMC Prototype Filter Design via Convex Optimization," in *IEEE Transactions on Vehicular Technology*, vol. 68, no. 1, pp. 393-404, Jan. 2019.

[142] D. H. Kwon, S. H. Yang and S. K. Han, "Modulation bandwidth enhancement of white-LED-based visible light communications using electrical equalizations", *Proc. SPIE 9387, Broadband Access Communication Technologies IX*, 7 February 2015. [Online]. Available: https://doi.org/10.1117/12.2078680

[143] N. Fujimoto and H. Mochizuki, "477 Mbit/s visible light transmission based on OOK-NRZ modulation using a single commercially available visible LED and a practical LED driver with a pre-emphasis circuit," *Optical Fiber Communication Conference and Exposition and the National Fiber Optic Engineers Conference (OFC/NFOEC)*, Anaheim, CA, 2013.

[144] S. K. Sharma, I. Woungang, A. Anpalagan and S. Chatzinotas, "Toward Tactile Internet in Beyond 5G Era: Recent Advances, Current Issues, and Future Directions," in *IEEE Access*, vol. 8, pp. 56948-56991, 2020.

[145] J. Yli-Kaakinen, J. Alhava, M. Renfors and H. Tuomivaara, "Multicarrier waveform processing for HF communications," *2018 International Conference on Military Communications and Information Systems (ICMCIS)*, Warsaw, Poland, pp. 1-8, 2018.

[146] Ihalainen, T., Hidalgo Stitz, T., Rinne, M. *et al.*, "Channel Equalization in Filter Bank Based Multicarrier Modulation for Wireless Communications, " EURASIP J. Adv. Signal Process. 2007, 049389 (2006).

[147] T. Wang, F. Yang, C. Pan, L. Cheng and J. Song, "Spectral-Efficient Hybrid Dimming Scheme for Indoor Visible Light Communication: A Subcarrier Index Modulation Based Approach," in Journal of Lightwave Technology, vol. 37, no. 23, pp. 5756-5765, 1 Dec.1, 2019.

[148] Haas, R., Belfiore, JC., " A Time-Frequency Well-localized Pulse for Multiple Carrier Transmission," Wireless Personal Communications 5, 1–18 (1997). [Online]. Available: https://doi.org/10.1023/A:1008859809455.

[149] M. G. Bellanger, "Specification and design of a prototype filter for filter bank based multicarrier transmission," *2001 IEEE International Conference on Acoustics, Speech, and Signal Processing. Proceedings (Cat. No.01CH37221)*, Salt Lake City, UT, USA, pp. 2417-2420 vol.4, 2001.

[150] M. T. Rahman, M. Bakaul and R. Parthiban, "Analysis of the effects of multiple reflection paths on high speed VLC system performance," 2018 28th International Telecommunication Networks and Applications Conference (ITNAC), Sydney, NSW, Australia, pp. 1-6, 2018.

[151] C. E. Yew, M. B. Hidayab and C. C. Leong, "Visible Light Communication for Robotic Control," *2018 IEEE 4th International Symposium in Robotics and Manufacturing Automation (ROMA)*, Perambalur, India, 2018, pp. 1-5,

[152] M. Khan and J. Chakareski, "Visible Light Communication for Next Generation Untethered Virtual Reality Systems," *2019 IEEE International Conference on Communications Workshops (ICC Workshops)*, Shanghai, China, pp. 1-6, 2019.

[153] G. Qiao, X. Liu, L. Ma, S. Mazhar and Y. Zhao, "Residual Doppler Effect Analysis of the FBMC/OQAM Communication System in Underwater Acoustic Channel," in *IEEE Communications Letters*, vol. 25, no. 9, pp. 3090-3093, Sept. 2020.

[153] Y. Li, H. Qiu, X. Chen and Jielin Fu, "A novel PAPR reduction algorithm for DCO-OFDM/OQAM system in underwater VLC," *Optics Communications*, vol. 463, 2020. [Online]. Available: https://doi.org/10.1016/j.optcom.2020.125449.